STANFORD UNIVERSITY
ENGINEERING IN MEDICINE AND BIOLOGY

NONLINEAR ANALYSIS OF PRESSURE- AND SHOCK WAVES IN BLOOD VESSELS

PH. D. DISSERTATION

BY

ROBERT L. ROCKWELL

FACILITY FORM 602
N70-36857 (ACCESSION NUMBER)
122 (PAGES)
CR-112864 (NASA CR OR TMX OR AD NUMBER)
(THRU)
(CODE)
04 (CATEGORY)

BIOMECHANICS LABORATORY

DEPARTMENT OF AERONAUTICS AND ASTRONAUTICS

DECEMBER 1969

Reproduced by
NATIONAL TECHNICAL
INFORMATION SERVICE
Springfield, Va. 22151

This work was carried out at the Ames Research Center of NASA under a collaborative research arrangement with Stanford University (NASA Grant NGL 05-020-223).

Department of Aeronautics and Astronautics
Stanford University
Stanford, California

NONLINEAR ANALYSIS OF PRESSURE- AND SHOCK WAVES IN BLOOD VESSELS

Ph. D. Dissertation

by

Robert L. Rockwell

Certified by:

Max Anliker (Adviser)

I-Dee Chang

Herbert N. Hultgren
(Professor of Medicine, Cardiology)

SUDAAR NO. 394
December 1969

This work was carried out at the Ames Research Center of NASA under a collaborative research arrangement with Stanford University (NASA Grant NGL 05-020-223)

ACKNOWLEDGEMENT

First and foremost I must thank my adviser, Professor Max Anliker, for his expert counsel and many suggestions. His excellence as a teacher and guide is reflected throughout this dissertation.

Professor I-Dee Chang from Aeronautics and Astronautics and Professor Herbert Hultgren from the Division of Cardiology at the Stanford Medical School were kind enough to review the preliminary manuscript. Their pertinent comments are gratefully acknowledged. Space does not allow me to name individually the other members of the Stanford University faculty who without exception have contributed to my education through their stimulating lectures. I thank them all.

In spite of deadline pressures and other commitments, Miss Kathy Hunt and Mrs. Jane Fajardo have done their best in typing the final manuscript. I appreciate the availability of their exceptional skills.

This research was carried out at the Ames Research Center of the National Aeronautics and Space Administration under a collaborative research arrangement with Stanford University (NASA Grant NGL 05-020-223). Thanks are due Dr. Eric Ogden of the Environmental Biology Division for encouraging my work in this fascinating field of Biomechanics. For sponsoring my graduate studies I express appreciation to the Naval Weapons Center at China Lake and especially to my immediate supervisor, Mr. Judson C. Smith.

Finally I must apologize to my family for my neglect as a husband and father during these past few years. I deeply appreciate their understanding. To Sheila I owe special thanks for her faith, encouragement and infinite patience.

PRECEDING PAGE BLANK NOT FILMED.

ABSTRACT

A nonlinear analysis of large amplitude pressure waves was made for a theoretical model of the canine aorta and its continuation beyond the saphenous artery. In particular the changes in the pressure and flow pulses produced by the heart were assessed for meaningful variations in the system parameters. To allow for the interpretation of relatively small changes in the pressure and flow patterns it was considered necessary to take nonlinearities into account as accurately as possible. According to recent experimental evidence, the propagation of the natural pressure pulse should be strongly affected by nonlinear phenomena such as the wave speed variations with pressure and flow and the large local changes in cross-sectional area with pressure.

Pressure and flow pulses induced in the aorta and other large arteries were predicted by prescribing the ejection pattern of the heart and the physical and geometric features of the system. The effects of branches and bifurcations were modeled by a continuous outflow pattern which varies with location and pressure. At the distal end of the vessel the terminal condition was specified either in the form of a peripheral resistance or in terms of a constant end pressure. The basic geometry was defined by an exponential decrease of the cross-sectional area of the artery with distance from the heart. Instead of being prescribed directly, the elastic properties of the vessel wall were given through the wave speed and its dependence on location and pressure. This information was also used to determine the cross-sectional area variation with pressure and distance by integrating the wave speed-distensibility relation. In this way, the experimental measurements were incorporated in a most direct manner.

The nonlinear equations for one-dimensional incompressible fluid flow were transformed according to the method of characteristics and solved on

the digital computer for cardiovascular parameter values corresponding to a hypothetical 30 kg dog. The parameters were systematically varied to determine their effects and to investigate possible manifestations of certain pathological conditions such as arteriosclerosis. In the numerical solutions the effects of reflections arising from the boundary conditions, taper and changes in the local wave velocity are inherently included by employing the method of characteristics.

Many familiar features of the natural pulse induced by the heart are predicted by the mathematical model, including the incisura, the growth and subsequent decay of the pulse pressure, and the gradual development of the dicrotic wave. As the pulse wave propagates down the aorta, there is a marked steepening of the wave front which was not observed when the basic equations were linearized.

The results suggest that the dicrotic wave is caused by reflections from the distal regions of the artery. However, the degree to which the dicrotic wave is due to the geometric taper and due to outflow has yet to be determined.

A comparison of the flow and pressure profiles obtained by postulating a peripheral resistance relation as the distal boundary condition with those computed for a constant pressure at the distal end shows that the concept of peripheral resistance yields good approximations for arterial models with a distal diameter less than 10% of that at the root of the aorta.

Aortic insufficiency was simulated by prescribing a cardiac ejection rate with an inordinate degree of regurgitation. The corresponding pressure pulses were shown to exhibit the familiar features of shock waves, which appear to be responsible for the so-called pistol shot sounds heard over the femoral or radial arteries of patients with highly incompetent aortic valves.

TABLE OF CONTENTS

	Page
TITLE PAGE	i
ACKNOWLEDGEMENT	iii
ABSTRACT	iv
TABLE OF CONTENTS	vi
NOTATION	viii
I. INTRODUCTION	1
II. DERIVATIONS	7
A. Basic Equations	7
B. Cross-Sectional Area as a Function of Pressure and Distance	14
C. The Friction Expression	17
D. The Outflow Expression Ψ	19
E. Boundary Conditions	25
F. Initial Conditions	29
III. TYPICAL RESULTS	30
A. Standard Case	30
B. Effect of Diameter	36
C. Effect of Wave Speed Increase	39
D. Effect of Pulse Rate	42
E. Effect of a Change in Outflow Distribution	45
F. Effect of Stroke Volume	45

Page

IV. SPECIAL PROBLEMS 52

A. Semi-Infinite Tubes with Uniform Cross Section 52

B. Linearized Treatment 56

C. Effect of Friction 62

D. Peripheral Resistance 68

E. Wave Front Velocity 73

F. Harmonic Analysis 76

G. Two Limiting Cases of Arterial Wall Properties 81

H. Effect of Generalized Vasoconstriction and Vasodilatation . . . 84

I. Effect of Cardiac Arrest 89

J. A Quiescent State as Initial Conditions 89

K. Aortic Insufficiency and Shock Waves 91

V. DISCUSSION AND CONCLUSIONS 102

APPENDIX A 107

APPENDIX B 110

REFERENCES 112

NOTATION

A = cross-sectional area of artery at the reference pressure p_o

c = local wave speed

c_o, c_1 = parameters in wave speed expression

c_f = friction coefficient

c_L = local wave speed for linearized analysis

C, C' = designations for general curves in z, t plane

D_o = diameter at aortic valve when $p = p_o$

D_t = diameter at distal end of artery when $p = p_o$

E = circumferential Young's modulus

f = axial frictional force per unit mass of fluid

h = wall thickness

L = total length of artery

n = parameter in wave speed expression

p = intraluminal pressure

$\bar{p}$ = calculated mean pressure

p_o = reference pressure

p_c = capillary pressure

p_L = pressure at distal end of artery

$q = Sv$ = local volume flow rate

$q_o = q_o(t)$ = volume flow rate ejected by heart

r = radial coordinate

R = internal radius of artery

R_e = Reynolds number for steady flow

R_L = peripheral resistance

s = curvilinear coordinate

S = cross-sectional area of artery

S_L = cross-sectional area for linearized analysis

t = time

T = circumferential wall tension

u = axial velocity

v = axial velocity averaged over cross section

x = axial distance coordinate

x^* = distance from aortic valve to femoral artery

α = outflow parameter

β = exponent in cross-sectional area expression

ϵ = differential strain

θ = circumferential coordinate

λ = undetermined multiplier

μ = blood viscosity coefficient

ρ = blood density

σ = differential wall stress

τ_w = frictional stress in the axial direction on the arterial wall

ψ = outflow function simulating effect of side branches

I. INTRODUCTION

The intermittent ejection of blood from the left ventricle produces pressure and flow pulses in the arterial tree. Experimental studies of these pulses reveal that they are propagated with a characteristic pattern. The pressure and flow pulses are interrelated and constitute a mechanical phenomenon whose features are defined by the physical and geometric properties of the arterial tree. We know from actual measurements on animals and on man that the pressure and flow pulses undergo well-defined changes in their wave form as they propagate away from the heart[1,2]. These changes are expected to be quite sensitive to certain variations in the properties of the cardiovascular system, and the question arises to what extent can deviations of the wave forms from their normal patterns be used as diagnostic indicators. With the recent development of ultrasound echo-ranging devices and pulsed doppler shift flowmeters which allow us to detect the flow pattern in major arteries without penetrating the skin[3,4,5], this question seems to be particularly relevant. However, a meaningful interpretation of changes in the pulse waves is only possible if we have a thorough quantitative understanding of how the various cardiovascular parameters can affect the phenomenon. As an attempt to answer some of these questions we have therefore begun a nonlinear analysis of large-amplitude waves in blood vessels which takes into account recently established experimental facts[6,7,8]. One of the principal reasons for undertaking this work is the need for a noninvasive method of determining possible changes which may occur in the cardiovascular system of astronauts as a result of prolonged exposure to weightlessness[9]. While preventive measures are being contemplated which are designed to inhibit the space adaptation of the circulatory system, the effectiveness of these measures has to be ascertained in a reliable fashion through transcutaneous measurements.

A thorough study of blood flow in arteries or veins presents formidable obstacles. For example, we do not yet know what constitutes a sufficiently accurate mathematical model for the mechanical behavior of the vessel wall and its surroundings. Also, we have yet to establish criteria which indicate when certain simplifying assumptions such as linearity in the system behavior, inviscid flow, one-dimensional flow, etc., are justified. So far, most theoretical studies of the arterial pressure and flow pulses have been based on linear analyses[1,2,10,11,12] even though there has been increasing evidence of the presence of strong nonlinear phenomena[6]. Some of the first serious attempts at including nonlinear effects were made by Lambert[13], Streeter et. al.[14], Rudinger[12,15], Barnard et. al.[16,17], and Jones[18] who considered the flow to be one-dimensiona and made use of the method of characteristics. The essential advantage of their approach is that the method of characteristics includes automatically the effects of reflections and makes it possible to account for the variations in cross-sectiona area with distance and pressure, and also the convection of the signal by the flow. While to-date no realistic analysis of the generation and evolution of the natural pulse wave in arteries has been made, the referenced investigations have clearly indicated the potential usefulness of the method of characteristics. The availability of faster digital computers and more detailed quantitative information on the mechanical behavior of arteries render the extension of earlier efforts feasible and timely.

Recent experimental observations[6,19] suggest that the propagation of large-amplitude pressure waves in arteries or veins is strongly influenced by nonlinear effects. It has been shown that the phase velocities of small sinusoidal pressure signals increase appreciably with transmural pressure and flow velocity. Consequently, the natural pressure pulse should exhibit a marked steepening of

its wave front with propagation and also an increase in pulse amplitude. Such a behavior can be interpreted as being similar to that observed during the initial phases of shock wave formation in a compressible flow field. In the present study we shall examine this similarity and explore the possibility of shock waves evolving from large-amplitude pressure pulses with steep wave fronts such as those encountered with incompetent aortic or tricuspid valves*) [20,21,22].

For sufficiently small pressure perturbations, such as those shown in Figure 1, a linearized treatment of the problem can be justified. Also, it can be used to demonstrate that the propagation characteristics of artificially induced signals vary with the naturally occurring pressure and flow fluctuations [6,19].

Since arteries do not seem to be significantly dispersive for pressure waves the phase velocity can be approximated by the speed of signals in the form of finite trains of sine waves [6]. This has been corroborated extensively for the canine aorta in the frequency range from 40 to 200 Hz. In our analysis we shall assume that the nondispersive property is valid also for frequencies as low as 1 Hz. In addition, we shall utilize in an approximate manner the pressure dependence of the wave speed shown in Figure 2 for the thoracic segment of the aorta [23].

The system of one-dimensional nonlinear differential equations for the present problem is hyperbolic which means that the occurrence of shock waves must be considered a distinct possibility. As a matter of fact the idea of shock waves in blood vessels is not new [21]. Their possible occurrence has been postulated at times in the past [11,12] but not been considered seriously because

---

*) In patients with aortic insufficiency, i.e., incompetent or leaking aortic valves, there is extensive regurgitation of arterial blood from the aorta back into the left ventricle. Likewise, in patients with severely leaking tricuspid valves we find regurgitation of venous blood from the right ventricle back into the vena cava. In both cases extremely large pressure pulses may be generated.

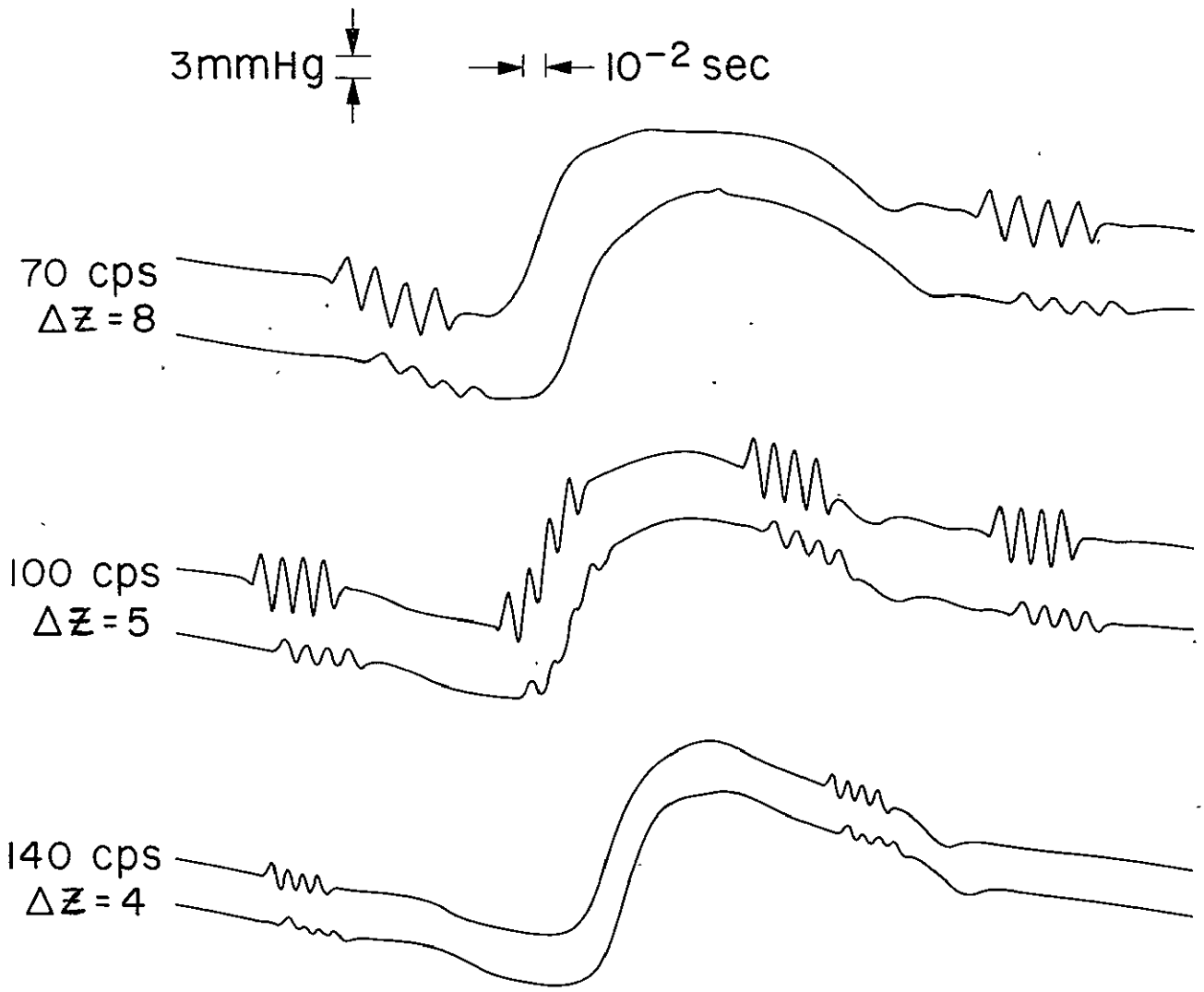

Figure 1. Representative tracings of recordings of the natural pulse wave in the thoracic aorta of an anesthetized dog, with artificially superimposed trains of sinusoidal waves of various frequencies. The transient signals were induced at different times during the cardiac cycle. Note that the sine waves are highly damped but retain their sinusoidal character during propagation. All of the pressure curves are drawn to the same relative scale, as indicated. However, each of the curves has a different zero point since they were separated for illustration purposes. Δz represents the distance between the two catheter-tip manometers used to record the pressure signals. These tracings are copied from Reference 6.

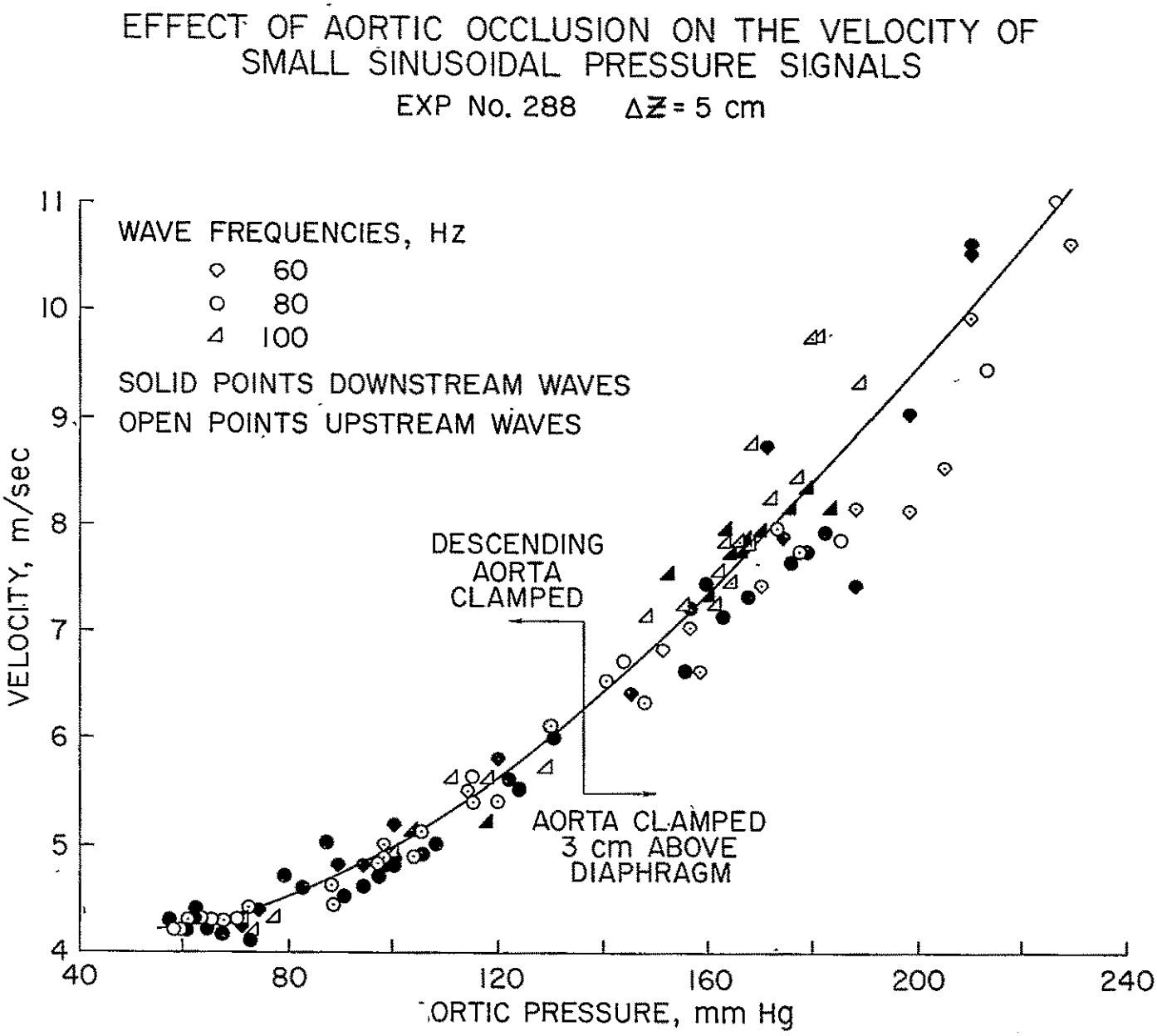

Figure 2. Wave speed-pressure data obtained for thoracic aorta of an anesthetized dog. Each point represents the average speed of a peak and successive valley of a sine wave. Taken from Reference 23.

under normal conditions the distances required for their development exceed physiologically meaningful values. However, for very strong pressure pulses with steep wave fronts, the distances at which shock waves can be identified could well be within the physiological range. If we can verify this hypothesis, we could possibly arrive at an explanation for the genesis of the pistol shot sounds which can be heard over arteries in the extremities of patients with incompetent aortic valves[20] or over the corresponding veins in cases of leaking tricuspid valves[22].

Compared with other theoretical investigations the present study differs insofar as it introduces the mechanical properties of the arterial wall in a very direct manner through the wave speed as a function of pressure and distance from the heart. In the past, the mechanical properties of the arterial wall were in most cases given in terms of a constant Young's modulus. However, if the pressure dependence of this modulus is not taken into account, the wave speed decreases with pressure[14], contrary to experimental observations.

II. DERIVATIONS

In this study of large-amplitude wave propagation in arteries we assume one-dimensional motion of the blood. We model the vessel as a tapered elastic tube and allow for continuously distributed seepage through the wall to simulate the outflow through the branches in a manner which approximates the regional blood flow pattern. The blood is treated as an incompressible fluid and the effects of viscosity are accounted for in an approximate fashion. Rather than specifying the elastic properties of the vessel wall in terms of a Young's modulus in order to define the interaction of the blood with the elastic wall we prescribe the mechanical behavior of the tube through the speed of small pressure waves and the variation of this speed with pressure and location. With the pressure dependence of the local wave speed we are also stipulating how the cross-sectional area changes when the pressure fluctuations can not be considered small. The equations governing the fluid flow and the fluid-wall interaction are then transformed according to the method of characteristics and put into a form suitable for machine computation. Adhering to such an approach we include automatically reflection phenomena and the essential nonlinearities of the system. It also permits us to give solutions corresponding to arbitrary initial conditions and realistic boundary conditions. For the most part, the notation used here is the same as that introduced by Skalak[11] and Rudinger[12] in their survey papers.

A. BASIC EQUATIONS

We begin with the formulation of conservation of mass and momentum for the fluid. Although this analysis assumes the cross section of the artery to be circular, it can readily be extended to vessels with non-circular cross sections. By postulating one-dimensional flow we treat the pressure and flow

velocity as uniform over the entire cross section. This is obviously an approximation of reality and means that we are essentially considering spatial average values of the dependent flow variables at each cross section. While the pressure is inherently nearly constant over the cross section, the average velocity can be expressed as

$$v(z,t) = \frac{1}{\pi R^2} \int_0^{2\pi} \int_0^{R} u(r,\theta,z,t)\, r\, dr\, d\theta$$

where $u(r,\theta,z,t)$ defines the velocity profile.

Conservation of mass requires that the rate of mass increase inside an element of the blood vessel is equal to the net influx of mass. For an incompressible fluid and allowing for outflow of fluid through the arterial wall we have, as indicated in Figure 3

$$\frac{\partial}{\partial t}(\rho S \Delta z) = \rho v_1 S_1 - \rho v_2 S_2 - \rho \Psi \Delta z$$

where Ψ is the rate of volumetric outflow (leakage) per unit length of artery. By expanding the flux at station 2 in a Taylor series about station 1 we obtain

$$\rho v_2 S_2 = \rho v_1 S_1 + \frac{\partial}{\partial z}(\rho v_1 S_1)\Delta z + \dots$$

and therefore

$$\frac{\partial}{\partial t}(\rho S \Delta z) = -\frac{\partial}{\partial z}(\rho v_1 S_1)\Delta z - \rho \Psi \Delta z - \dots$$

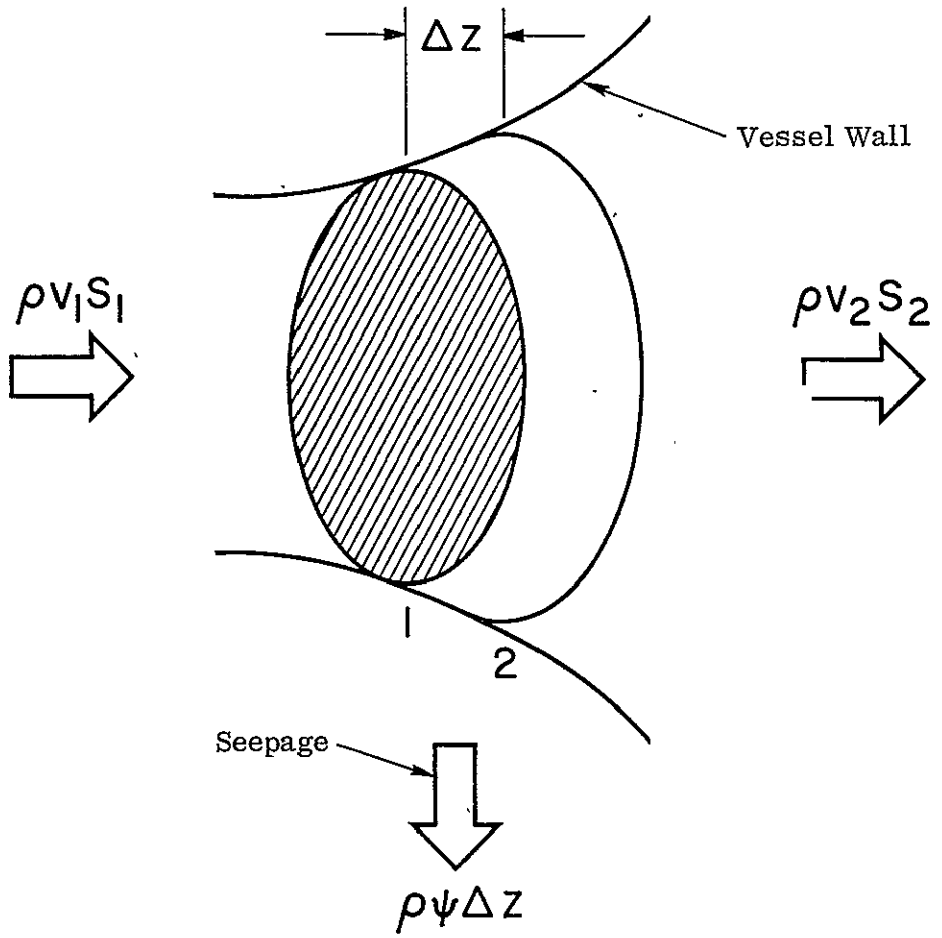

Figure 3. Fluid element in blood vessel. Schematic illustration for the formulation of the conservation of mass.

Recalling that ρ is constant and z is an independent variable we find for the limit $\Delta z \rightarrow 0$

$$\frac{\partial S}{\partial t} + \frac{\partial (S v)}{\partial z} + \psi = 0 \qquad (1)$$

For the time being, the nature of ψ is left undefined. Its inclusion in the equation simulates the outflow of blood from the artery of interest through discrete bifurcations and branches.

As in references (11) and (12) we write for conservation of momentum

$$\frac{\partial v}{\partial t} + v \frac{\partial v}{\partial z} + \frac{1}{\rho} \frac{\partial p}{\partial z} = f \qquad (2)$$

where f represents the effect of any forces acting on the fluid other than pressure forces. f is a force per unit mass of fluid in the z direction and has the dimensions of an acceleration. Like ψ it is temporarily also left undefined but will ultimately be restricted to represent only the effects of viscosity.

Since arteries are distensible and tapered, the cross-sectional area varies with pressure and distance z from the heart:

$$S = S(p, z) \qquad (3)$$

We now assume that the functional form of this equation is algebraic. It would be quite easy to include an explicit dependence of cross-sectional area on time (such as with respiration or during transient responses to vaso-active drugs). A dependence on velocity could also be incorporated but there appears to be no need to do so for the normal range of flow velocities in arteries.

Relations (1) - (3) constitute three equations for the three unknowns v, p and S. With the aid of (3) we can eliminate S as a dependent

variable:

$$\frac{\partial S}{\partial t} = \left(\frac{\partial S}{\partial \rho}\right)_z \frac{\partial \rho}{\partial t}$$

$$\frac{\partial S}{\partial z} = \left(\frac{\partial S}{\partial \rho}\right)_z \frac{\partial \rho}{\partial z} + \left(\frac{\partial S}{\partial z}\right)_\rho$$

Inserting these expressions into (1) we have

$$S \frac{\partial v}{\partial z} + \left(\frac{\partial S}{\partial \rho}\right)_z \frac{\partial \rho}{\partial t} + v\left(\frac{\partial S}{\partial \rho}\right)_z \frac{\partial \rho}{\partial z} + \nu\left(\frac{\partial S}{\partial z}\right)_\rho + \psi = 0 \qquad (4)$$

At this stage we restrict the expressions f and ψ to be algebraic functions of ρ and ν. For such expressions (2) and (4) represent a pair of quasi-linear (the coefficients in the equations depend on the unknowns, but not on their derivatives), first order partial differential equations. To apply the method of characteristics, we first form a linear combination of the equations. With $\lambda = \lambda(\rho, v, z, t)$ as an undetermined multiplier, we multiply (4) by λ and add to (2):

$$\frac{\partial v}{\partial t} + (v + \lambda S)\frac{\partial v}{\partial z} + \lambda\left(\frac{\partial S}{\partial \rho}\right)_z \left[\frac{\partial \rho}{\partial t}\right.$$

$$\left. + \left(\frac{1}{\lambda \rho \left(\frac{\partial S}{\partial \rho}\right)_z} + v\right)\frac{\partial \rho}{\partial z}\right] - f + \lambda v\left(\frac{\partial S}{\partial z}\right)_\rho + \lambda\psi = 0 \qquad (5)$$

For any curve C in the z,t plane, the parametric equations of C can be given in terms of a curve parameter s as

$$z = z(s)$$

and

$$t = t(s)$$

Along C,

$$\left.\frac{dv}{ds}\right|_C = \frac{\partial v}{\partial t}\left.\frac{dt}{ds}\right|_C + \frac{\partial v}{\partial z}\left.\frac{dz}{ds}\right|_C$$

We choose C so that

$$\left.\frac{dt}{ds}\right|_C = 1$$

$$\left.\frac{dz}{ds}\right|_C = v + \lambda S \tag{6}$$

Similarly along another curve C',

$$\left.\frac{dp}{ds}\right|_{C'} = \frac{\partial p}{\partial t}\left.\frac{dt}{ds}\right|_{C'} + \frac{\partial p}{\partial z}\left.\frac{dz}{ds}\right|_{C'}$$

Selecting C' such that

$$\left.\frac{dt}{ds}\right|_{C'} = 1$$

$$\left.\frac{dz}{ds}\right|_{C'} = \frac{1}{\lambda\rho\left(\frac{\partial \rho}{\partial S}\right)_z} + v \tag{7}$$

we can reduce (5) to

$$\left.\frac{dv}{ds}\right|_C + \lambda\left(\frac{\partial \rho}{\partial S}\right)_z \left.\frac{dp}{ds}\right|_{C'} - f + \lambda v\left(\frac{\partial \rho}{\partial z}\right)_S + \lambda\psi = 0 \tag{8}$$

We now attempt to find a λ for which the curves C and C' coincide, i.e., a λ for which expressions (6) and (7) are identical. This requirement is satisfied if

$$\lambda = \pm \frac{c}{S} \tag{9}$$

where c is defined by

$$c = \sqrt{\frac{S}{\rho\left(\frac{\partial S}{\partial p}\right)_s}} \tag{10}$$

Since $\frac{dt}{ds} = 1$ we have $\frac{dz}{ds} = \frac{dz}{dt}$ and the so-called characteristic directions, or base characteristics, are given by

$$I^{\pm} \qquad \frac{dz}{dt} = v \pm c \tag{11}$$

Inserting (9) and (10) into (8), we obtain the compatibility equations, or characteristic equations:

$$II^{\pm}: \quad dv \pm \frac{dp}{\rho c} = \left[f \mp \frac{vc}{S}\left(\frac{\partial S}{\partial z}\right)_p \pm \frac{c}{S}\psi\right] dt \tag{12}$$

The interpretation of these four equations is that II^+ (equation (12) with the upper signs) is meant to hold on the curve specified by I^+ (equation (11) with upper sign), and correspondingly II^- on I^-.

From equation (11) or from Appendix A, the meaning of c becomes clear: c is the local wave speed, the velocity at which small disturbances are propagated relative to the fluid at rest. Since the solutions for the base characteristics (11) are real the original system of equations (2) and (4) is hyperbolic.

The solution to the problem can be initiated once the functional form of $S = S(p, z)$ is known. To obtain $S(p, z)$ we could postulate a mathematical model for the mechanical behavior of the arterial wall and then derive the area-pressure relation and the corresponding wave speed expression. However, conventional models for the mechanical behavior of the wall often predict a decrease in wave speed with pressure[14] which, as can be noted from Figure 2, is in contradiction with experimental evidence. This difficulty is automatically avoided if we describe the mechanical behavior of the vessel in terms of the experimentally observed wave speed as a function of pressure and location[23]. The wave speed enters quite naturally into the characteristic equations (11) and (12) and the area-pressure relation can be obtained by integrating equation (10). Finally, by specifying f and ψ together with appropriate initial and boundary conditions we can arrive at numerical solutions to the problem on hand by integrating equations (11) and (12).

B. CROSS-SECTIONAL AREA AS A FUNCTION OF PRESSURE AND DISTANCE

Measurements in the thoracic aortae of anesthetized dogs[23] suggest that the wave speed changes with intraluminal pressure may be approximated by a linear function over the normal physiological range of pressure. Figure 2 displays typical results of wave speed measurements in which the normal range of pressure was extended by appropriate occlusions of the aorta. A quadratic function would approximate the curve in Figure 2 more closely and was in fact used for a number of computer runs. However the results did not differ significantly from the cases where a linear relationship was employed, and since the amount of computing time required was perhaps 50% greater due to the much more complicated expression for the cross-sectional area corresponding to the quadratic function, we consistently used a linear pressure dependence of the wave speed.

Assuming in addition that the wave speed varies linearly with distance along the aorta[7], we have

$$c(p,z) = (c_0 + c_1 p)(1 + nz) \tag{13}$$

By substituting (13) into (10) and integrating the resulting differential equation we find

$$S(p,z) = A(z)\, e^{\frac{p - p_0}{\rho c(p,z)\, c(p_0,z)}} \tag{14}$$

where p_0 is a reference pressure and $A(z)$ is an as yet unspecified function which defines the cross-sectional area of the blood vessel at the pressure p_0 as a function of the distance z from the heart: $A(z) = S(p_0,z)$.

Patel[24] has taken measurements on the major arteries of 11 moderately large dogs with an average weight of 22.1 kg. These measurements are considered as representative diameters at a given pressure p_0, say p_0 = 100 mm Hg. Assuming a wall thickness-to-radius value of 0.08 in the aorta and one of 0.25 in the external iliac artery, we converted his data to internal diameters corresponding to the pressure p_0 as plotted in Figure 4. However we are interested in larger animals (the ultimate application is to man), and we have therefore scaled these converted data upward to correspond to a 30 kg dog whose bifurcation was somewhat arbitrarily placed at 54 cm. This was done by increasing the internal diameters obtained from Patel's data by a factor of $\sqrt{\frac{30}{22.1}} = 1.165$ assuming that the ratio of weights is the same as the ratio of lumen areas. The new diameters are also shown in Figure 4.

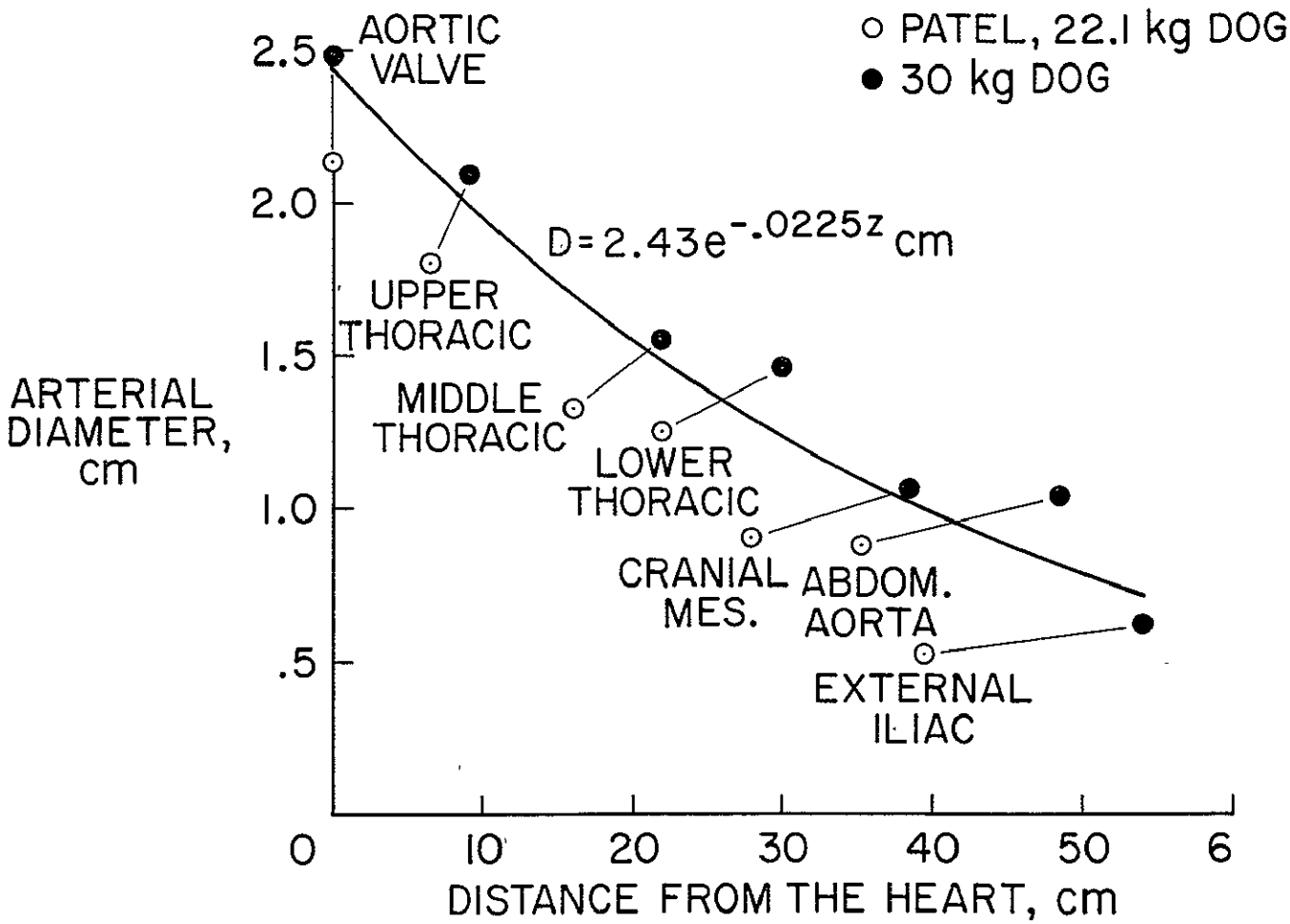

Figure 4. Internal diameter data for the dog aorta according to Patel.[24] The solid curve approximates the diameter variation with distance for the hypothetical 30 kg dog.

An exponentially decreasing diameter appears to be a reasonable approximation for the aorta according to the data published in the literature and given in Figure 4 (see also Ref. 25). We therefore could write for $A(z)$:

$$A(z) = S(p_o, z) = S_o(p_o)\, e^{-\beta z} \tag{15}$$

where $S_o(p_o)$ is the cross-sectional area at the root of the aorta at the pressure p_o. With (15) we have

$$S(p,z) = S_o(p_o)\, e^{-\beta z + \frac{p - p_o}{\rho c(p,z)\, c(p_o,z)}} \tag{16}$$

and thus a complete definition of the geometry and mechanical behavior of the aorta.

C. THE FRICTION EXPRESSION

The expression for the force parameter f in equations (2) and (12) will now be restricted specifically to one representing the effects of blood viscosity. As stated before, f must be an algebraic function which unfortunately rules out a more general modeling of the viscous friction including its proper phase relationship to the pressure. To obtain an approximate expression, we first consider a segment of fluid of unit mass in the aorta. For moderately tapered vessels this segment can, in a first approximation, be considered as a short cylinder of radius R and length Δz, where

$$\Delta z = \frac{1}{\rho S} \tag{17}$$

Denoting by τ_w the frictional stress on the arterial wall, we have

$$f = -(2\pi R \Delta z)\tau_w$$

or

$$f = -2\sqrt{\pi S}\,\Delta z\,\tau_w$$

The sign is negative because the flow is retarded by viscosity. The frictional stress τ_w is usually expressed as

$$\tau_w = c_f \cdot \tfrac{1}{2}\rho v^2 \tag{18}$$

with c_f called the friction coefficient. With this expression we can write

$$f = -c_f\sqrt{\frac{\pi}{S}}\,v^2 \tag{19}$$

We now restrict ourselves temporarily to steady flow and consider three cases:

1. Inviscid Flow

   Here $c_f = 0$ and

   $$f_{\text{inviscid}} = 0 \tag{20}$$

2. Laminar Flow

   From the well-known result for Poiseuille flow we conclude

   $$c_f = \frac{16}{R_e}$$

where R_e is the Reynolds number based on length, $R_e = \frac{\rho v D}{\mu}$.

Hence

$$c_f = \frac{8\mu}{\rho v R} = \frac{8\mu}{\rho v}\sqrt{\frac{\pi}{S}}$$

and

$$f_{\text{laminar}} = -8\pi \frac{\mu}{\rho}\frac{v}{S} \tag{21}$$

3. Turbulent Flow

According to the Blasius formula for steady turbulent flow in a pipe

$$c_f = .0791 \frac{1}{R_e^{1/4}} = .07675\left(\frac{\mu}{\rho v\sqrt{S}}\right)^{1/4}$$

and therefore

$$f_{\text{turbulent}} = -.1360\left(\frac{\mu}{\rho}\right)^{1/4} \frac{|v|^{7/4}}{S^{5/8}} \operatorname{sgn} v \tag{22}$$

where $\operatorname{sgn} v$ guarantees that f acts in the direction opposite to that of the velocity.

The friction expressions (21) and (22) are in a strict sense only vali for steady flow but are now assumed to be applicable also for nonsteady flow.

D. THE OUTFLOW EXPRESSION ψ

The outflow of blood from the aorta through discrete side branches and bifurcations is modeled by a continuously distributed leakage or seepage defined by the outflow function ψ. We use the data of Sapirstein[26] on regiona blood flow measurements to specify how much blood, in per cent of the total cardiac output, is lost per unit time through the major arteries (identified in Figures 4 and 5) emanating from the aorta. The results are summarized in Table 1 and Figure 6. It appears that these data are reasonably well

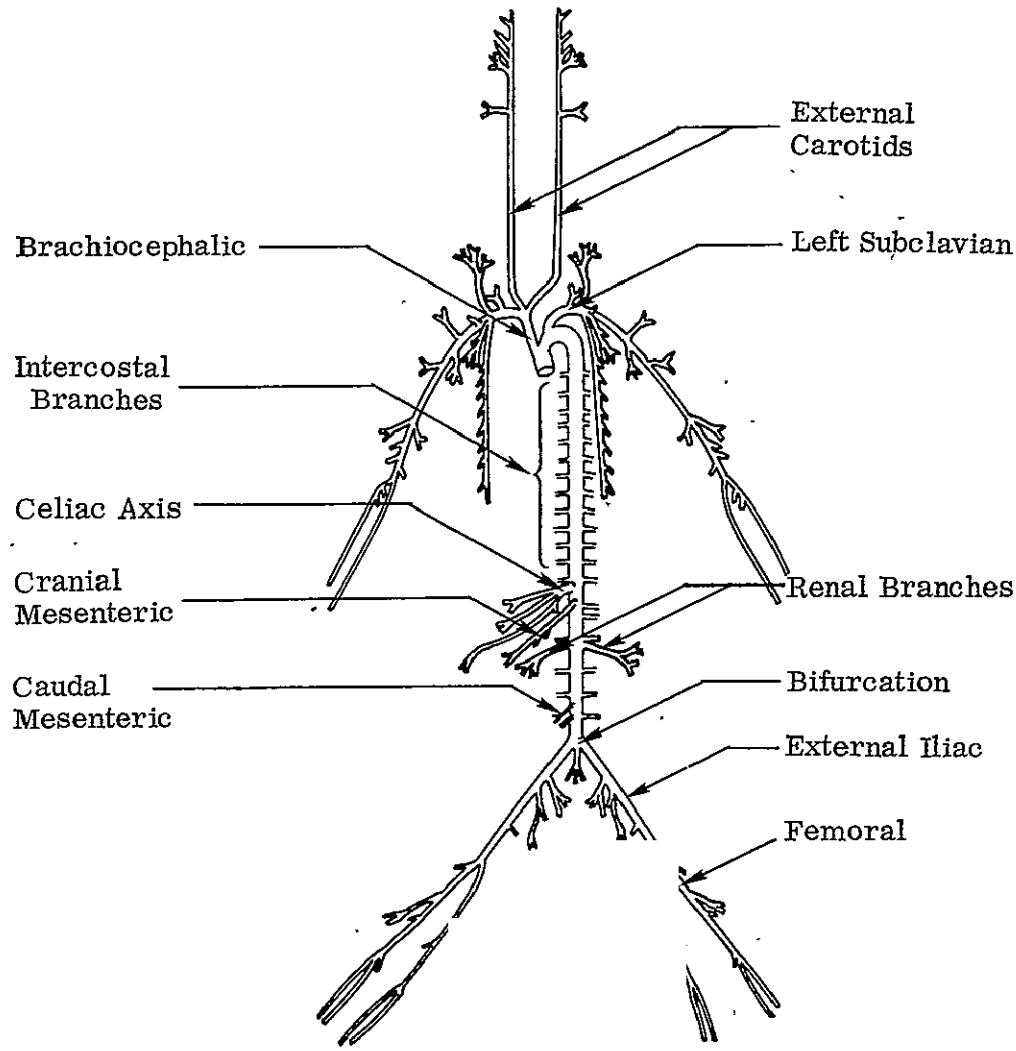

Figure 5. The major components of the canine arterial tree, copied from Reference 27.

TABLE 1

Distribution of Blood through the Major Arterial Branches of the Aorta According to Sapirstein[26]

Branch	Distance from Aortic Valve, cm	Fraction of Cardiac Output to Branch	Fraction of Cardiac Output Remaining
Aortic Valve	0		1.00
Coronary Arteries	0^+	.05	.95
Brachiocephalic	3	.17	.78
Left Subclavian	4	.02	.76
Intercostals, Bronchials, Diaphagmatic	distributed	.11	.65
Celiac Axis	38.5	.08	.57
Cranial Mesenteric	40.5	.18	.39
Right Renal	42	.06	.33
Left Renal	44	.06	.27
Caudal Mesenteric	51	.09	.18
Bifurcation	54	.09	.09

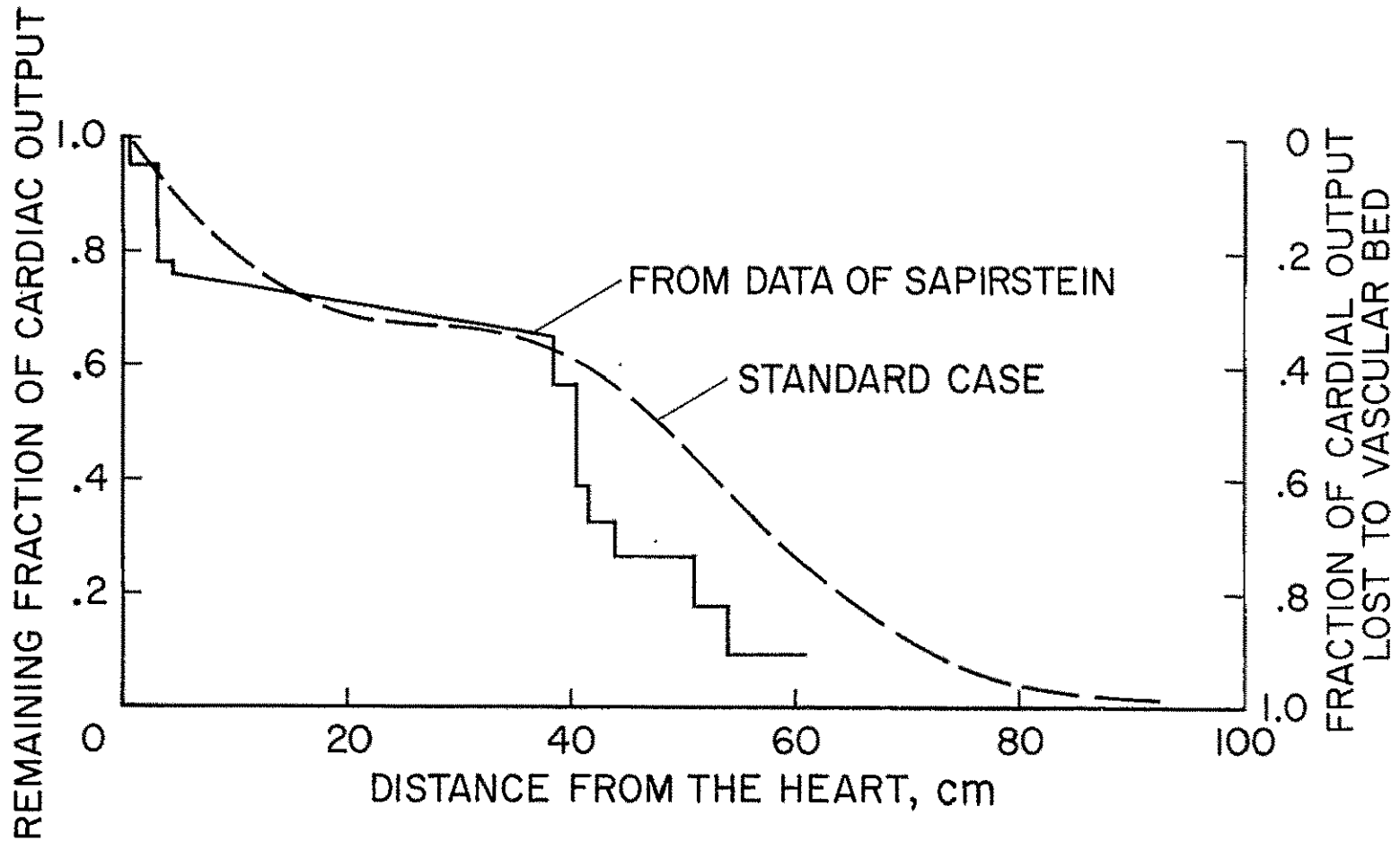

Figure 6. Average distribution of blood plotted from the data of Table 1. The dashed curve is the result of integrating the volume flow rates for the Standard Case (Chapter III, Section A) over a cardiac cycle.

approximated by an outflow function which stipulates that the local leakage rate is proportional to the difference $p - p_c$ between the local arterial pressure p and the capillary pressure p_c and which exhibits the gross features of the regional blood flow pattern. Among the various functions considered, the most realistic outflow distribution was obtained with

$$\psi(p,z) = \begin{cases} \alpha (p-p_c)\left(1.1 + \cos \frac{5\pi}{2} \frac{z}{z^*}\right) & \text{for } z \leq z^* \\ \alpha (p-p_c)(1.1) e^{-.08 (z-z^*)} & \text{for } z \geq z^* \end{cases} \tag{25}$$

in which z^* represents the distance from the aortic valve to the general region of the femoral artery and $\frac{1}{\alpha}$ is a measure of the outflow resistance. For the cases considered in this analysis z^* was taken to be 70 cm.

The seepage distribution defined by (25) is shown in Figure 7. Near the heart the outflow is large to simulate the blood flow into the brachiocephalic and left subclavian arteries at the top of the aortic arch. The seepage rate is low in the thoracic region, and again large near $z = 50$ cm to approximate the outflow to the abdominal organs and into the bifurcation. The exponential decrease in ψ for $z \geq z^*$ accounts for the diminishing outflow into the arteries distal to the femoral region. Since the pressure in the capillaries is of the order of 25 mm Hg we have chosen this value for p_c in all our computations. The parameter α was generally chosen such that the diastolic pressure at the heart was of the order of 80 mm Hg.

A typical outflow distribution obtained with this function is shown in Figure 6 (Standard Case). It can be seen that the gross behavior of the empirical data is mimicked by the computed results but the agreement is not altogether satisfactory. This indicates the need for a more appropriate accounting

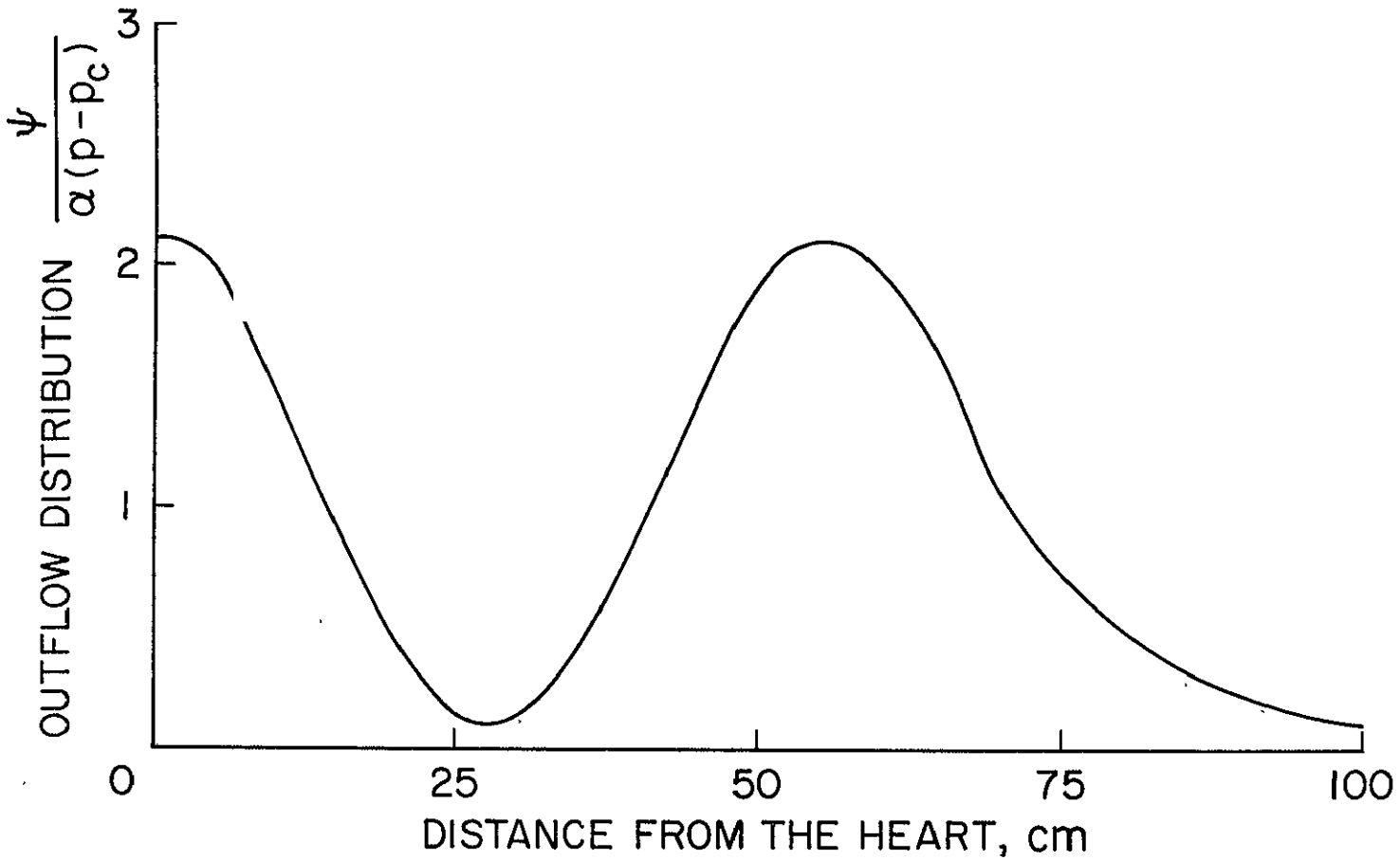

Figure 7. Outflow distribution of blood through the arterial wall as defined by equation (25).

for outflow, although perhaps this effort would be better expended on a model including discrete branches rather than on the purely continuous model considered here.

This procedure for modeling the effect of branches from the aorta is admittedly crude. However, until more accurate information is available on the true regional flow distribution and its dependence on pressure, approaches such as the one taken here are justifiable.

E. BOUNDARY CONDITIONS

The boundary conditions which must be specified at the proximal and distal ends of the artery of interest can each take different forms.

1. Proximal Boundary Condition

There were two types of boundary conditions utilized. The first was to prescribe the variation of the pressure at the aortic valve as a function of time:

$$p(0,t) = p_0(t)$$

Although this choice seemed a logical one in view of the abundance of actual pressure recordings taken near the aortic valve, it did not give very satisfactory results and was abandoned. The principal reason was that with a representative pressure recording as the proximal boundary condition we did not predict the experimentally observed flow profiles at the same location. There were often moderate positive and negative velocities during the latter two-thirds of the cardiac cycle, when the aortic valve is normally closed. (At this stage, we do not wish to deal with incompetent valves.) This finding reaffirms that the pressure variation just outside the heart as well as elsewhere in the arterial tree is related in a complex manner to the conditions in the entire circulatory system. If the true pressure fluctuation were used in conjunction with the actual

geometric and elastic parameters, heart rate and cardiac output, outflow function, etc., the corresponding flow pulses should be in close agreement with those observed experimentally provided we have a valid mathematical model for the mechanical behavior of the system. We infer from this that we either do not yet have a sufficiently accurate description of the mechanical properties of the circulatory system or that relatively small changes in the pressure pulse produce dramatic changes in the flow pulse and that therefore the pressure variation with time must be known to a high degree of accuracy.

Much more satisfactory results were obtained by specifying the volume rate of flow of blood from the left ventricle into the aorta:

$$q(0,t) = q_0(t)$$

The flow rate is an equally natural choice as a boundary condition. It is related directly to cardiac output and pulse rate both of which can readily be measured and are physically important parameters. Since q is equal to the product of spatial mean flow velocity and cross-sectional area, the boundary condition now takes the form

$$v(0,t) = \frac{q_0(t)}{S(p(0,t),0)} \tag{26}$$

In this analysis we shall use the curve shown in Figure 8[28] as representative of the cardiac ejection $q_0(t)$. Since p is not known apriori, iteration is necessary to satisfy the boundary condition (26) as stated.

2. Distal Boundary Condition

As in the case of the proximal boundary we considered two types of conditions at $x = L$. Recognizing that the pulsatile component of blood flow diminishes in the smaller arteries and arterioles and essentially vanishes in

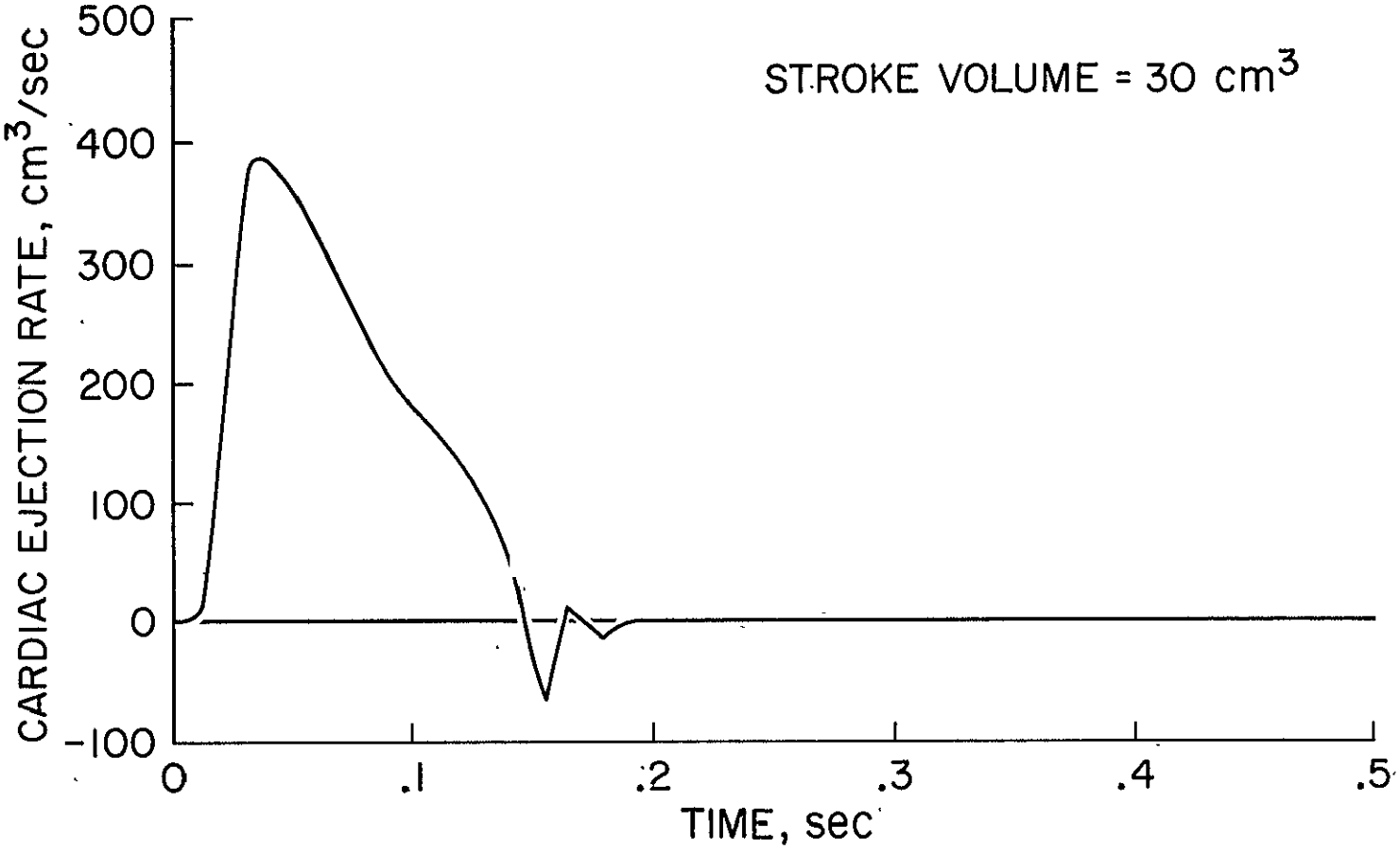

Figure 8. Cardiac ejection rate as a function of time. Adapted from Reference 28 by scaling to yield a net stroke volume of 30 cm^3. As heart rate we have assumed 120 beats per minute.

most precapillaries and capillaries, we assume that the terminal pressure is constant:

$$p(L,t) = p_L \tag{27}$$

This is a reasonable approximation only if the diameter at the distal end of the artery is sufficiently small.

The second type of terminal boundary condition considered is based on the concept of peripheral resistance, which is defined as the ratio of driving pressure Δp across the capillary bed to volume flow rate through this bed. If we take the pressure at the venous end of the capillary as p_c the driving pressure is $p(L,t) - p_c$. The peripheral resistance R_L can therefore be expressed as

$$R_L = \frac{p(L,t) - p_c}{q(L,t)} \tag{28}$$

which allows us to write the boundary condition as

$$v(L,t) = \frac{p(L,t) - p_c}{R_L S(p(L,t), L)} \tag{29}$$

The concept of flow rate being proportional to pressure has been widely used in the analysis of blood flow although it seems too simple to be very realistic. Small changes in R_L will usually cause relatively large changes in the pressure and flow along the artery. We decided to choose that value for R_L which produces a representative mean pressure at the heart.

The validity of the peripheral resistance idea will be tested by determining the relation between the actual driving pressures and flow rates for

specific distances from the heart when a constant end pressure is stipulated as the boundary condition (equation 27).

F. INITIAL CONDITIONS

Although initial conditions are of minor interest here since we are mainly concerned with the steady state solutions, they are necessary to complete the mathematical formulation of the problem. From an engineering point of view it might be logical to specify that the velocity is initially zero and that the pressure is at a nominally low level, say 25 mm Hg. Then by initiating the pulsatile ejection of blood from the heart one can study the "starting process." This could possibly be of some interest in studying the transient response of the cardiovascular system to normal heart beats following a period of cardiac arrest.

Similarly, one might want to study the response to sudden changes in the system parameters. Then the initial conditions for that problem would be the steady state conditions of the unperturbed circulation at the time instant of the occurrence of the change.

As a rule the initial conditions were usually chosen as close as possible to the anticipated steady state conditions in order to minimize computer time. In general we selected as the initial pressure and flow velocity patterns those of the Standard Case (see section III A) at the end of diastole. Of course, the effect of any initial conditions is ultimately damped out and does not influence the steady state solutions.

III. TYPICAL RESULTS

For the most part the IBM 360 computer was employed, although some final runs were made on the Univac 1108. The so-called method of specified time intervals was employed[14, 29]. The ordinary differential equations (11) and (12) were converted into finite difference equations. Provisions for iteration were included, but with computing intervals of $\Delta z = 2$ cm, $\Delta t = .001$ sec, they proved unnecessary. With this choice, the differences in the computed results were generally less than 1 mm Hg in pressure and 2 cm/sec in velocity when compared with results obtained with much smaller computing intervals. An exception was the case of aortic insufficiency (see section IV K) in which the large and rapid changes in pressure and flow required intervals of $\Delta z = 1$ cm and $\Delta t = .0001$ sec to maintain the desired accuracy.

Unless indicated otherwise the following parameter values were used throughout the study:

$\rho = 1.06$ grams/cm^3

$\mu = .049$ poise

$p_o = 100$ mm Hg $= 1.33 \times 10^5$ dynes/cm^2

$p_L = 25$ mm Hg $= 3.3 \times 10^4$ dynes/cm^2

$L = 150$ cm

The units of pressure used in performing the calculations were usually dynes/cm^2. However conversion to the more popular millimeters of mercury was generally made for presentation of the results.

A. STANDARD CASE

To establish a basis of comparison in studying the effects of certain parameters, we defined a Standard Case for the aorta and its continuation beyond

the saphenous artery in an anesthetized 30 kg dog. The following physical and geometric features were assumed.

1. Wave Speed:

$$c(p,z) = (97 + 2.03p)(1 + .02z) \quad \text{cm/sec} \tag{30}$$

where p is the pressure in mm Hg and z is the distance from the aortic valve in cm. This dependence of the wave speed on pressure and distance from the heart approximates the patterns given in the literature[7] and observed in our laboratory[23]. The experimental data shown in Figure 2 represent the wave speed as a function of pressure in the canine thoracic aorta at about 25 cm from the aortic valve.

2. Cross-Sectional Area:

Consistent with Equation (16) and the data plotted in Figure 4, we have taken

$$S(p,z) = \begin{cases} 4.63\, e^{-.045z + \frac{p-p_o}{\rho c(p,z)c(p_o,z)}} & \text{for } z \le 54 \\ 0.41\, e^{-.089(z-54) + \frac{p-p_o}{\rho c(p,z)c(p_o,z)}} & \text{for } z \ge 54 \end{cases} \tag{31}$$

The available anatomical data suggest that we choose for S slightly different exponential functions depending on $z \le 54$ cm or $z \ge 54$ cm. For $z \le 54$ cm we used the data shown in Figure 4, while for $z \ge 54$ cm we arranged it such that we have a terminal diameter of 100 microns when $L = 150$ cm. Both functions assume the same value at $z = 54$ cm. Originally a terminal diameter of 10 microns was used which approximates more closely the capillary size but requires

a larger value of L for the same function $S(p,z)$ and thus more extensive computation. However, the results did not differ noticeably and in order to minimize computer time we selected as terminal diameter 100 microns.

3. Heart Parameters and Outflow Expression:

For the Standard Case the pulse rate is 120 beats per minute and the net stroke volume 30 cm^3. This means that the cardiac output of the hypothetical 30 kg dog is 3.6 liters or 0.12 liters per minute per kg mass[30]. The value of α appearing in Equation (25) for the outflow function $\Psi(p,z)$ was determined to produce a diastolic pressure of 80 mm Hg. This was achieved for $\alpha = 9.29 \times 10^{-3}$ $cm^3/sec/mm\,Hg$.

Pressure and flow velocity profiles for the Standard Case are displayed in Figure 9 for six different locations beginning with $z = 0$ (the aortic valve) and continuing to $z = 100$ cm. Figure 10 shows the temporal mean values for pressure and flow velocity as a function of z together with the diameter at diastolic pressure.

The temporal pressure profiles plotted in Figure 11 for various distances from the aortic valve indicate the familiar gradual change in shape as the pulse wave propagates in the aorta. We clearly note the incisura in the pressure pattern at $z = 0$. Its sharpness however begins to disappear with increasing distance. In the course of our numerical studies we observed that the short interval of backflow or negative flow shown in Figure 8 was not necessary to produce the incisura. Abrupt decreases in the cardiac ejection rate can cause that feature even when there is no flow reversal. For the Standard Case no backflow was present beyond 30 cm. As the pulse wave propagates, the wave front steepens markedly with distance. The pulse pressure grows fastest

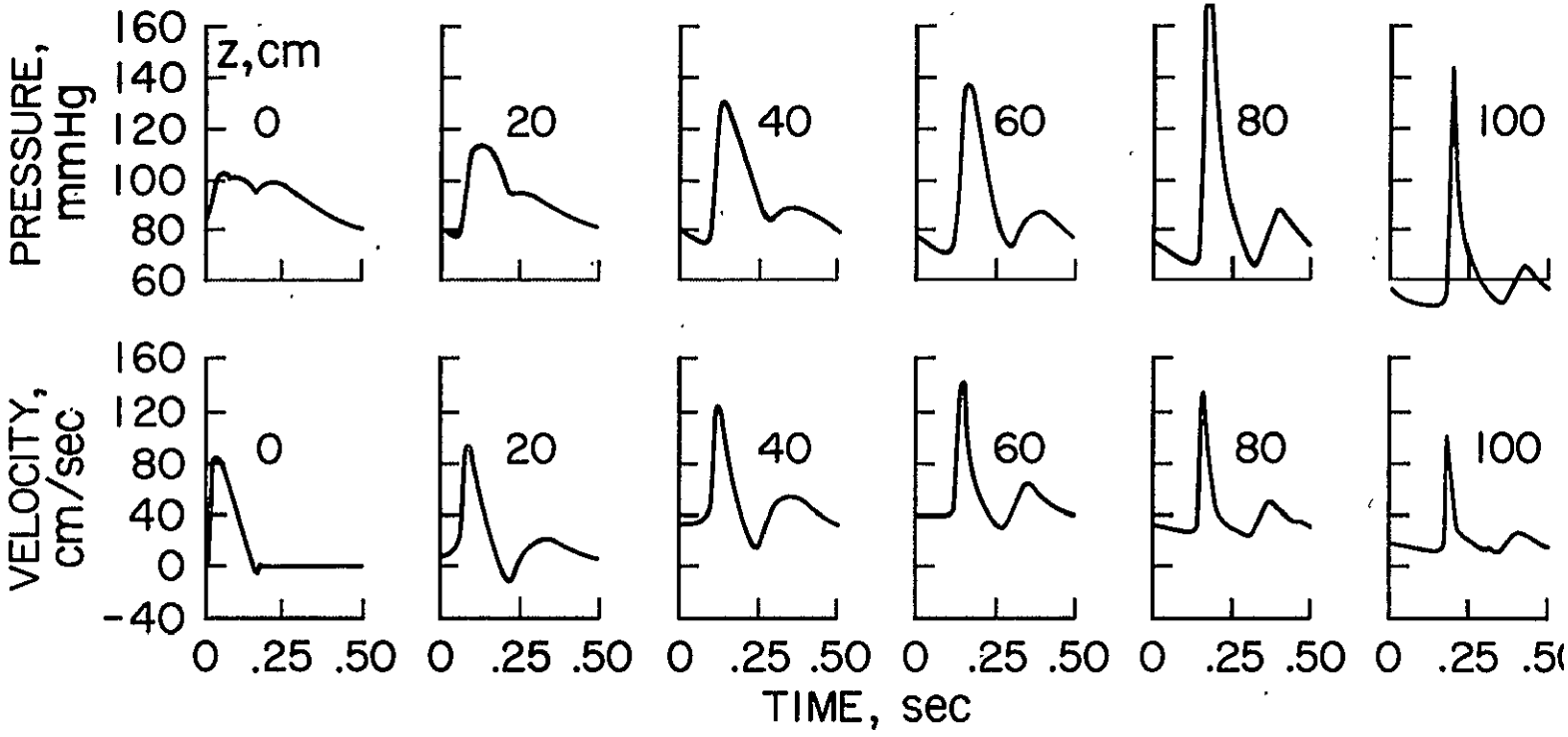

Figure 9. Pressure and flow velocity profiles at six different locations along the artery for the Standard Case. z=0 is the location of the aortic valve. Note steepening of the wave front and peaking of the pulse with propagation. Flow patterns computed at intermediate stations show that flow reversal persists to z=30 cm in this case.

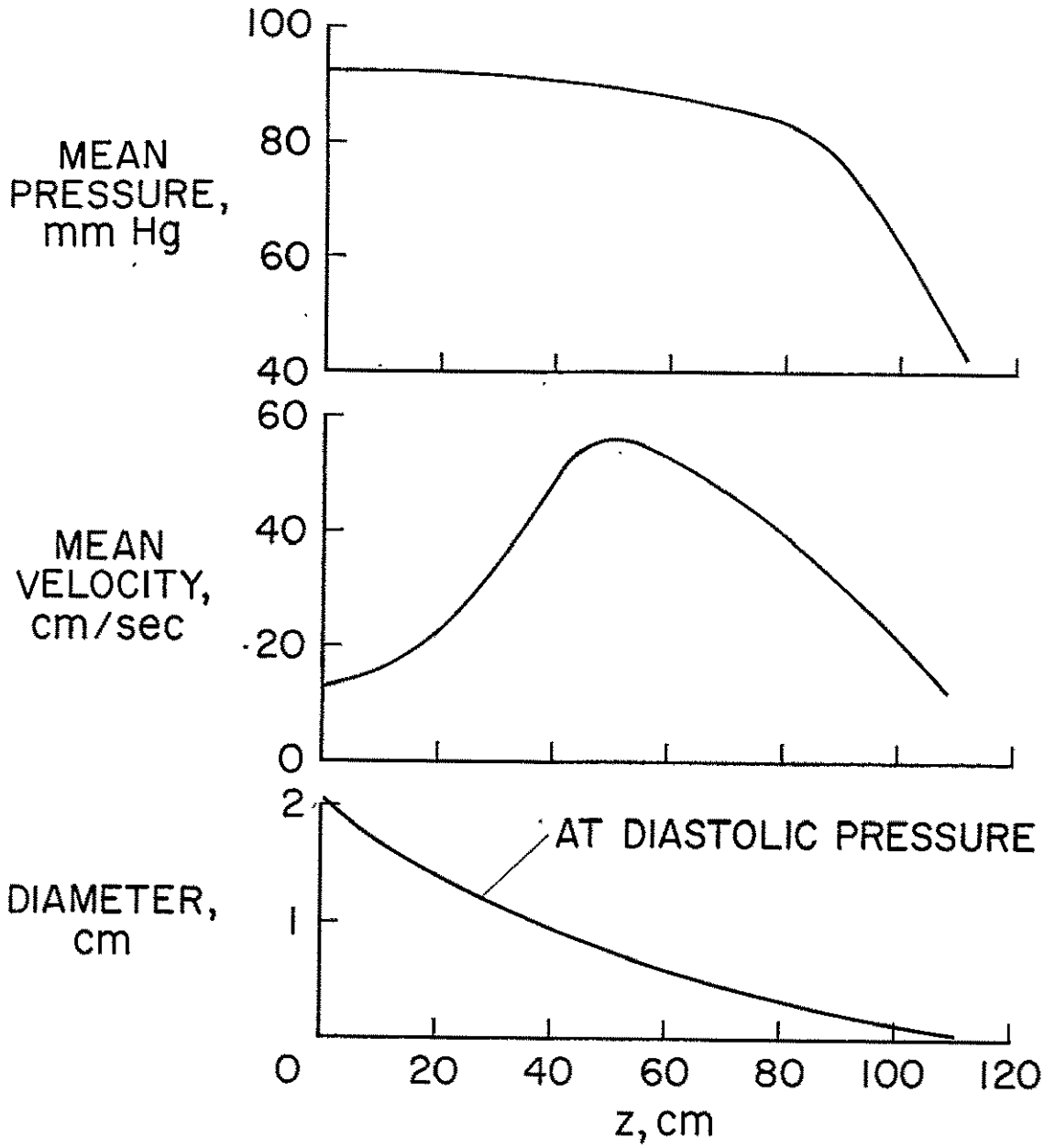

Figure 10. Pressure and flow velocity averaged over the cardiac cycle and plotted as a function of distance from the heart for the Standard Case. Also internal diameter at diastolic pressure.

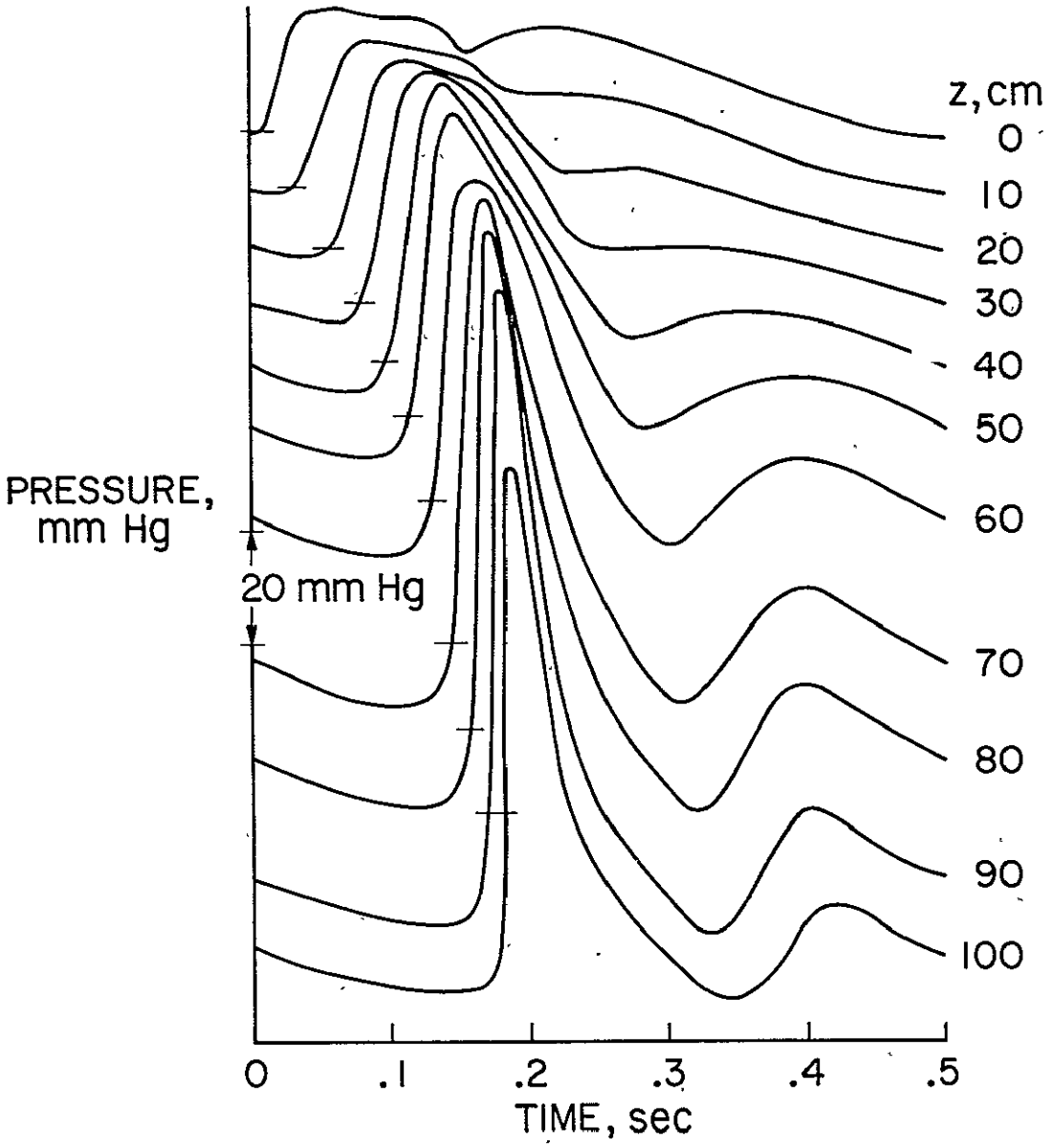

Figure 11. Pressure - time profiles for the Standard Case at different distance from the aortic valve, illustrating the evolution of the natural pressure pulse. The pressure corresponding to 80 mm Hg is denoted at the beginning of each profile.

near $z = 70$ cm and reaches a maximum near $z = 90$ cm.

The dicrotic wave first becomes noticeable at $z = 40$ cm and is fully developed past $z = 60$ cm. It will be indicated later that the dicrotic wave appears to be the result of reflection phenomena.

By integrating the product of area and velocity at each station over a cardiac cycle, we obtain the volume flow at each point. The corresponding results for the Standard Case are given in Figure 6 for comparison with the empirical data of Ref. 26.

The growth of pulse pressure with increasing distance from the heart correlates well with in vivo observations. That the diastolic pressure decreases with distance has also been noted in experimental studies[2]. However the variation of the mean flow velocity with distance from the aortic valve as predicted by this analysis has not been mentioned in the literature. As a matter of fact the graphs in Ref. 2 seem to suggest that the mean velocity decreases monotonically with distance. This could be interpreted as an indication of a deficiency in our present model, although the equipment necessary for reliable and accurate measurements of flow velocity in blood vessels has not been generally available.

B. EFFECT OF DIAMETER

Figures 12 and 13 show the effects of a general reduction of the mean diameter of the aorta by 20% which amounts to a decrease in cross-sectional area by 36%. All other parameter values are the same as in the Standard Case. A decrease in the cross-sectional area apparently causes higher flow velocities and pulse pressures. The velocity is higher because the same amount of blood must flow through the smaller aorta (the stroke volume remains 30 cm^3). The pulse pressure is increased as a consequence of lowering the distensibility of

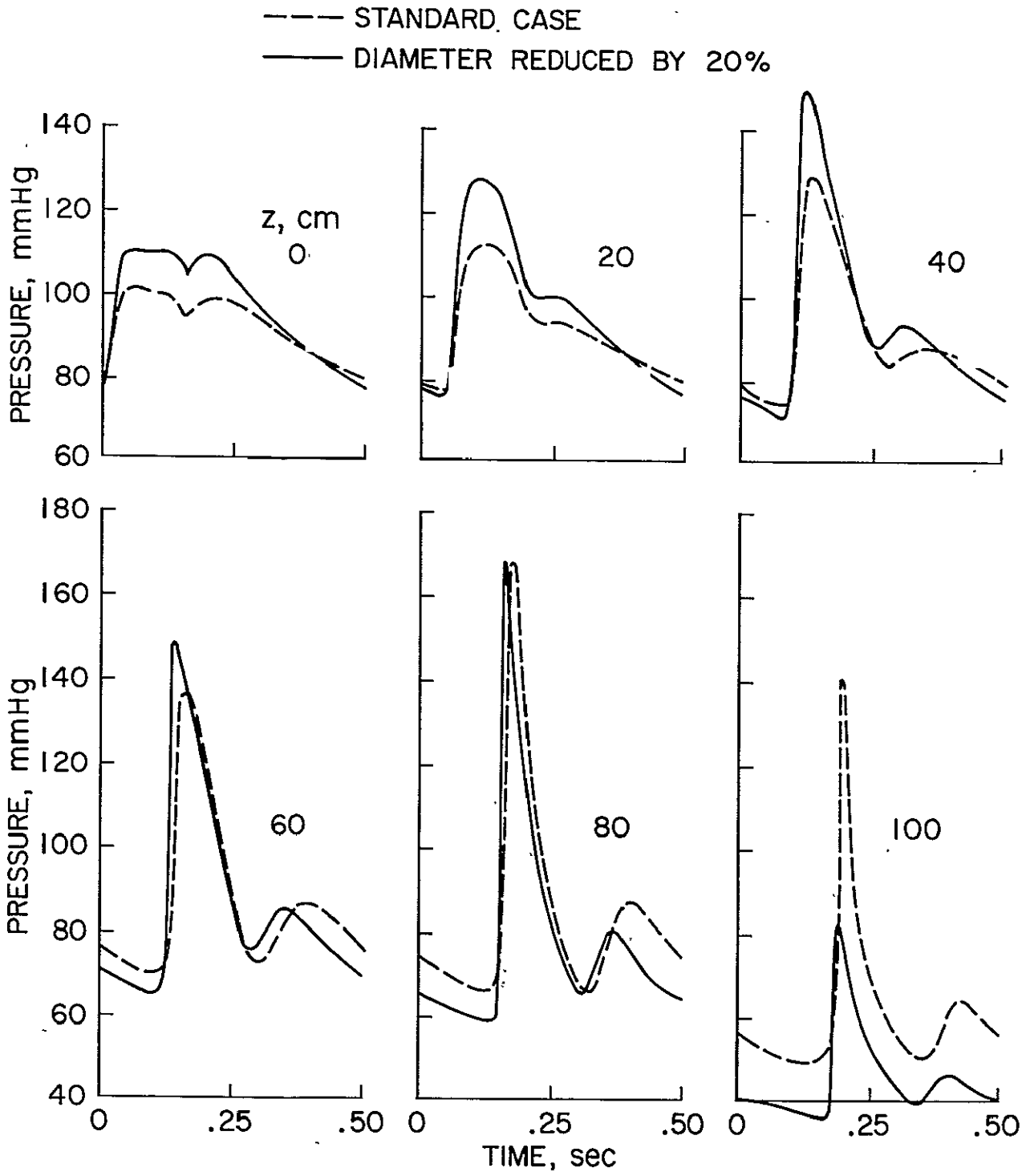

Figure 12. Pressure - time profiles at various distances from the heart for reduced arterial diameters, with other cardiovascular parameters unchanged from the Standard Case.

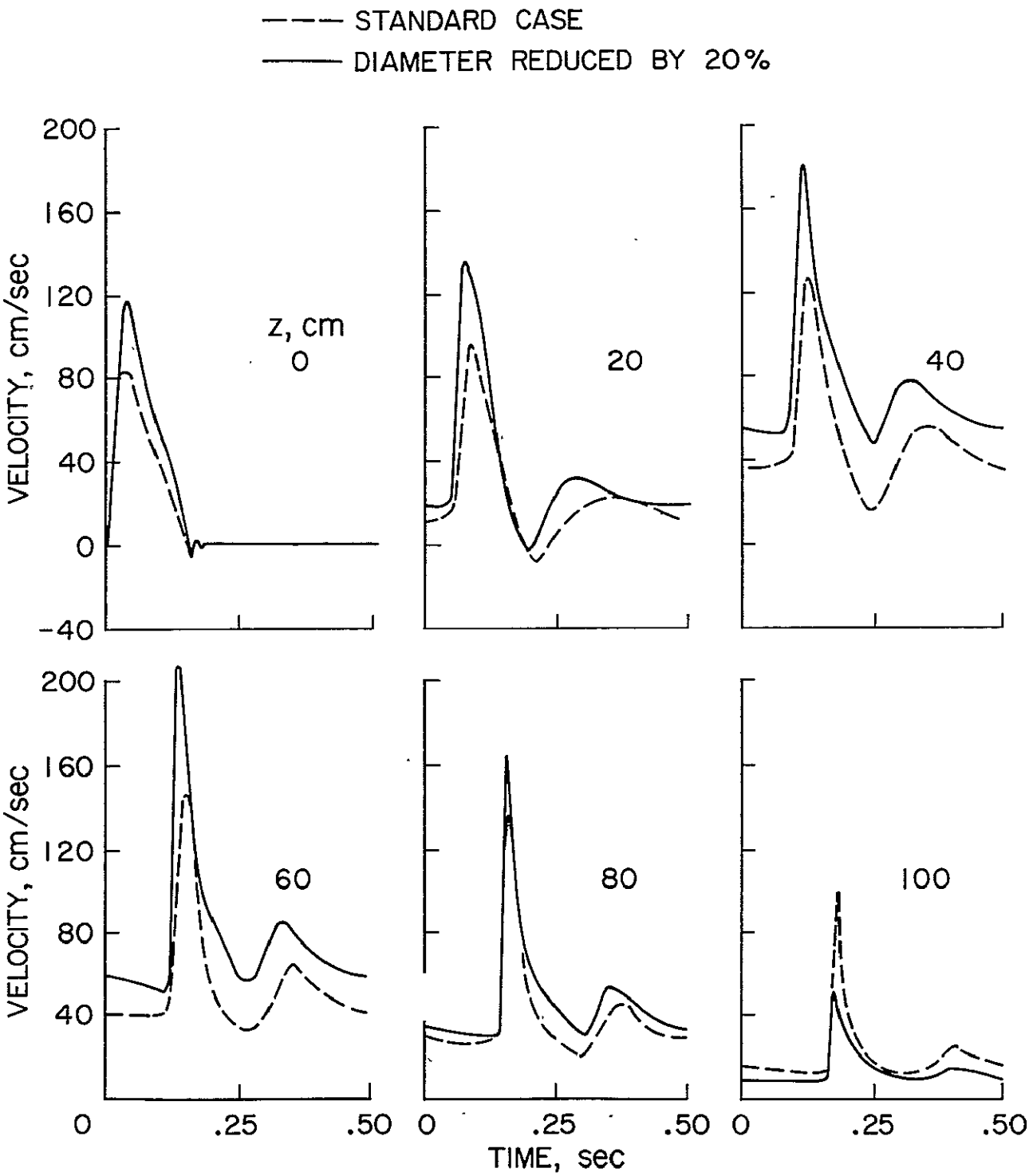

Figure 13. Velocity - time profiles at various distances from the heart for reduced arterial diameters, with other cardiovascular parameters unchanged from the Standard Case.

the artery by reducing the cross-sectional area. With ρ and $c(p, z)$ unchanged, a 36% decrease in S means a decrease in the distensibility $\left(\frac{\partial S}{\partial p}\right)_z$ by the same percentage according to Equation (10). If the dicrotic wave is a manifestation of reflections from the distal end of the arterial tree, the overall reduction in diameter should lead to a dicrotic wave which is more distinct at closer distances from the heart than in the Standard Case. Figures 12 and 13 seem to confirm this. Also, as z increases the diastolic pressure assumes lower values than in the Standard Case, which appears to be due to the larger outflow from the proximal aorta due to the higher pressures during systole. The higher pressures also lead to higher average wave speeds which in turn causes the pressure peaks to occur earlier in time.

C. EFFECT OF WAVE SPEED INCREASE

It is known that the wave speed in arteries increases with age[31] and possibly also as a result of arteriosclerosis. We have therefore examined the effects of a general increase in wave speed by 40% which, according to the Moens-Korteweg equation (see Appendix A, equation 4A), is equivalent to a doubling of the elastic modulus of the vessel wall. Since any increase in wave speed amounts to a reduction of the distensibility we expect the pressure and flow pulses to exhibit similar changes as in the case of a general reduction in the diameter. Indeed, the results shown in Figures 14 and 15 confirm this. We note again a higher systolic pressure and a steeper wave front. The pressure peaks and valleys occur much earlier due to the increase in wave speed. However the flow pulse is not as strongly affected by a 40% increase in wave speed which amounts to a lowering of the distensibility by 96%, as it is by a decrease in the distensibility by 36% through a reduction in the cross-sectional area without a change in wave speed. The higher wave speed also appears to induce what could be

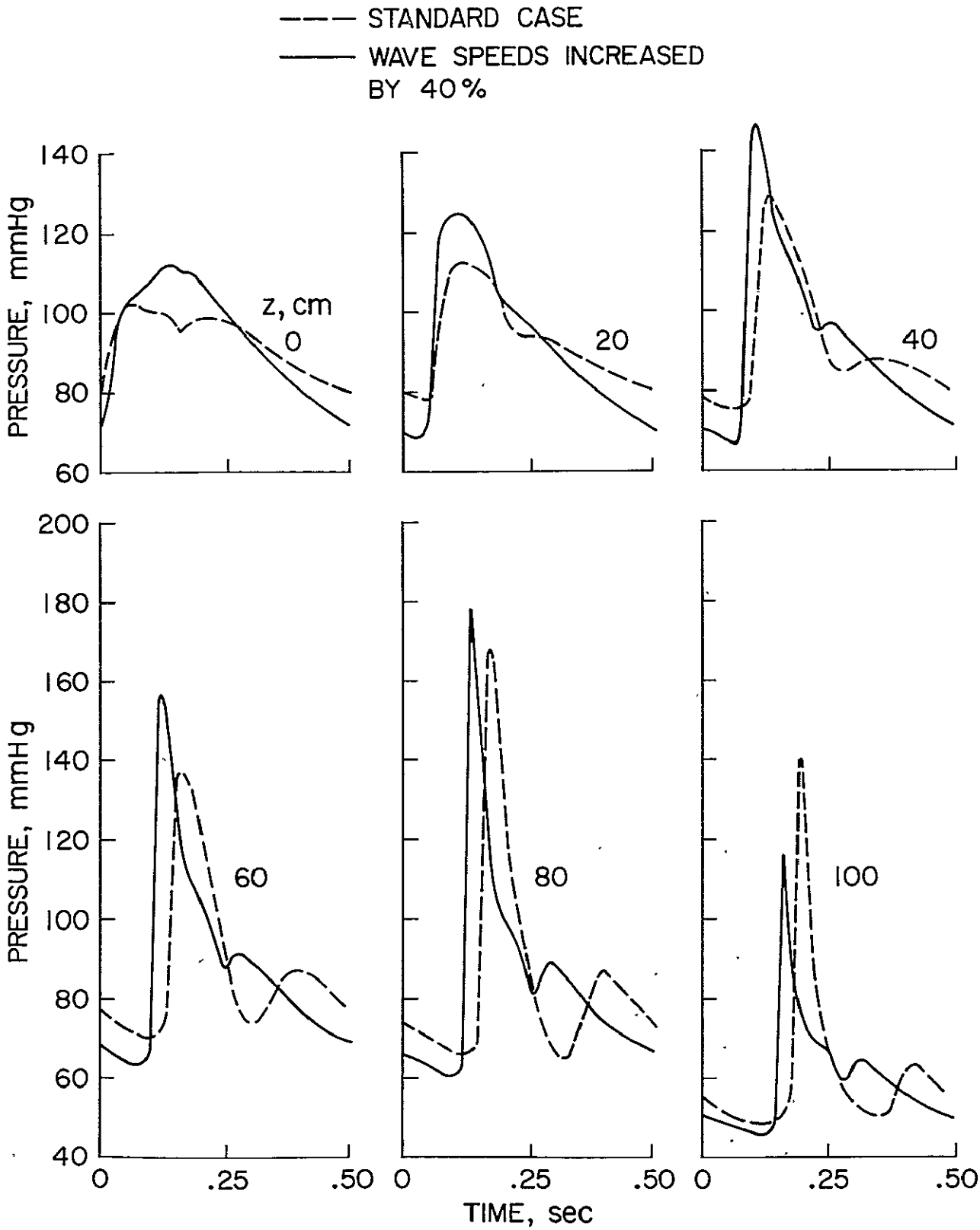

Figure 14. Pressure-time profiles for wave speeds 40% higher than with the Standard Case, but with all other cardiovascular parameters unaltered. As expected, the pressure peaks and valleys develop earlier in time for the higher wave speeds.

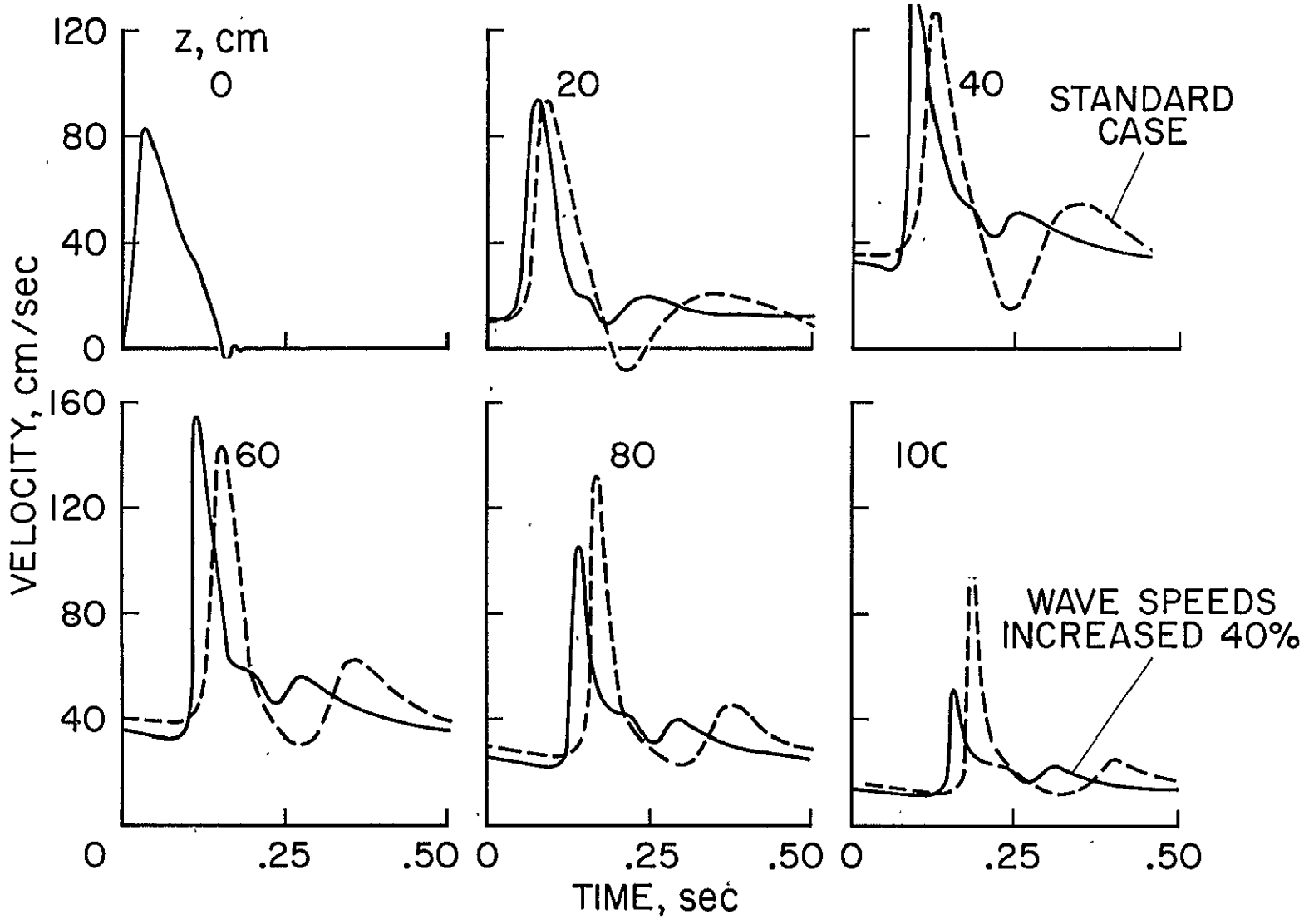

ure 15. Velocity – time profiles for wave speeds 40% higher than with the Standard Case, but with all other cardiovascular parameters unaltered. With higher wave speeds or stiffer vessels the phenomenon of flow reversal is increasingly restricted to shorter distances from the heart.

interpreted as the onset of a second dicrotic wave at the larger distances from the heart.

D. EFFECT OF PULSE RATE

Figures 16 and 17 display the effects of changing the heart rate from the standard value of 120 to 180 and 60 beats per minute. The systolic interval, i.e., the ejection time, was left unchanged and the stroke volume was also held constant. Therefore the cardiac output was changed by factors of 3/2 and 1/2 respectively. Since physiologic responses will cause changes in the outflow pattern when the cardiac output is altered to this degree, the outflow constant α was changed by the same factor in each case. Thus the pulse rate of 180 per minute is taken to simulate exercise, and 60 per minute to simulate rest. We recognize that these variations are only gross approximations. For example, in exercise certain organs receive more blood and others less which means that scaling the outflow distribution by changing α is somewhat artificial.

For the lower pulse rate of 60 beats per minute, the pulse pressure is generally larger than in the Standard Case because we have also reduced α for this case and therefore increased the resistance to outflow while the ejection phase of the cardiac cycle is the same as the Standard Case. We note that a short interval of negative flow persists well past $z = 40$ cm. Also, we find additional "dicrotic waves." Actually, such additional waves during diastole were observed experimentally on anesthetized dogs[27]. It is of interest that the first extra wave appears to coincide in time with the next primary wave of the Standard Case. A similar statement can be made about the second extra wave, which has a relatively small amplitude, and the dicrotic wave of the Standard Case. This suggests that some of the prominent features of the natural pulse are directly related to reflection phenomena.

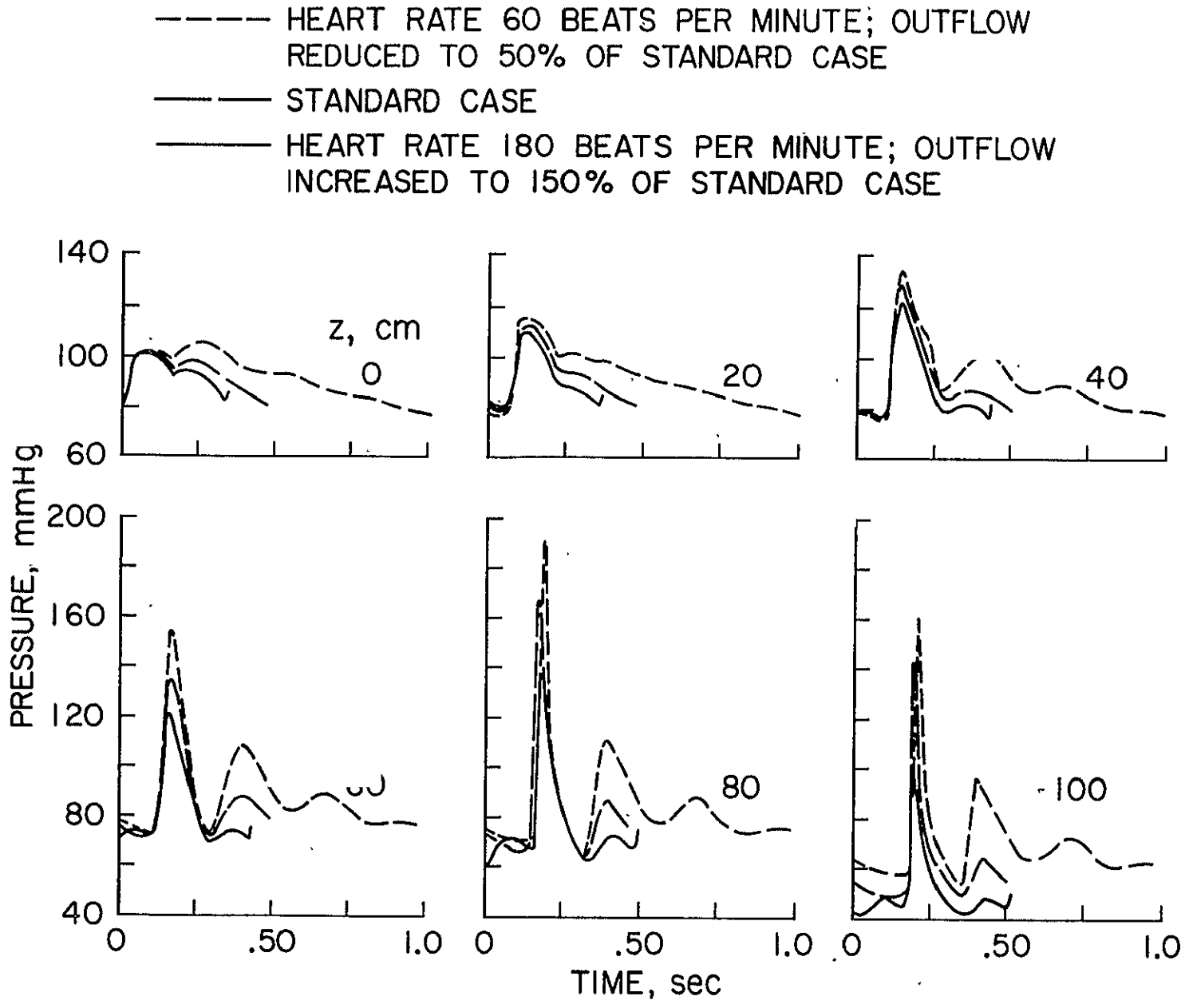

Figure 16. Pressure-time profiles showing the effect of heart rates different from that of the Standard Case (H.R. = 120 beats per minute). The outflow constant α was adjusted as indicated in order to maintain essentially the same diastolic pressure at the heart.

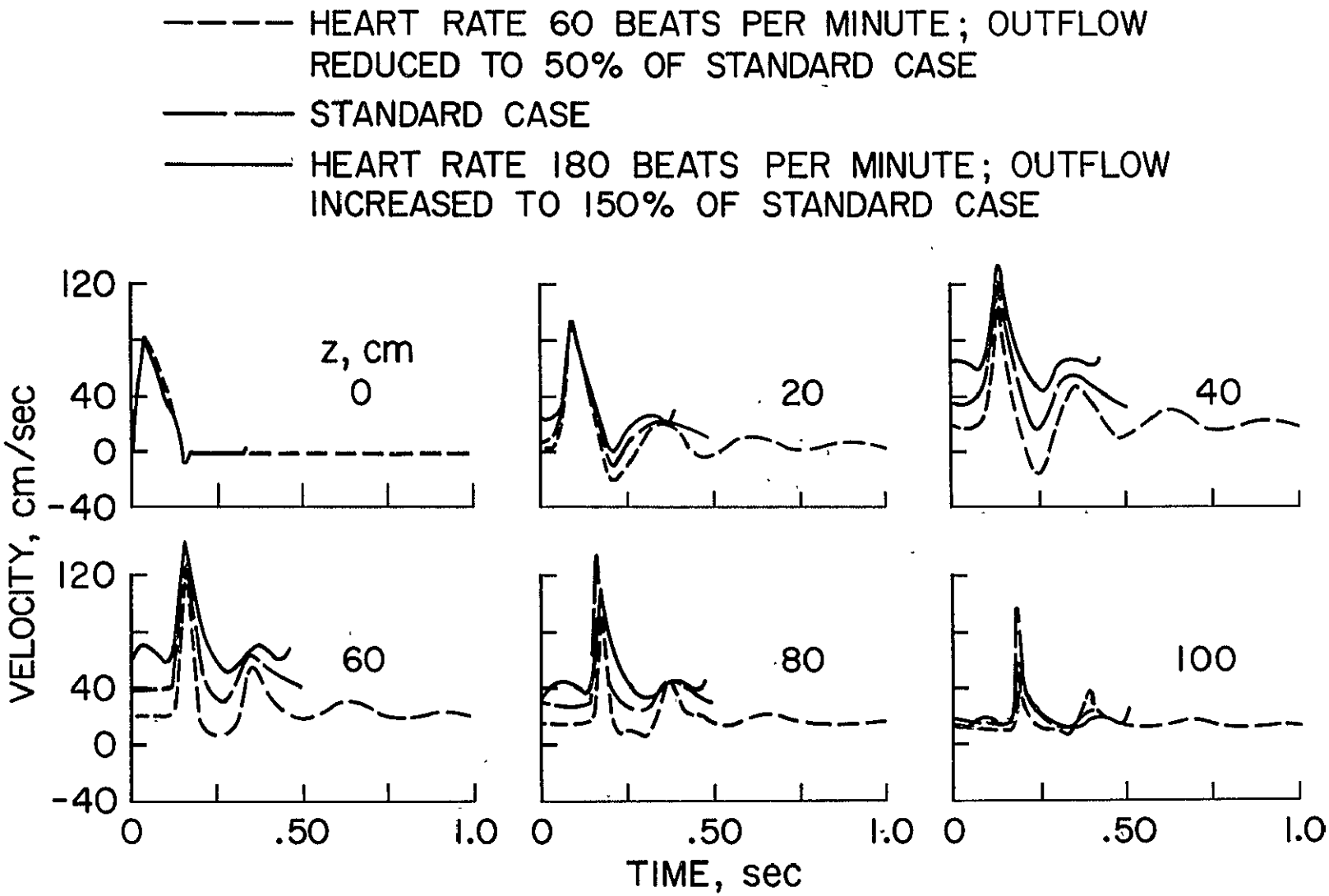

Figure 17. Velocity - time profiles for different heart rates corresponding to the pressure curves of Figure 16.

The increase in pulse rate from 120 to 180 beats per minute generally leads to opposite effects relative to the Standard Case than does a reduction in heart rate from 120 to 60. The pulse pressure is diminished since we have lowered the outflow resistance. Also, the short interval of negative flow is no longer present at $z = 20$ cm.

E. EFFECTS OF A CHANGE IN OUTFLOW DISTRIBUTION

As stated in Chapter II the model for outflow pattern Ψ is not entirely satisfactory. In order to assess the effects of the variation of Ψ with distance along the artery we have modified the outflow function of the Standard Case to simulate what might occur as a result of reducing the outflow into the abdomen as illustrated in Figure 18. Since we are leaving the outflow constant α and the cardiac output unchanged, the pressure must increase. This is corroborated by the results shown in Figure 19. A higher pressure leads in turn to an increase in the outflow rates and a larger distension of the vessel which together account for the reduction in the flow pulse evident in Figure 20. The results given in Figures 19 and 20 show that any marked change in outflow distribution, with all other cardiovascular parameters left unaltered, should cause clearly noticeable deviations from the Standard Case.

F. EFFECT OF STROKE VOLUME

The result of altering the stroke volume was studied for both larger (50 cm^3) and smaller (20 cm^3) values than in the Standard Case (30 cm^3). In order to maintain near normal diastolic pressure levels, the outflow was adjusted by a corresponding factor. All other cardiovascular parameters were left unchanged. Therefore an increase in the stroke volume should produce an increase in the pressure and flow pulse while conversely a decrease in stroke volume should diminish them. Accordingly we expect a more pronounced

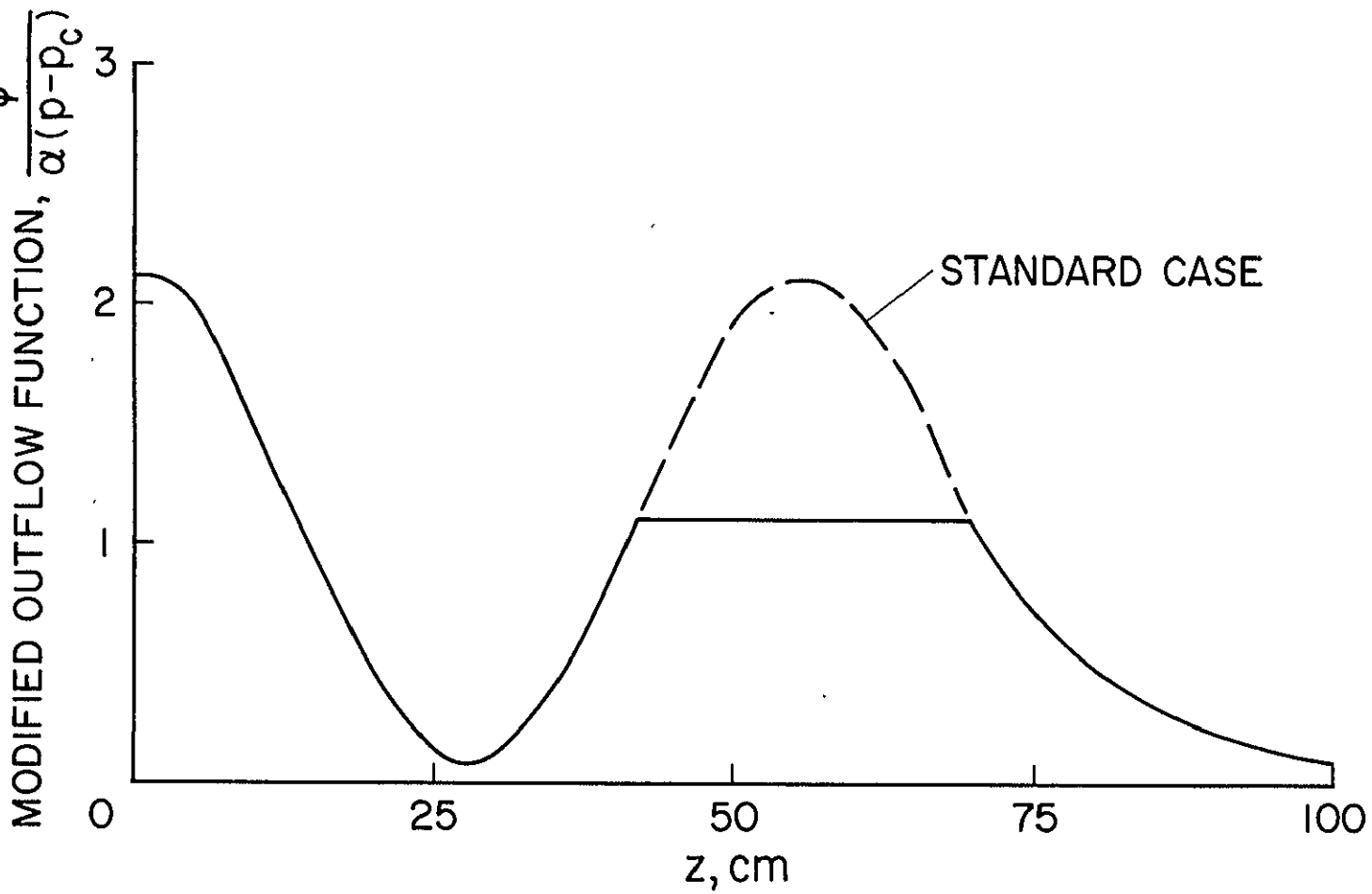

Figure 18. Outflow distribution function (solid curve) used to simulate reduction of blood flow into the abdomen by approximately 1/3.

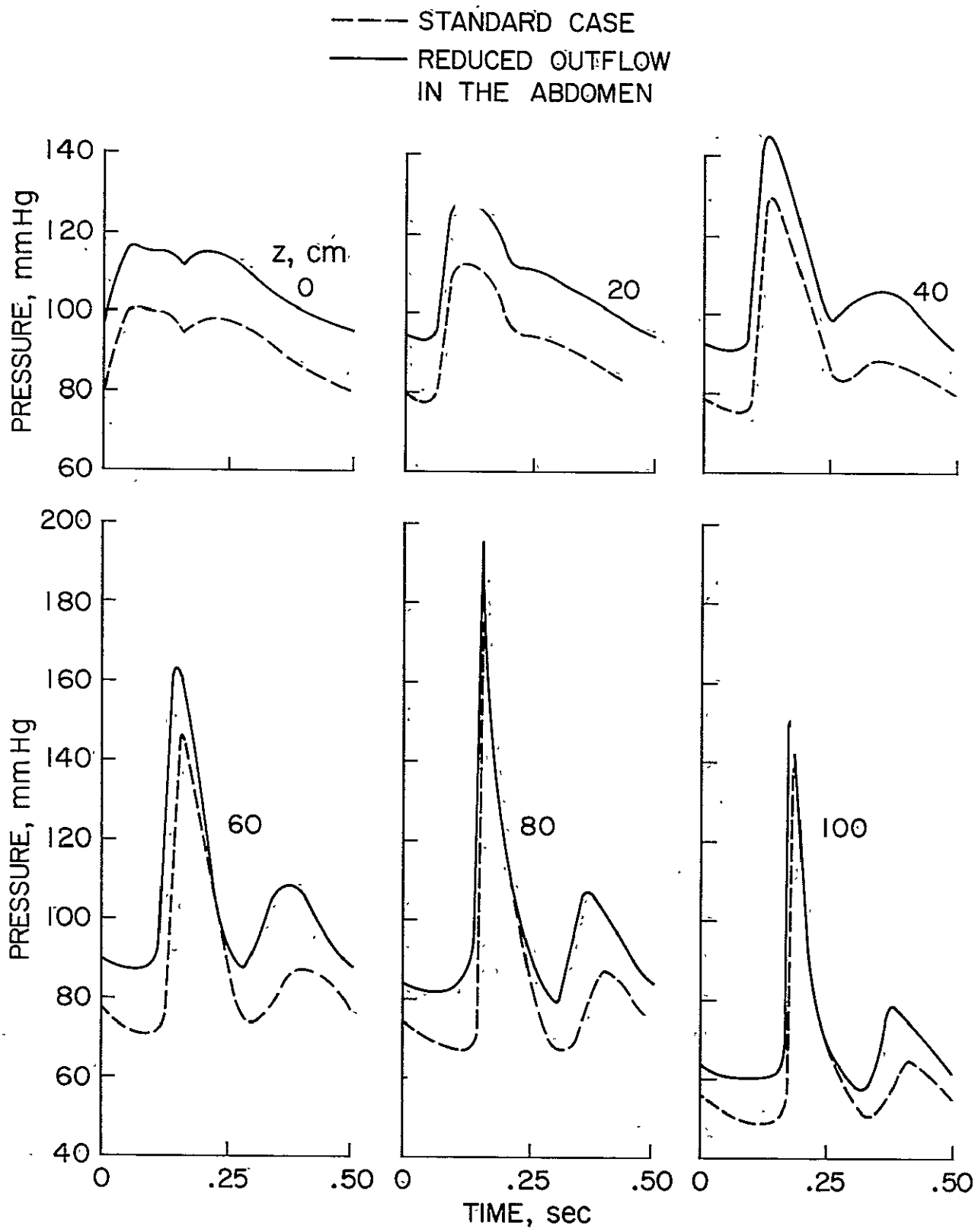

Figure 19. Pressure profiles computed using the outflow function of Figure 18 all other parameter values and functions remaining unchanged.

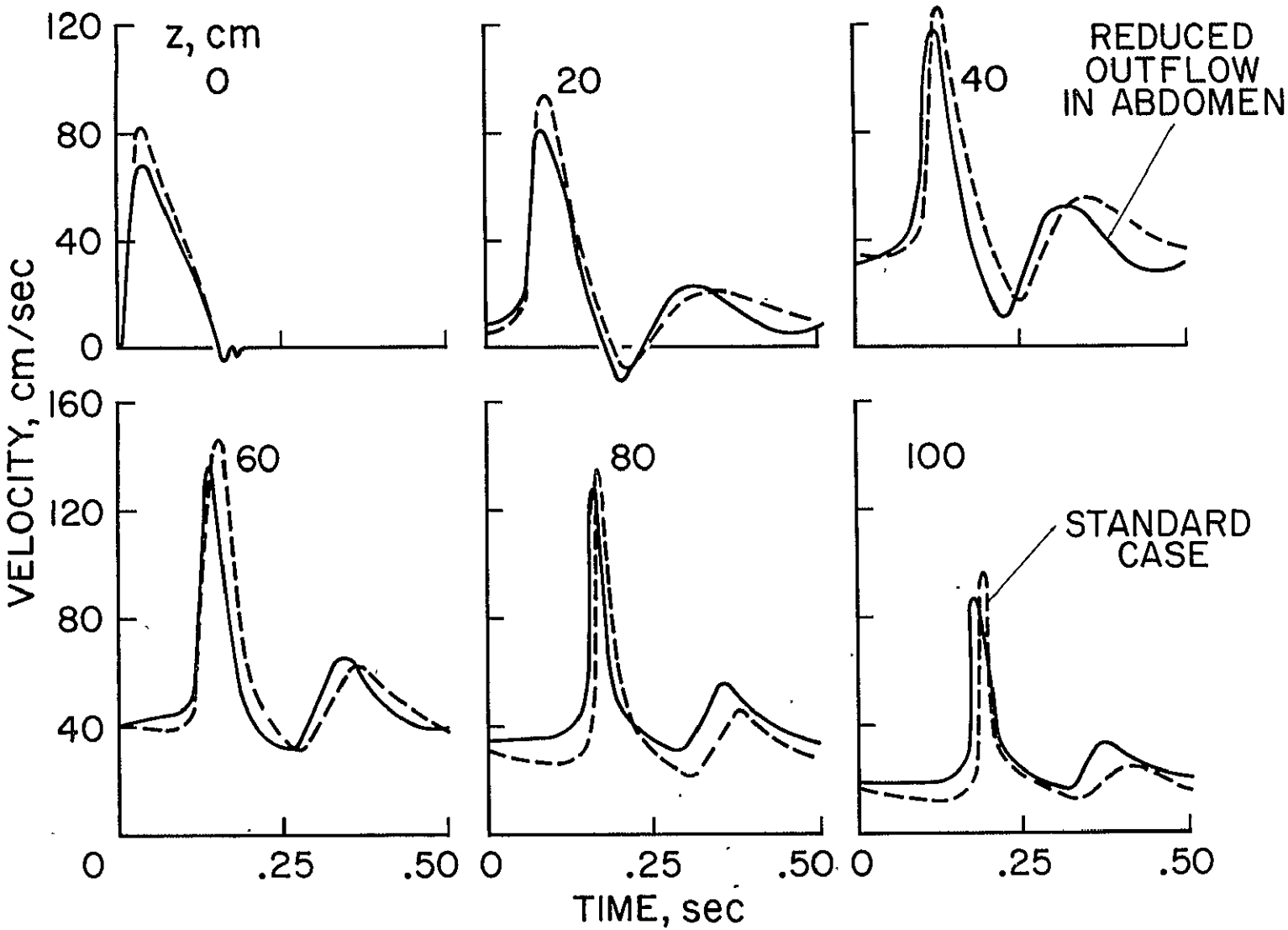

Figure 20. Velocity profiles corresponding to the modified outflow distribution shown in Figure 18 and to the pressure pattern given in Figure 19.

steepening of the wave front at the higher stroke volume and a more gradual one when we reduce it. We note that the results plotted in Figures 21 and 22 confirm these predictions. The flow pulse patterns given in Figure 22 also indicate that for the small stroke volume we have flow reversal even at relatively large distances from the heart.

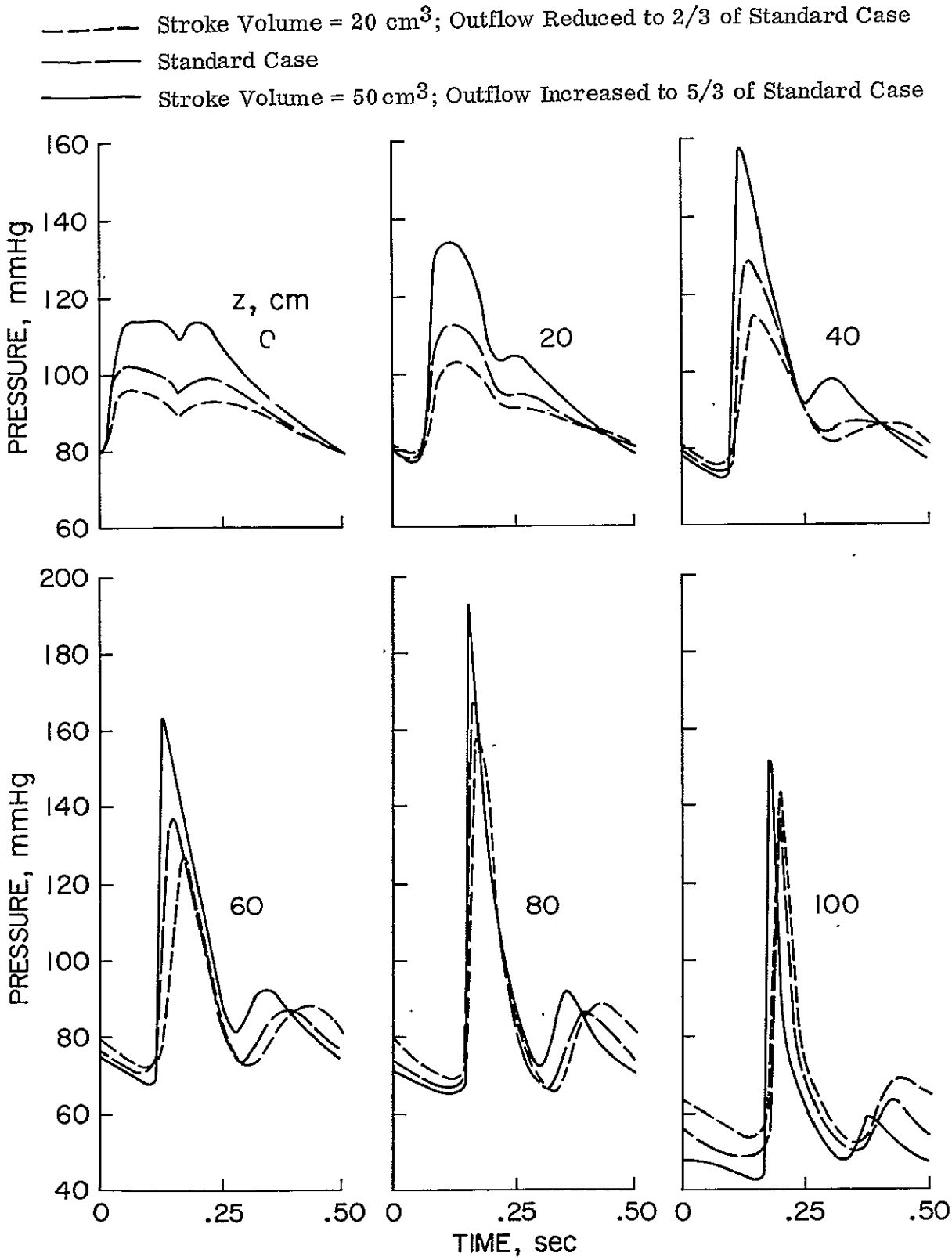

Figure 21. Effect of stroke volume on the pressure pattern. The cardiac ejection rates used were obtained by scaling the ejection rates given in Figure 8. The outflow constant α was changed by the same factor, but all other parameter values are those of the Standard Case. As expected, the pulse pressure varies in a direct manner with the stroke volume. Also, with increasing pressure the peaks and valleys of the pressure pulse are advanced in time.

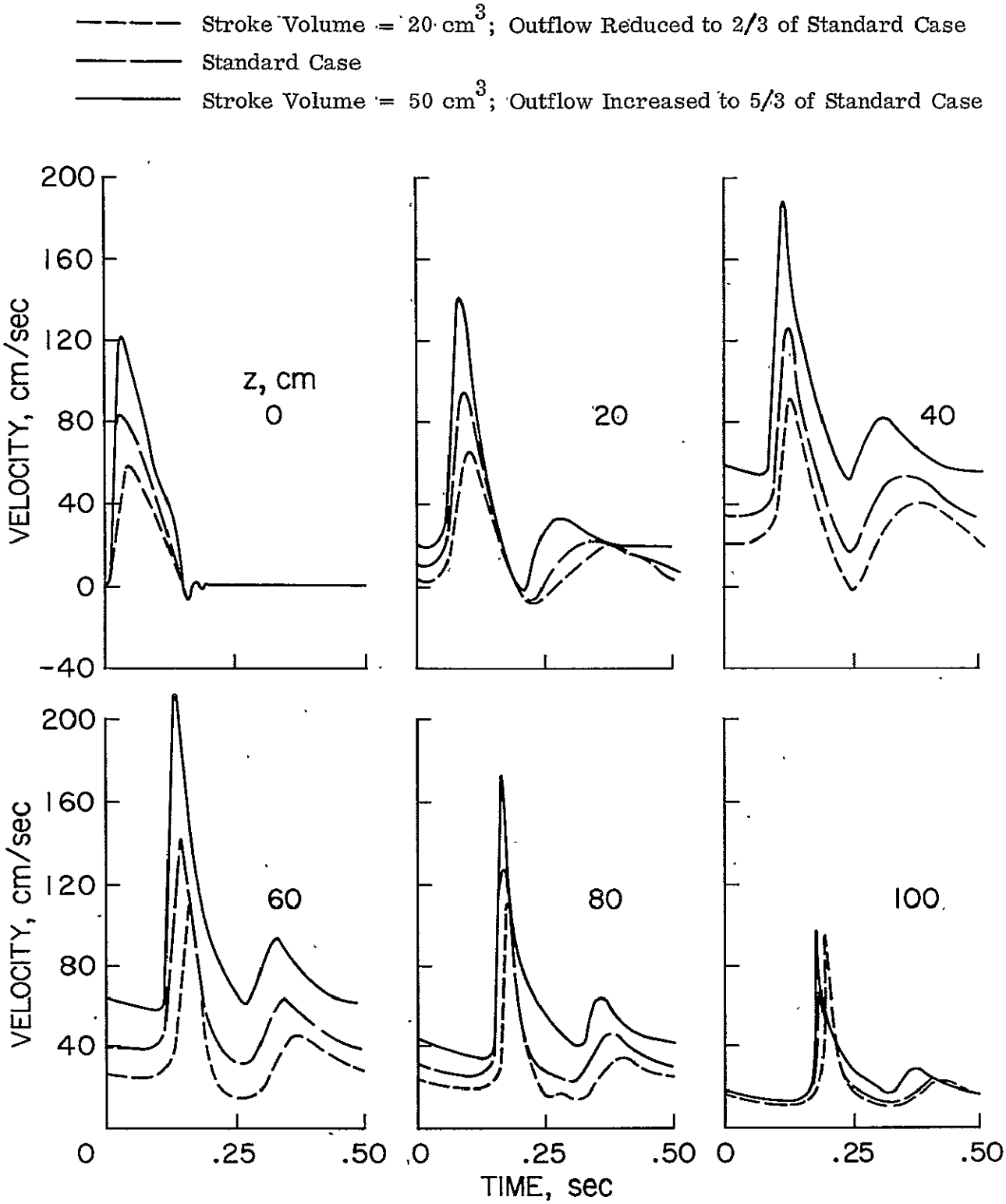

Figure 22. Velocity patterns corresponding to different values of the stroke volume and pressure patterns shown in Figure 21.

IV. SPECIAL PROBLEMS

Having a mathematical model which yields reasonable predictions for the characteristic features of the actual pressure and flow pulses generated by the heart, we intend to study the consequences of making certain changes in this model. We are particularly interested in assessing the effects of simplifications which are frequently introduced in elementary theories on blood flow. Whenever we compare the results from any of the altered models with those of the Standard Case, it should be kept in mind that even though the Standard Case solution is used as a reference, it represents an approximation to the pressure and flow pulses observed in reality. However the computer results discussed are sufficiently accurate to be considered as exact solutions of the mathematical problems defined by the various models.

A. SEMI-INFINITE TUBES WITH UNIFORM CROSS SECTION

In order to study the pulse waves in the absence of geometrically induced reflections we treat the case of a semi-infinite elastic tube of constant diameter. To simplify the problem further, we assume that there is no outflow. For such tubes and various functions $c(p, z)$ we shall examine the flow and pressure pulses induced by a single stroke with an ejection pattern as shown in Figure 8.

The inside diameter of the tube is taken to be 2.43 cm at a pressure of 100 mm Hg. Since there is no geometric taper, the pressure and flow fluctuations should be much lower than those occurring in a moderately tapered tube. Therefore in order to attain reasonable fluctuations in pressure and flow we double the stroke volume by doubling the values of cardiac ejection rate given in Figure 8. The initial conditions are zero velocity and a constant pressure of 80 mm Hg everywhere in the tube.

Figures 23 and 24 illustrate the results for four different wave speed functions:

(1) $c = c(p,z) = (97 + 2.03p)(1 + .02z)$ cm/sec (Standard Case)

(2) $c = c(z) = (97 + 2.03 \times 100)(1 + .02z)$ (independent of p)

(3) $c = c(p) = (97 + 2.03p)$ (no variation with distance)

(4) $c = \text{constant} = (97 + 2.03 \times 100)$

In all these expressions the pressure p is measured in mm Hg and the distance z in centimeters from the heart.

Function (1) exhibits the wave speed variation with pressure and distance as it has been assumed in the Standard Case. Taking in (1) the pressure to be 100 mm Hg we obtain function (2). Disregarding in (1) the wave speed increase with distance from the heart we arrive at the expression (3). Finally, by neglecting the spatial variation of the wave speed and assuming an average pressure of 100 mm Hg everywhere, we have a constant wave speed function as given by (4).

From Figures 23 and 24 it is clear that the pressure and flow pulses are noticeably changed when we have a wave speed which increases with z. This implies that a meaningful prediction of the natural pressure pulse in the aorta is only possible if we take into account the variation of the wave speed with distance.

The influence of pressure dependence of the wave speed appears to be less significant here than is the increase of c with distance. We notice, however, an increase in the slope of the wave front when c is pressure dependent and a more gradual decrease in the pressure or flow for the wave back as might be anticipated. Since the slopes are already steep the differences in slope are not readily apparent in the figures but they do in fact amount to factors of two or three.

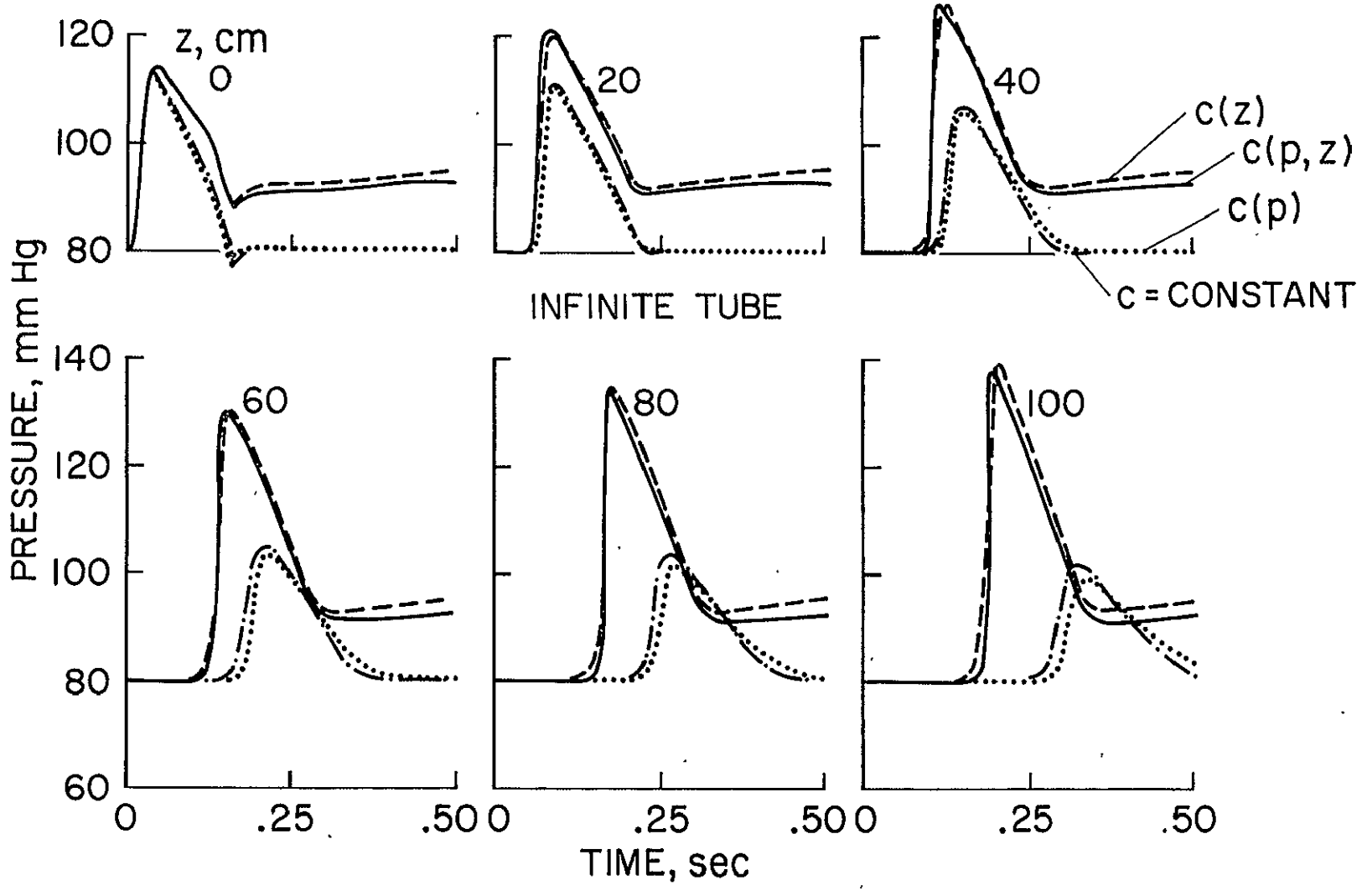

Figure 23. Pressure profiles in semi-infinite tubes with different wave speed functions. The tubes are untapered and there is no outflow through the wall. Ejection pattern is that for Figure 8 but scaled to yield a stroke volume of 60 cm^3. The solid lines represent the results corresponding to $c = c(p, z)$ as defined by (1); dashed lines correspond to $c = c(z)$ (expression (2)). The dotted lines are obtained for $c = c(p)$ (expression (3)) and the dash-dot lines illustrate the results for a constant wave speed, expression (4).

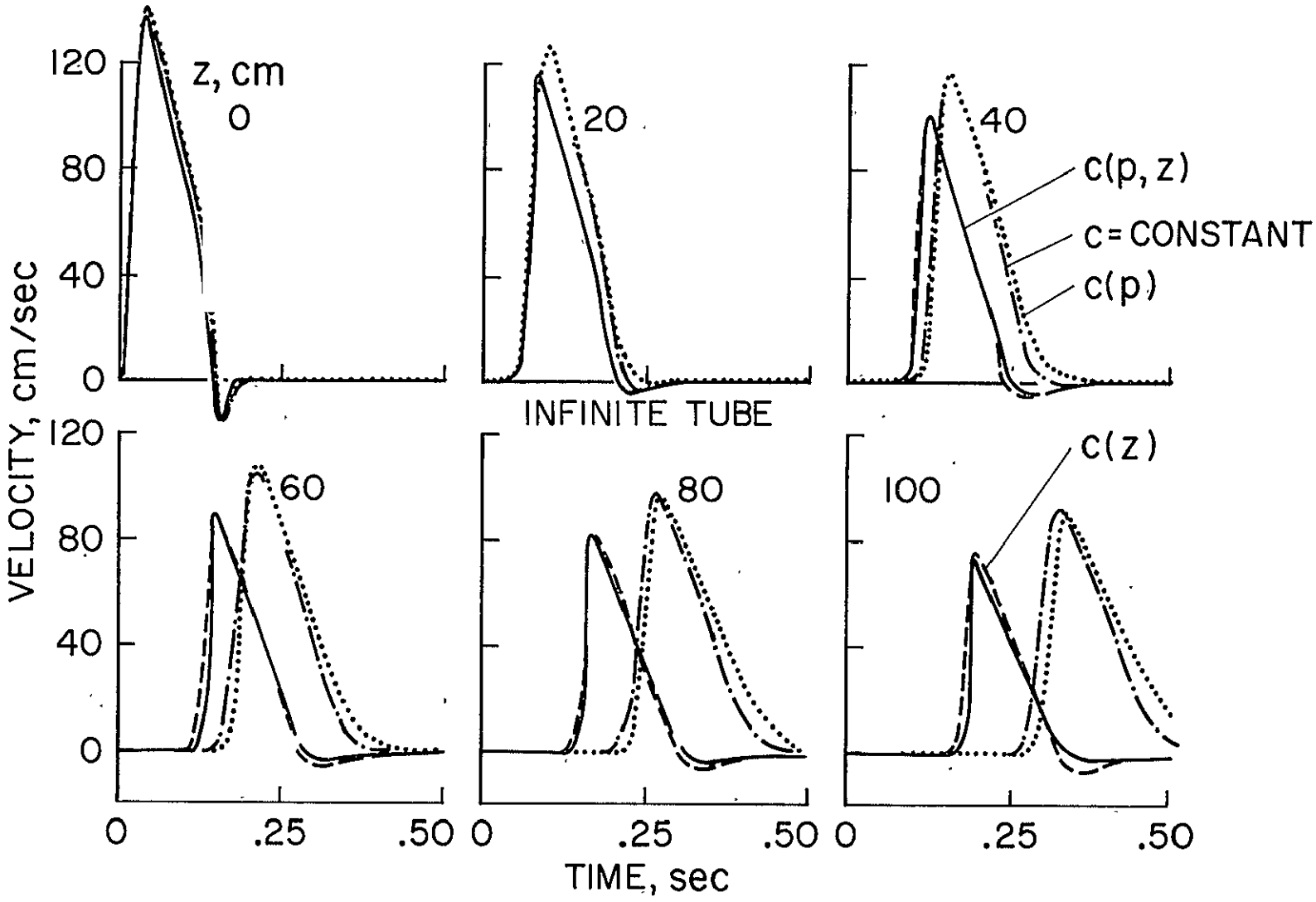

Figure 24. Velocity profiles corresponding to Figure 23 for an elastic tube with constant cross section and different expressions for the wave speed.

Expressions (1) and (2) stipulate higher wave speeds and thus a stiffer arterial wall than do either (3) or (4). Therefore, with (1) or (2) the pressure pulses arrive at each station sooner and have larger amplitudes than the pulses corresponding to expressions (3) and (4). We also note that for functions (3) and (4) the pressure returns to 80 mm Hg after the ejection ceases, whereas for the cases of the tube becoming stiffer with increasing distance from the origin the pressure remains elevated for the time periods considered.

For the functions (2) and (4) the individual changes in shape of the pressure and flow pulses with increasing distance from the origin can at least in part be attributed to fluid viscosity. The nonlinear effects due to the wave speed variation with flow velocity, to the local changes in cross-sectional area with pressure, and to the local taper generated by the pressure pulse are still present and also cause modifications of the results.

For the wave speed functions considered there is no evidence of a dicrotic wave in any of the pressure pulses.

B. LINEARIZED TREATMENT

The differential equations (2) and (4) for one-dimensional fluid flow are inherently nonlinear. If we linearize these equations we reduce the problem to one which can be treated by conventional methods such as Fourier analysis. As a matter of fact most of the past studies of pulsatile blood flow are based on linearized equations, even though it has been recognized that linearization constitutes an approximation. While for some applications such an approximation may be tolerable, it is expected to introduce excessive errors in the predicted pressure and flow patterns. To determine the magnitudes of these errors in our case we have set out to examine the differences between the solutions of nonlinear and linear analyses.

If we consider the fluid velocity and the deviation of the pressure from a mean value $\bar{p}$ as perturbations, the linear approximations to the governing differential equations (2) and (4) can be written as

$$\frac{\partial v}{\partial t} + \frac{1}{\rho}\frac{\partial p}{\partial z} = f(\bar{p}, v, z) \tag{32}$$

and

$$S_L(\bar{p}, z)\frac{\partial v}{\partial z} + \left(\frac{\partial S_L}{\partial p}\right)_z\Bigg|_{p=\bar{p}} \frac{\partial p}{\partial t}$$

$$+ v\left(\frac{\partial S_L}{\partial z}\right)_p\Bigg|_{p=\bar{p}} + \Psi = 0 \tag{33}$$

$S_L(p, z)$ denotes the cross-sectional area relation for the linearized problem. The outflow expression Ψ is linear in the dependent variables and does not have to be modified.

The method of characteristics applied to these equations yields

$$I^{\pm}: \quad \frac{dz}{dt} = \pm c_L \tag{34}$$

and

$$II^{\pm}: \quad dv \pm \frac{dp}{\rho c_L} = \left[f(\bar{p}, v, z) \right.$$

$$\left. \mp \frac{v c_L}{S_L}\left(\frac{\partial S_L}{\partial z}\right)_p\Bigg|_{p=\bar{p}} \mp \frac{c_L \Psi}{S_L(\bar{p}, z)} \right] dt \tag{35}$$

where the wave speed is now independent of pressure.

$$c_L(z) = \sqrt{\frac{S_L(\bar{p}, z)}{\rho \left(\frac{\partial S_L}{\partial p}\right)_z \Big|_{p=\bar{p}}}} \tag{36}$$

As before, we prescribe the spatial variation of the wave speed and then integrate Equation (36) to determine the dependence of the cross-sectional area on pressure. Specifying the geometric taper again by (15) we obtain

$$S_L(p, z) = S_0(p_0)\, e^{-\beta z + \frac{p - p_0}{\rho c_L^2}} \tag{37}$$

We note that S_L grows exponentially with pressure whereas in the nonlinear analysis the cross-sectional area defined by (16) approaches an upper limit with $p \to \infty$, namely

$$\lim_{p \to \infty} S(p, z) = S_0(p_0)\, e^{-\beta z + \frac{1}{\rho c_1 (1 + nz) c(p_0, z)}}$$

Especially relevant would be a comparison of linear and nonlinear analysis for the Standard Case. We choose the mean pressure of the nonlinear solution as the pressure $\bar{p}$, about which the linearization is made. Accordingly we take $\bar{p} = 88$ mm Hg. For the wave speed expression we use Equation (30) with the pressure set identically equal to 88 mm Hg.

Figures 25 and 26 illustrate the solution of both the linear and nonlinear problems. In the linearized case the systolic pressure is higher in the

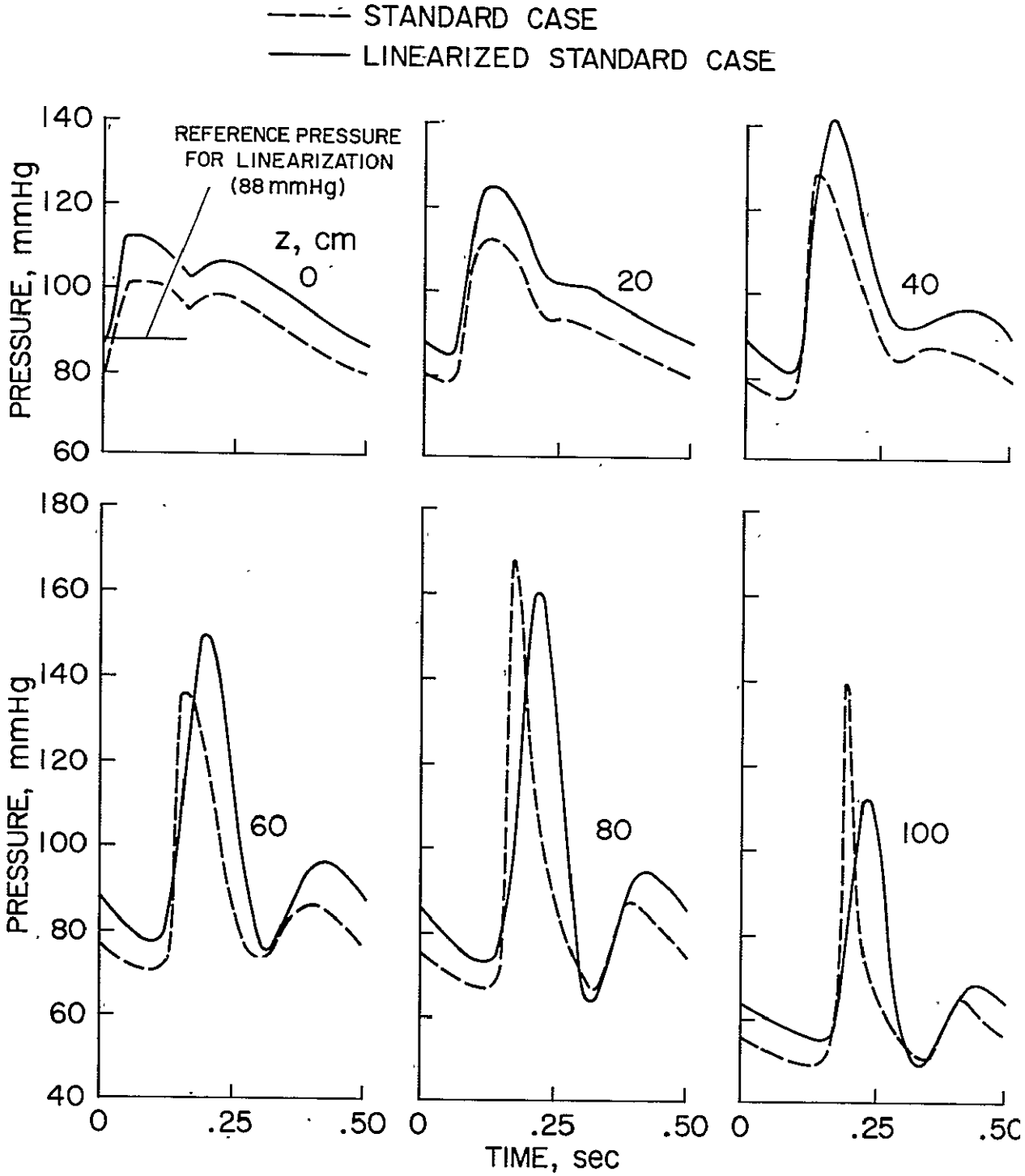

Figure 25. Pressure patterns corresponding to the Standard Case in which nonlinear effects have been taken into account, and patterns computed from the linearized equations. Aside from the mean pressure, the differences in shape become more pronounced with increasing distance from the heart.

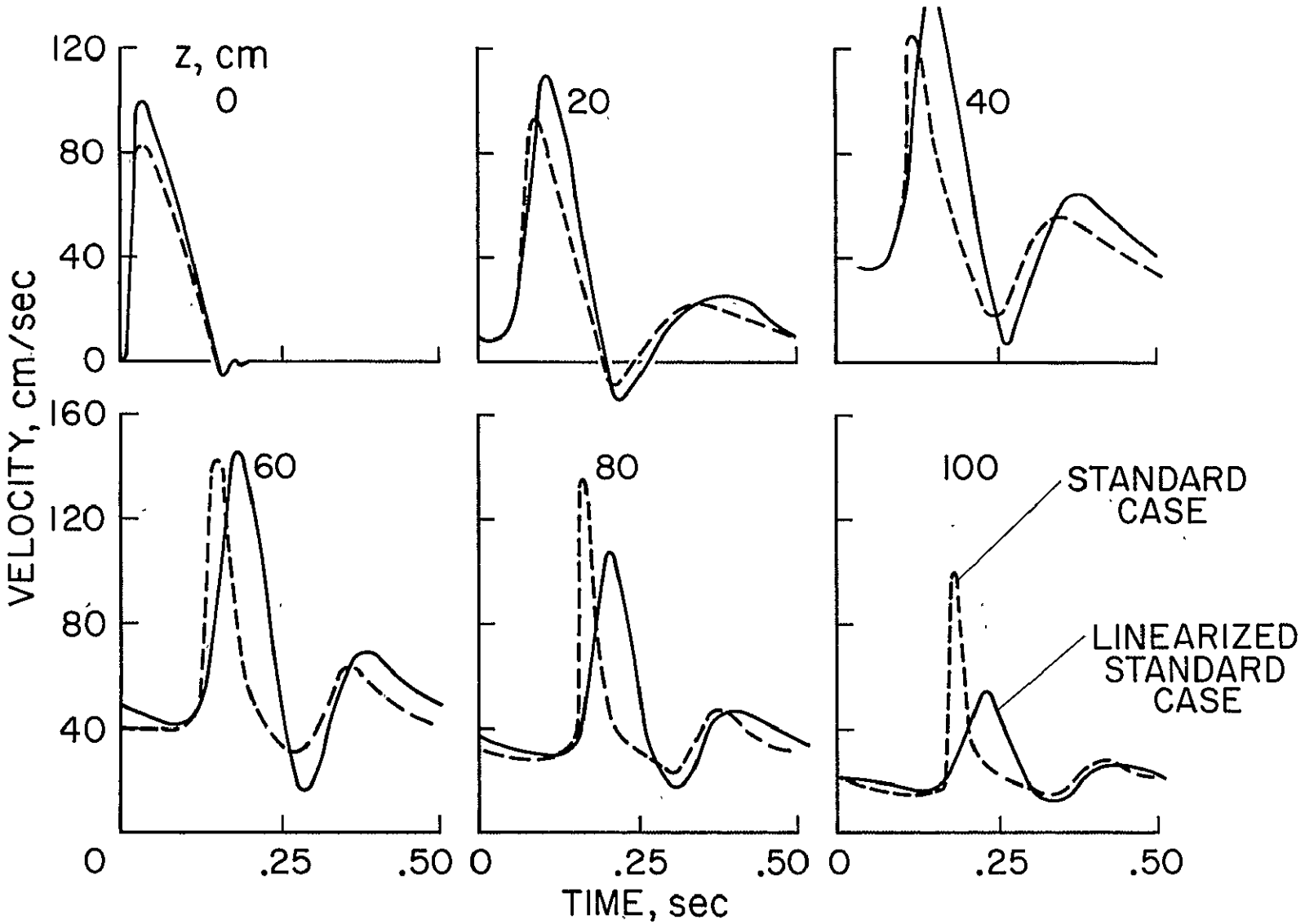

Figure 26. Velocity patterns for the Standard Case computed on the basis of nonlinear and linear analyses. The corresponding pressure patterns are shown in Figure 25.

proximal aorta than predicted by the nonlinear treatment because the increase in cross-sectional area (distension) with pressure is no longer taken into account as a pressure-alleviating phenomenon. As z increases the difference between the systolic pressures diminishes and changes its sign. This may in part be due to the fact that the outflow from the proximal aorta is higher for the linear analysis than for the nonlinear one. (The outflow is proportional to the pressure.) Therefore a smaller flow pulse reaches the distal portions of the artery in the linear case giving rise to a smaller pressure pulse there.

In the linear case the wave fronts are considerably less steep and do not increase their slopes appreciably with distance. The wave backs are steeper so that the wave peaks are delayed but the valleys occur at approximately the same time. As the pressure increases above the average value $\bar{p}$ the arterial wall becomes stiffer in the nonlinear analysis which causes a progressive steepening of the wave front; conversely, as the pressure falls below the average value the vessel becomes more distensible which in turn causes more moderate slopes. These differences become more pronounced with increasing distance from the heart. It is evident that the slope does not vary appreciably between the bottom and top of each pulse in the linear solution. Also, the rate of pressure rise at the front of the pulse is approximately equal to the rate of decay at the back.

We also note that the dicrotic wave is larger in the linear approximation. One possible explanation for this could be the increased stiffness of the distal portion of the artery in the linear case which was introduced by selecting $\bar{p} = 88$ mm Hg for all z. Since the dicrotic wave appears to be caused by the reflection of the primary pressure pulse from the distal portions of the artery, it can be expected that the larger dicrotic wave is due to a stiffer distal end, i.e., a harder reflection region in the linear analysis.

The prominent differences seen between the two solutions indicate that a reliable interpretation of the possible causes for relatively small changes in the naturally occurring pressure and flow pulses can only be made if nonlinear phenomena are taken into account.

C. EFFECT OF FRICTION

Since it has been anticipated that fluid friction does not play an important role in the large arteries[32], the effects of viscosity have been accounted for only in an approximate way. The results discussed so far are all based on a friction coefficient corresponding to steady laminar flow.

In order to assess to some degree the importance of frictional effects, different values of the viscosity coefficient μ were assumed and the results compared with the Standard Case. It has been stated[33] that the "effective" viscosity coefficient for pulsatile flow in the large arteries is of the order of eight times that associated with steady flow. Therefore the effect of increasing μ ten-fold as compared with the Standard Case was examined. In addition the inviscid approximation was investigated.

An increase in the viscosity coefficient produces a higher flow resistance and therefore a decrease in the flow velocity and an increase in the pressure, at least in the proximal aorta. The inviscid case should essentially yield opposite results. With the retarding effects of friction removed, the flow velocity pulse, and correspondingly the pressure pulse should have a larger magnitude for smaller diameters.

The results plotted in Figures 27 and 28 confirm these expectations. For the larger viscosity coefficient the overall pressures are higher when $z < 40$ cm, and the pulse pressure at the heart has increased slightly. The resistance to outflow along the artery should actually be greater for a more

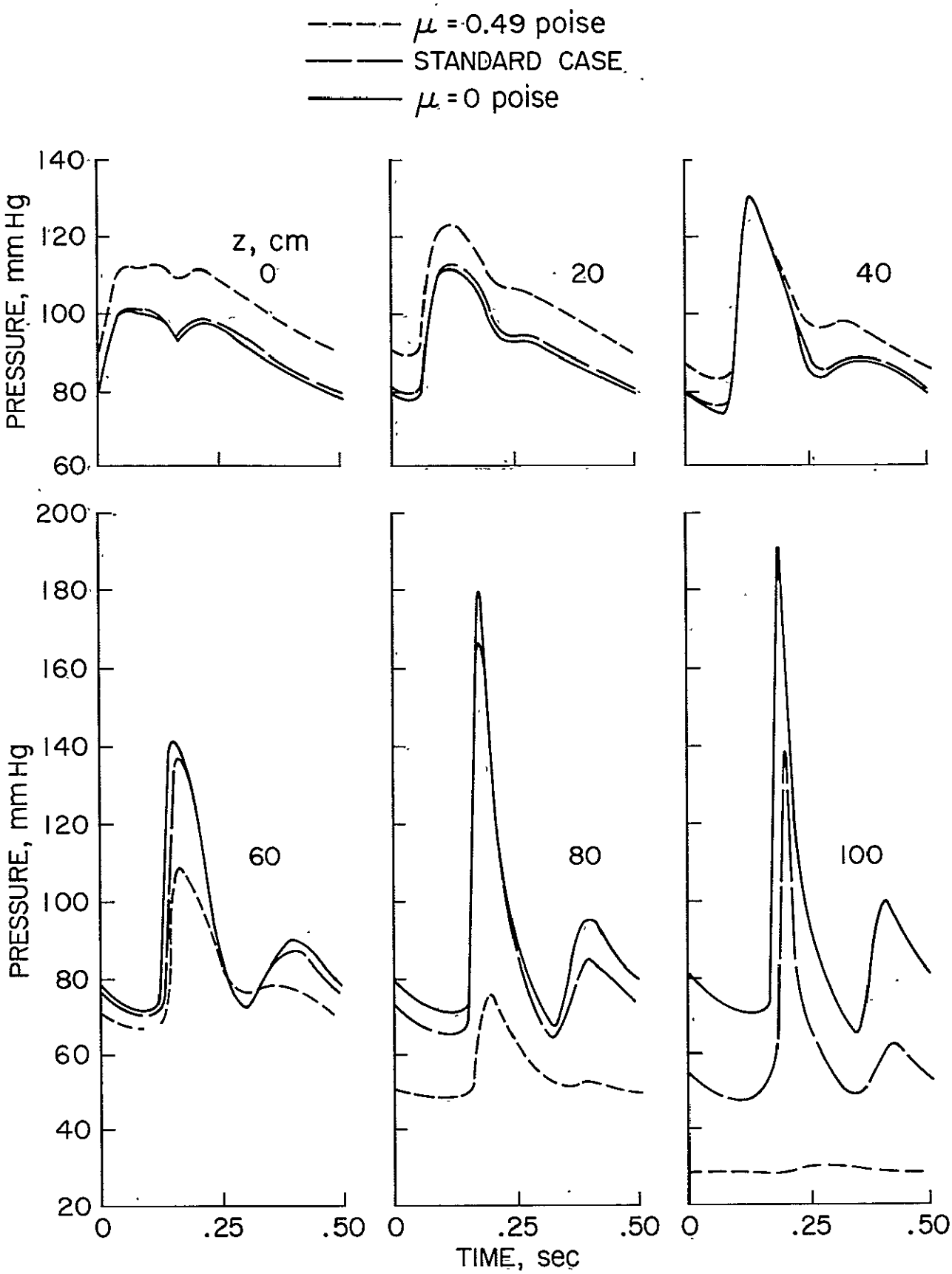

Figure 27. Pressure - time profiles for different values of effective viscosity coefficient in the laminar model for the friction term. The Standard Case ($\mu = .049$ poise) is shown for comparison.

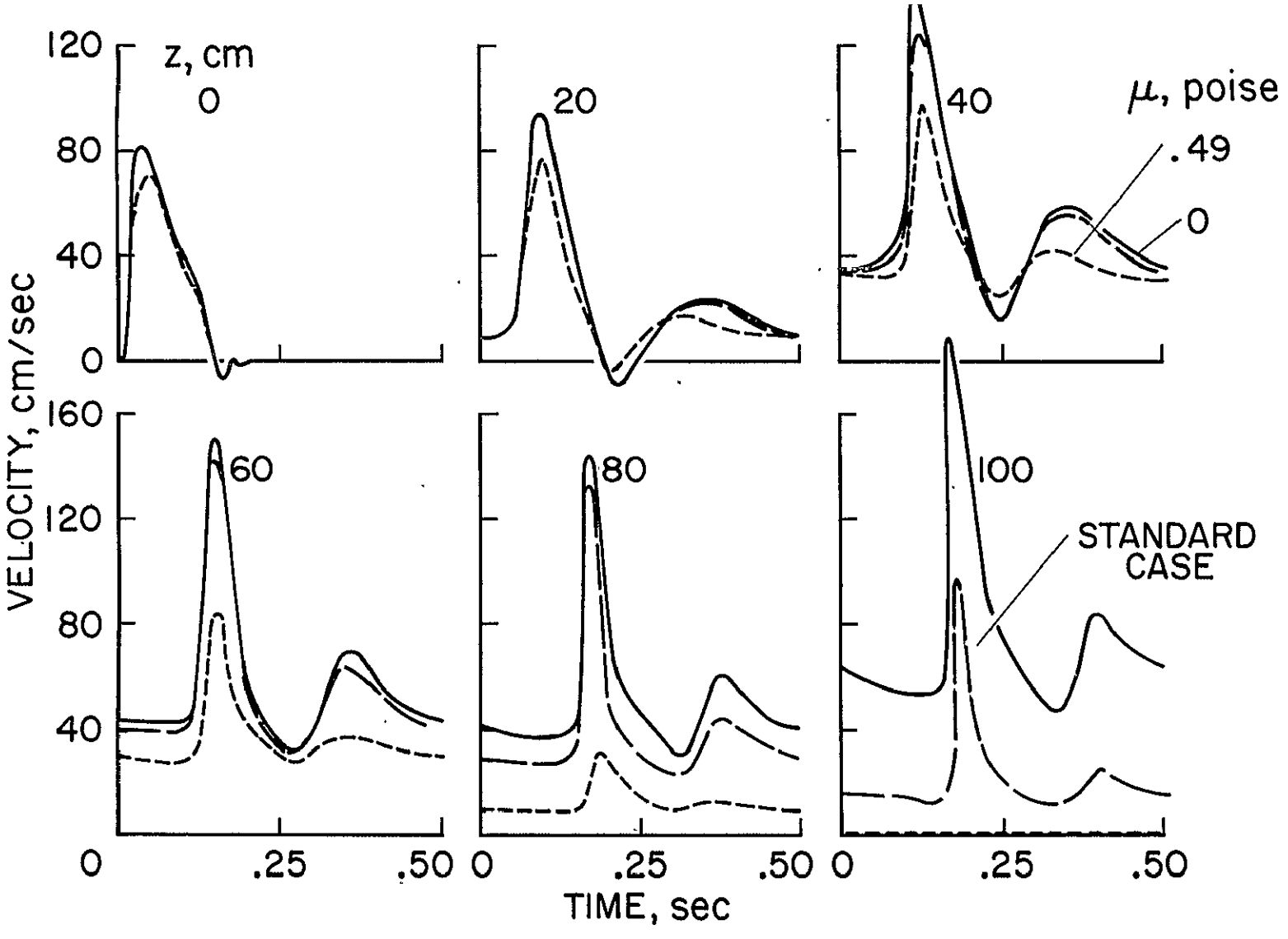

Figure 28. Velocity – time profiles for different values of viscosity coefficient corresponding to the pressure profiles shown in Figure 27.

viscous fluid but this detail was not included in the model for the outflow function Ψ. Its proper inclusion would tend to increase the pressures further. Beyond 40 cm the cumulative effects of increased friction cause such a rapid decay of the pressure and velocity pulses that they are virtually damped out at 100 cm from the heart. Percentagewise, the amplitude of the dicrotic wave has been reduced more markedly than the primary pulse. One possible explanation for this can readily be given. If the dicrotic wave is indeed caused by reflection it must exhibit the effects of friction in a compounded fashion.

The case for $\mu = 0$ is not quite a true inviscid solution because the terminal pressure, left unaltered at 25 mm Hg, is probably strongly influenced by viscous effects in the arterioles. While a true inviscid formulation would lead to a different terminal condition, the investigation of that problem would not be of practical interest. Our intention here is to approximate reality as closely as possible, and we have therefore left the distal boundary condition unchanged.

For the larger viscosity coefficient of $\mu = .49$ poise the pressure and flow pulses are significantly different from those of the other cases ($\mu = 0$, .049). If the "effective" viscosity coefficient is in fact of this order of magnitude then fluid viscosity does play an important role even in arteries as large as the aorta. On the other hand, the comparison of the case $\mu = 0$ with the Standard Case suggests that the differences due to friction are not great for $z \leq 60$ cm where the mean diameter is larger than 0.6 cm. Beyond that region the pressure and velocity fluctuations for $\mu = 0$ progressively depart from those of the Standard Case.

Aside from the laminar Poiseuille expression (21), the Blasius formula for steady turbulent flow in a pipe was also used for the cases $\mu = .049$ poise and $\mu = .49$ poise. As can be noted from Figures 29 and 30

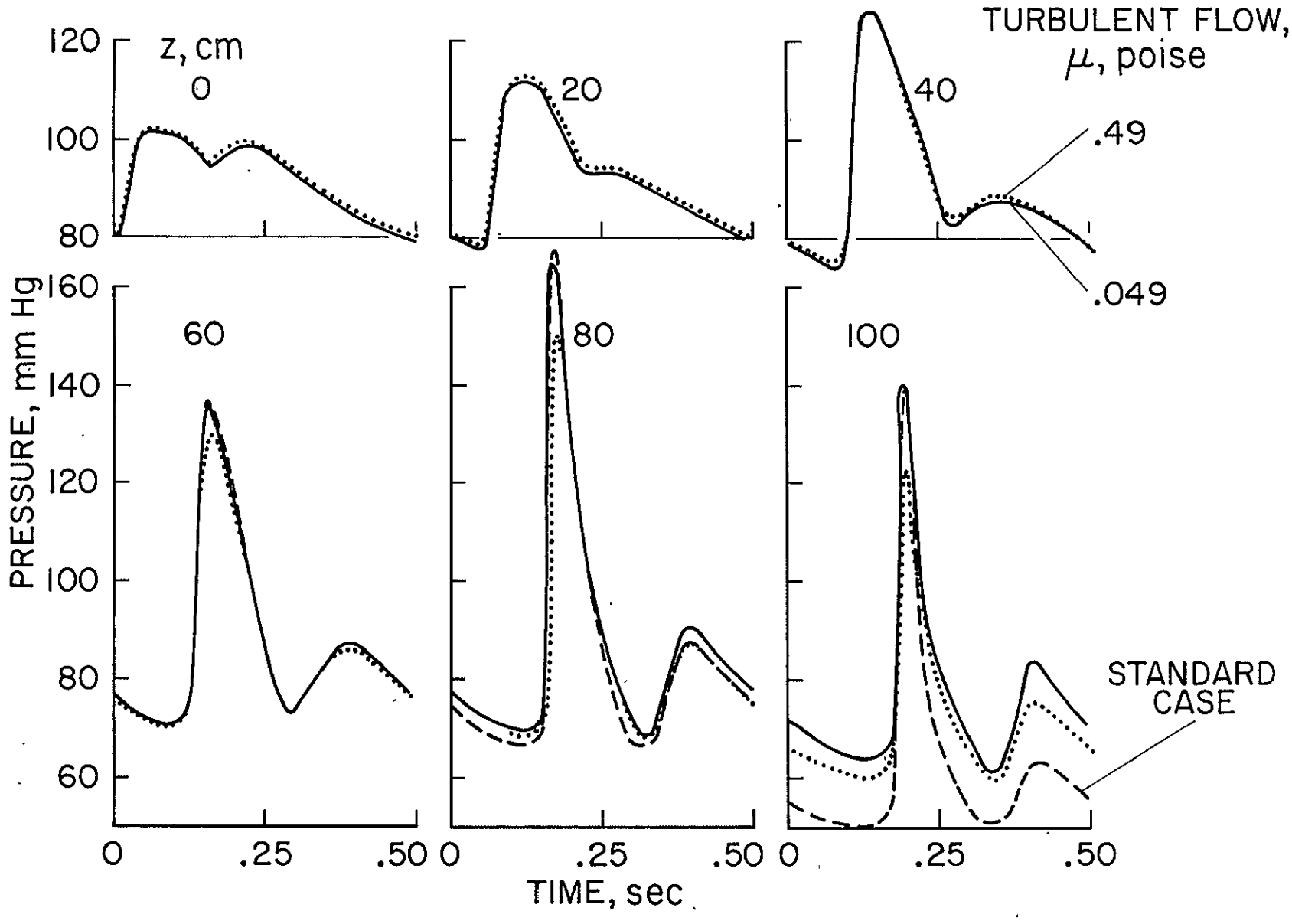

Figure 29. Changes in the pressure patterns resulting from different values of effective viscosity coefficient in the turbulent model for fluid friction. The Standard Case (laminar flow, $\mu = .049$ poise) is also shown.

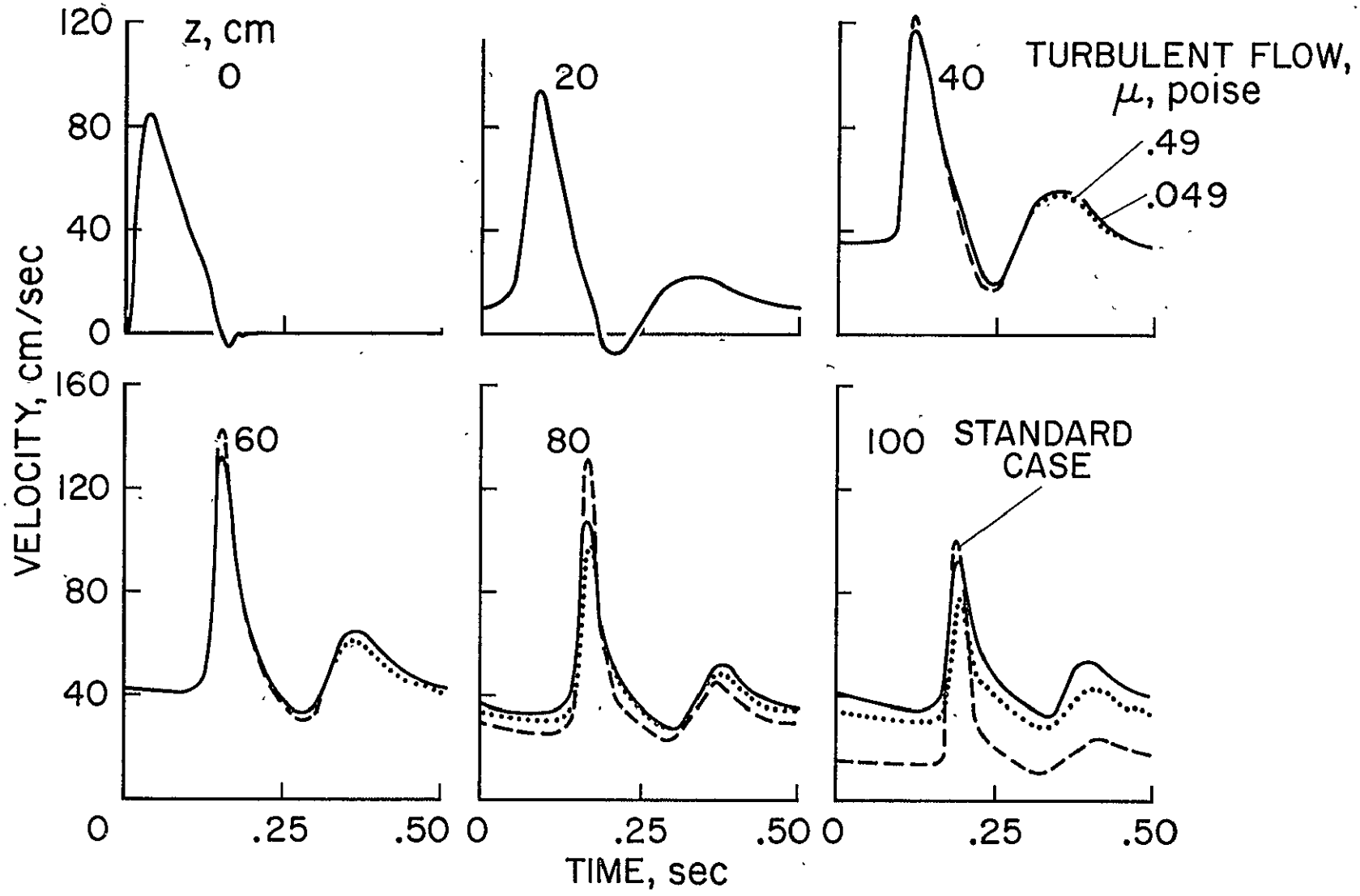

Figure 30. Velocity patterns for turbulent friction and corresponding to pressure patterns shown in Figure 29.

the pressure and flow pulses are remarkably unaffected by turbulent friction, especially for $z < 80$ cm. Deviations are observed only for $z \geq 80$ cm or for diameters less than 0.3 cm where the flow is unlikely to be turbulent. Only near the heart is turbulent flow normally considered possible. The differences between results for the two values of μ are not profound because the turbulent expression for friction (22) includes the coefficient of viscosity raised to the one-fourth power.

Since we are dealing here with friction models which are in some sense artificial we can not perform a true investigation into the importance of fluid viscosity. All we can say is that an increase of the viscosity coefficient from 0.049 to 0.49 poise in our laminar frictional term produces considerable changes in the pressure and flow pulse particularly at larger distances from the heart. By contrast the same increase in μ does not induce significant changes when the turbulent friction term is utilized. However, it remains to be shown whether the expressions chosen for the frictional term are adequate representations of the true situation. Clearly, a thorough investigation of the effects of fluid viscosity on large-amplitude pulsatile flow in distensible tubes should be conducted.

D. PERIPHERAL RESISTANCE

The notion of peripheral resistance is applicable when the pressure and flow pulses are linearly related. The adequacy of such a concept for the distal boundary condition should be investigated. We are doing this by utilizing as distal boundary condition the fact that the pressure is essentially constant in the vicinity of the capillaries. The corresponding solution for the Standard Case is then examined as to the pressure-flow relationship at various distances from the heart. Figure 31 gives the results in terms of the instantaneous blood

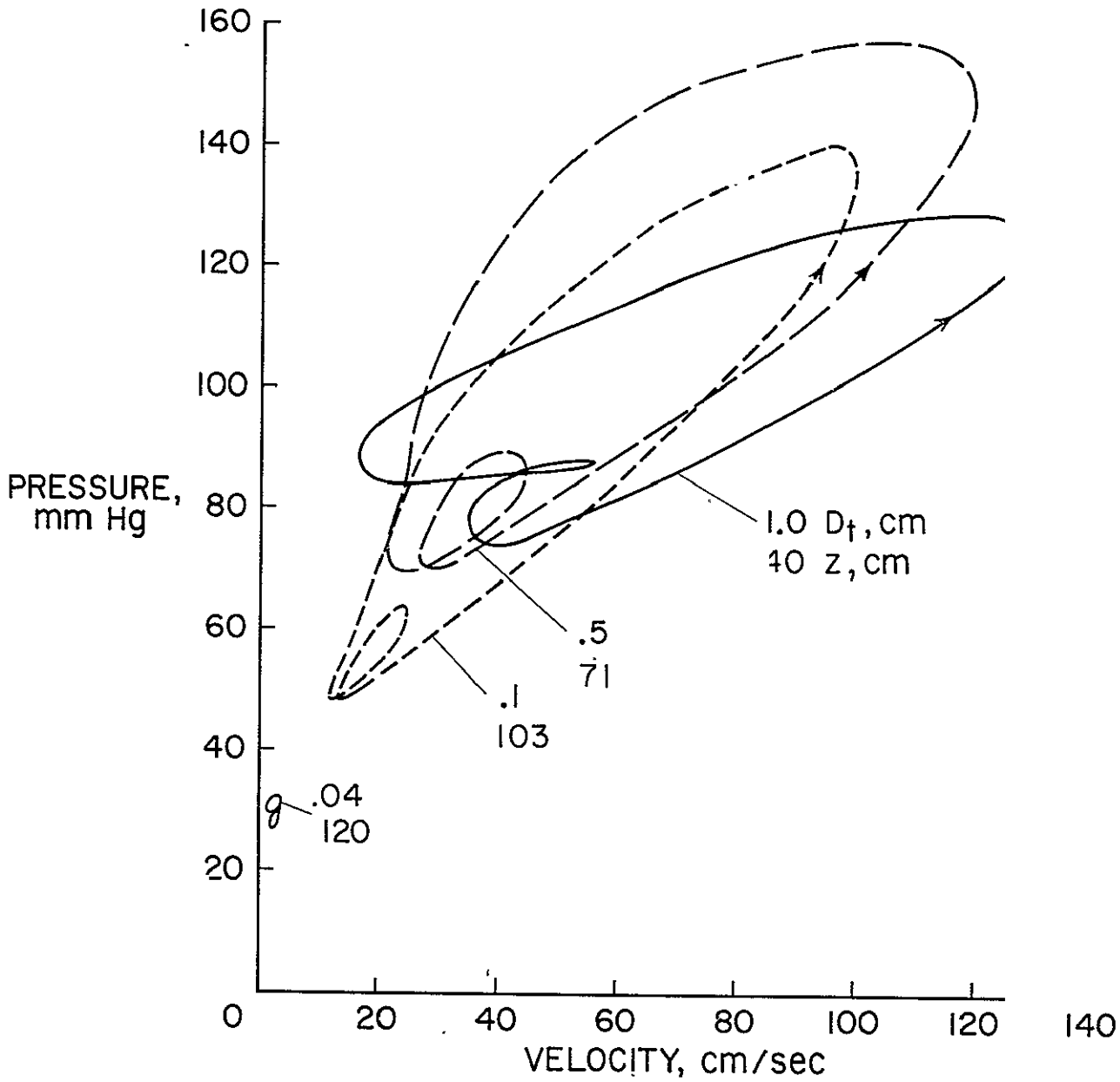

Figure 31. Pressure - velocity relation for the Standard Case at four different distances from the heart. Each of the four closed curves represents the variation of pressure and flow during a full cardiac cycle. If the peripheral resistance concept were strictly valid, each of the four curves would be a straight line.

velocity as a function of instantaneous pressure at four different distances from the heart. If we can disregard the cross-sectional area changes with pressure the local blood velocity is directly proportional to the local blood flow. For small diameters we may indeed neglect the cross-sectional area changes and therefore interpret the curves in Figure 31 as approximations of the pressure-flow relations. We note that with decreasing distance from the heart the pressure-flow relationship deviates progressively from a linear one.

To further assess the effects of prescribing a peripheral resistance R_L we have considered the Standard Case artery and suitably selected a value for R_L at each of the various distances z from the heart indicated in Figure 31. This means we have computed the pressure and flow pulses for four arteries with the same initial diameter, taper, $c(p,z)$, $\psi(p,z)$, ejection pattern and heart rate, but different lengths, terminal diameters and peripheral resistances. The values used for R_L are given in Table 2. In each case R_L was selected such as to yield at the root of the aorta the same diastolic pressure as does the Standard Case. The corresponding results are illustrated in Figures 32 and 33.

TABLE 2

Peripheral Resistance for Different Terminal Diameters

Diameter cm	Length cm	R_L dyne sec/cm^5
.04	120	2.39×10^6
.1	103	3.82×10^5
.5	71	9.93×10^3
1.0	40	2.60×10^3

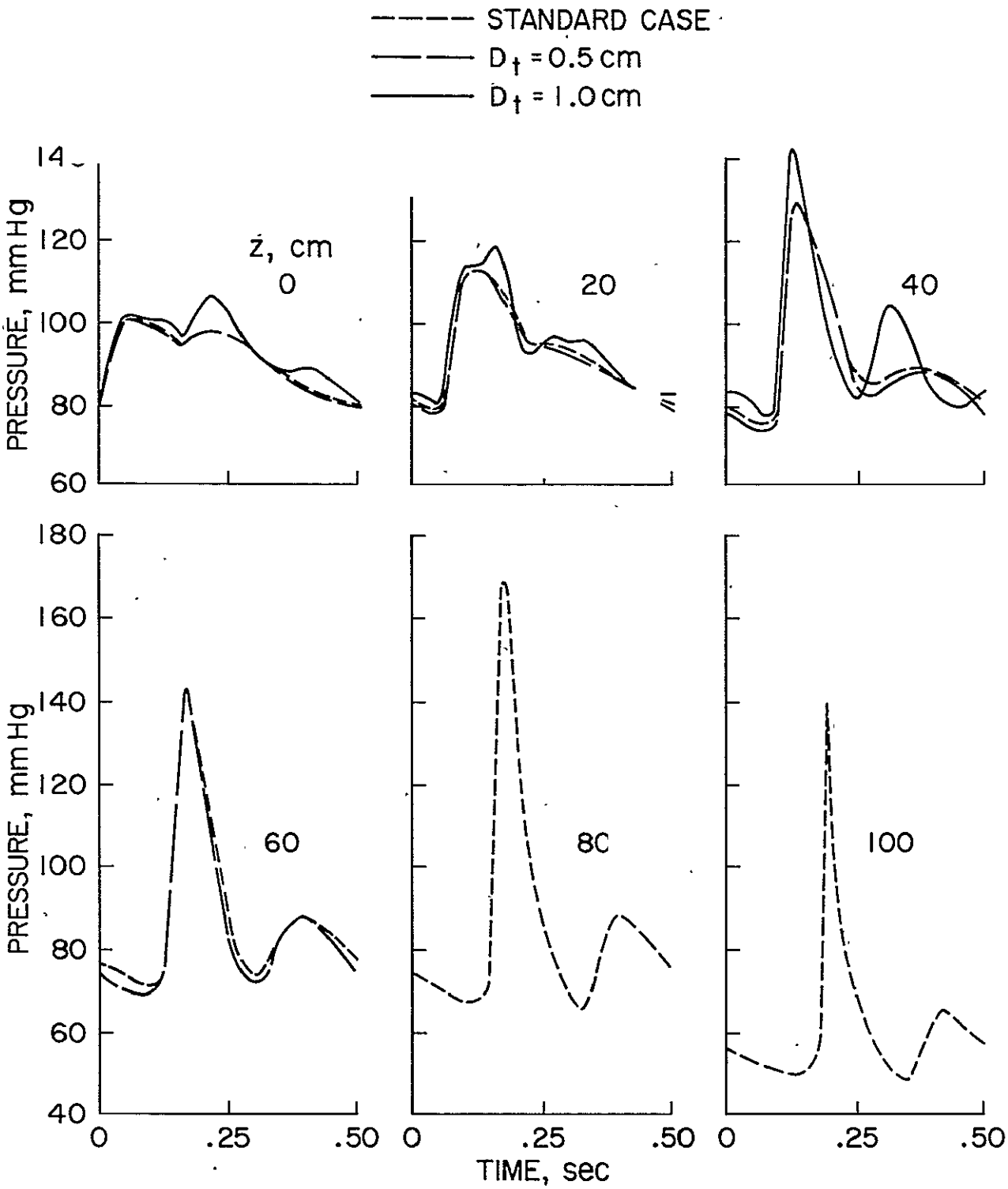

Figure 32. Pressure-time profiles obtained by specifying a peripheral resistance relation for different terminal diameters. The taper of the artery and other parameter values are the same as for the Standard Case.

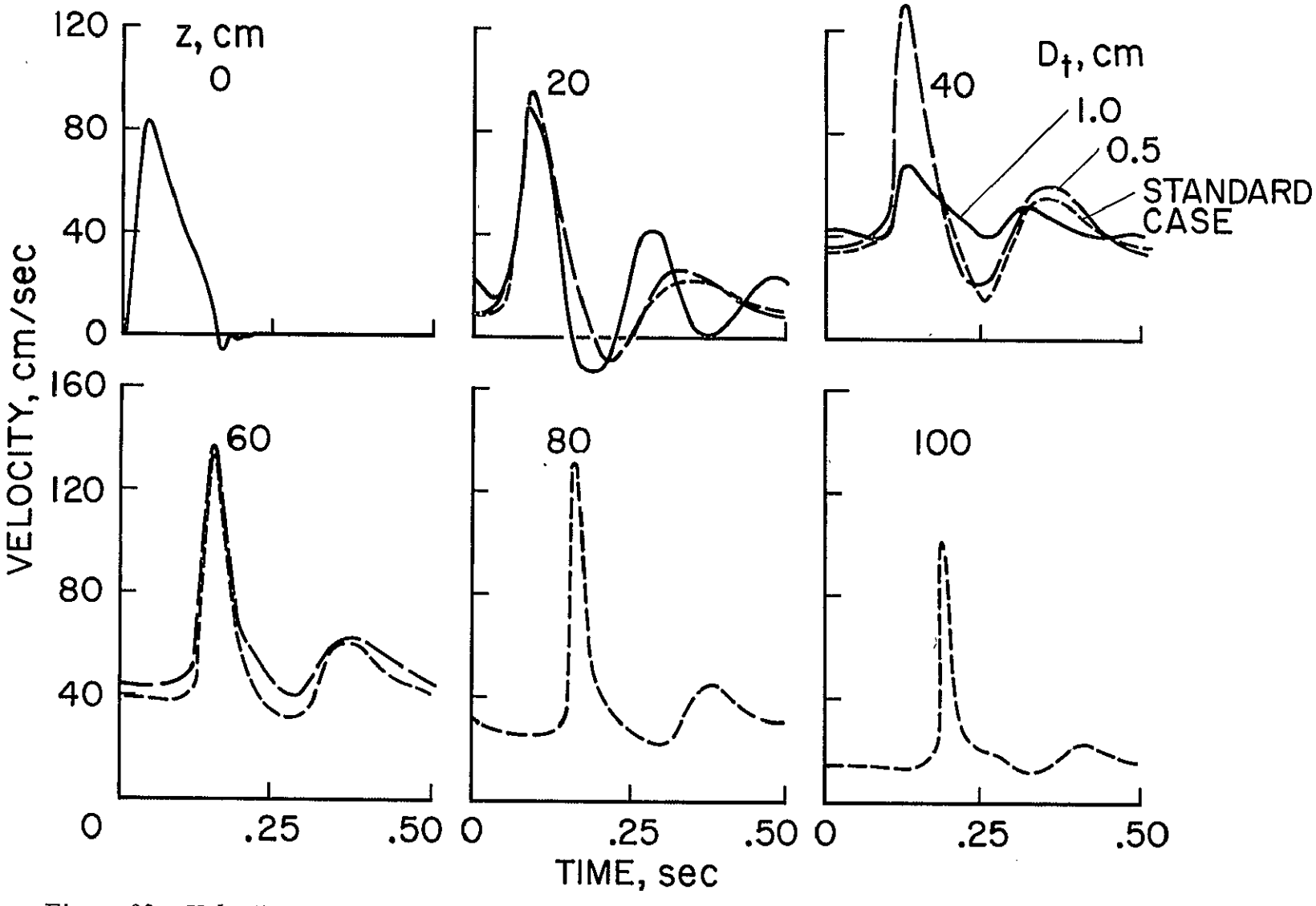

Figure 33. Velocity - time profiles corresponding to the pressure patterns shown in Figure 32, obtained by specifying a peripheral resistance relation at the distal end of the artery.

The pressure and flow velocity profiles for the case with a terminal diameter of 0.04 cm can not be distinguished within drawing accuracy from those for the Standard Case. The same is true for the artery with an end diameter of 0.1 cm. Hence for the mathematical model used here the concept of peripheral resistance appears to be a very good approximation for arteries with end diameters of 0.1 cm or less. For a terminal diameter of 0.5 cm the agreement is not as good. In this case we have deviations up to 4 mm Hg in pressure and up to 12 cm/sec in velocity.

When the terminal diameter is taken as 1.0 cm at $L = 40$ cm we note that extra waves begin to appear; the pressure and flow pulses are distorted and their magnitudes altered considerably. The peripheral resistance concept leads to results which can no longer be considered as acceptable approximations.

Within the framework of the mathematical model used here for the aorta and its continuation, the elementary concept of peripheral resistance appears to yield fairly accurate results provided that the terminal diameter does not exceed 0.5 cm. Since in our case this value is reached at a distance of 71 cm from the aortic valve, it appears that prescribing a peripheral resistance may not be advisable at any point of the aorta.

E. WAVE FRONT VELOCITY

It has been shown that the familiar features of the natural pulse generated by the heart are predicted by the present model. The wave front velocity offers another comparison between theory and experiment. To define a characteristic point of the wave front on which to base the calculations of the velocity from the transmission time over a given distance, a straight line was drawn tangent to the front of the pressure pulse at the location of maximum slope (inflection point). Another line was drawn tangent to the pressure curve

at the end of diastole preceding the beginning of the pulse. The intersection of these two lines was used as the characteristic point, whose speed is interpreted as the wave front velocity. The results for the pressure pulse of the Standard Case are shown in Figure 34.

McDonald[7] has published some data on the wave front velocities for a situation where the mean pressure was 121 mm Hg. After scaling his distances to correspond to the hypothetical dog considered here, those velocities are also given in Figure 34. The comparison of McDonald's values with the results from the Standard Case is generally satisfactory. However such a comparison is not strictly proper because the mean pressure of the Standard Case is only 88 mm Hg. Therefore an additional computer run was made using the parameters of the Standard Case except that the mean pressure was raised to 121 mm Hg by decreasing the outflow constant α. The larger wave speeds due to the higher pressures should naturally cause larger values of the wave front velocity and the calculations, also given in Figure 34, confirm this. Further, recent measurements taken in the canine ascending aorta[34] indicate that the wave front velocity averages 3.3 m/sec at pressures of 100 to 110 mm Hg. Assuming that a value of $\ell \cong 5$ cm characterizes the region of the ascending aorta, we see that this data point also agrees with the computer results given in Figure 34.

It seems that our mathematical model of the aorta can be used to predict actual wave front velocities with reasonable accuracy. Of course, it would be more meaningful to compare the velocities obtained by direct measurements on a dog with those predicted by our model on the basis of the physical and geometric parameters for the same dog.

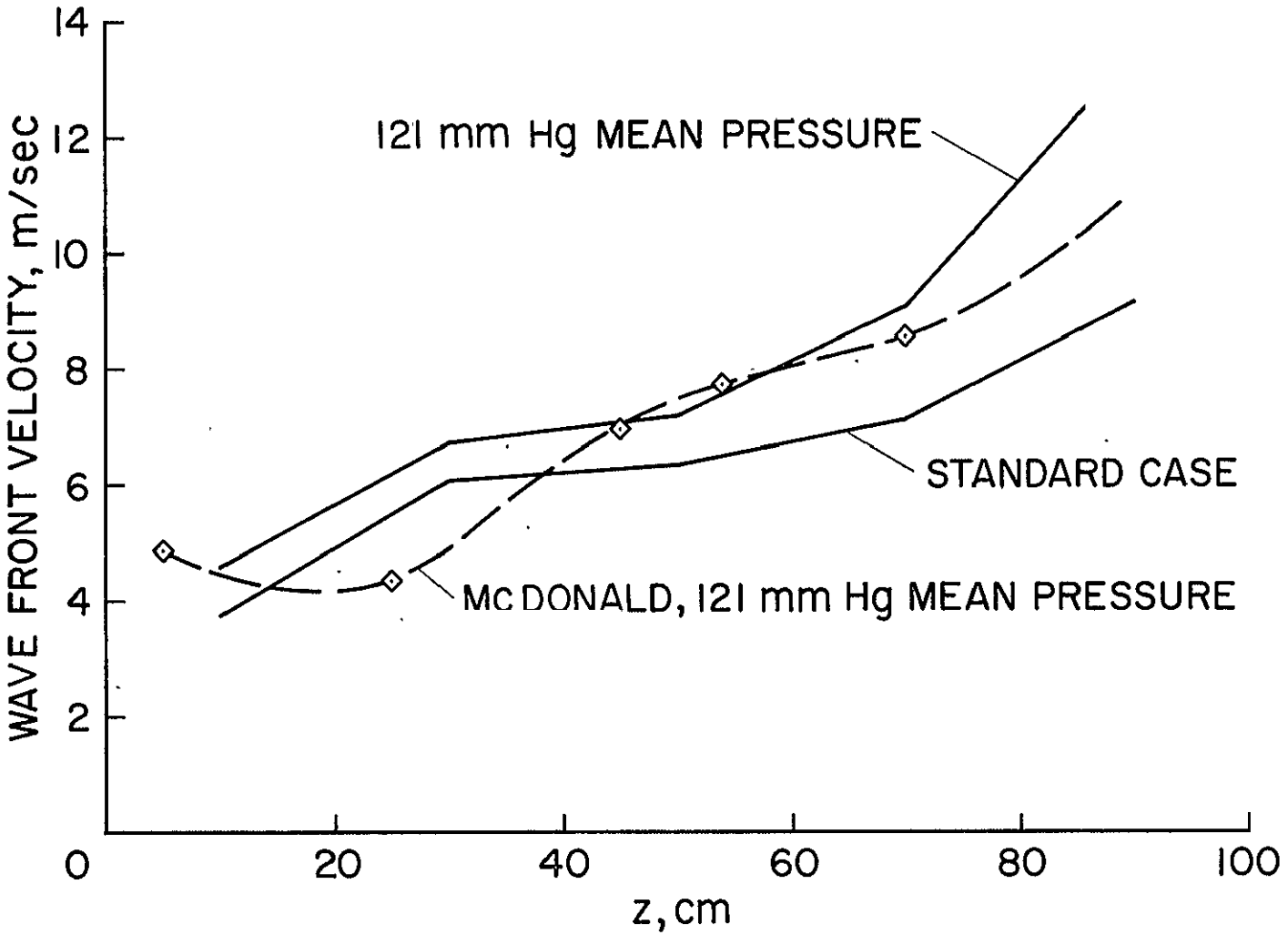

Figure 34. Wave front velocity of the pressure pulse as a function of distance from the aortic valve for the Standard Case (mean pressure = 88 mm Hg) and for a mean pressure of 121 mm Hg. Included for comparison is a curve extracted from Reference 7.

F. HARMONIC ANALYSIS

If we were dealing with a linear system, then a logical way to solve the present problem would be to first calculate the pressure and flow velocity pulses produced by sinusoidal ejections of blood from the heart. Superposition of the contributions from each harmonic of the actual cardiac ejection curve would then yield the actual spatial and temporal patterns of pressure and velocity.

As an approximation to the true situation, linear analyses of blood flow have been extremely popular in the past. Specific quantities which have been examined and interpreted by such linear analyses are the apparent phase velocity and impedance (defined as the ratio of the magnitudes of pressure and flow velocity) for each harmonic component. Numerous investigators have published plots of phase velocity and impedance as functions of frequency and have attempted to relate certain features of these plots to properties of the circulatory system. Although linear theories may have legitimate applications, we have sufficient evidence that we can not disregard nonlinear phenomena for our purposes.

Nevertheless we have decomposed the pressure and velocity profiles of the Standard Case into Fourier components at different locations along the artery and have computed the apparent phase velocities for pressure and flow velocity and also the impedance moduli and phase angles. The corresponding results are given in Figures 35 to 38. For comparison purposes we have also shown in Figure 37 an example of an impedance curve taken from in vivo measurements in the femoral artery of a dog[35].

The graphs in Figures 35 to 38 generally approximate the data given in the literature. This was to be expected since the pressure and flow pulses of the Standard Case and their shape change during propagation are reasonably close approximations of experimental observations.

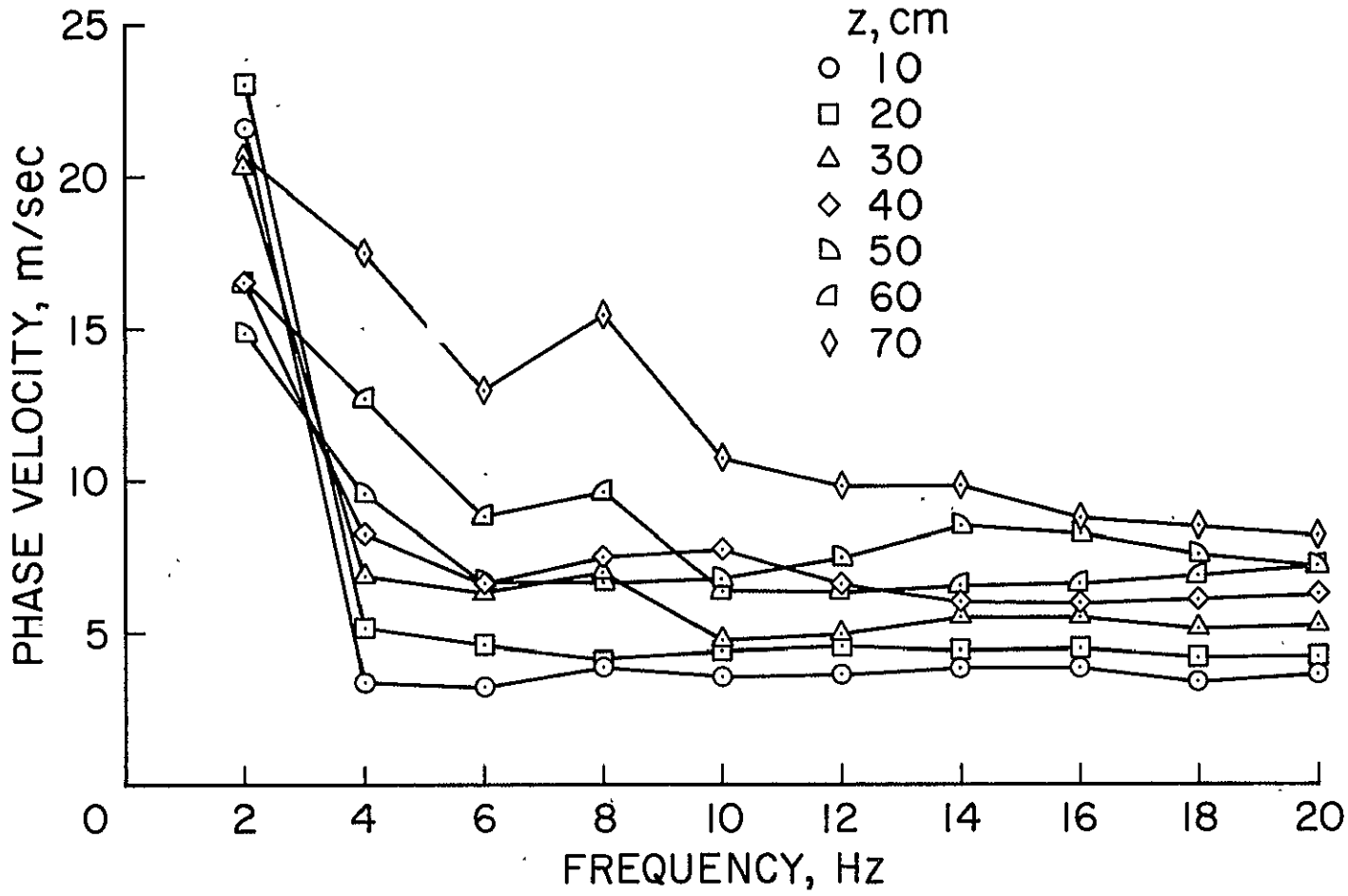

Figure 35. Apparent phase velocities as functions of frequency obtained by Fourier analysis of the pressure pulse of the Standard Case (heart rate 120 beats per minute) for different locations along the artery.

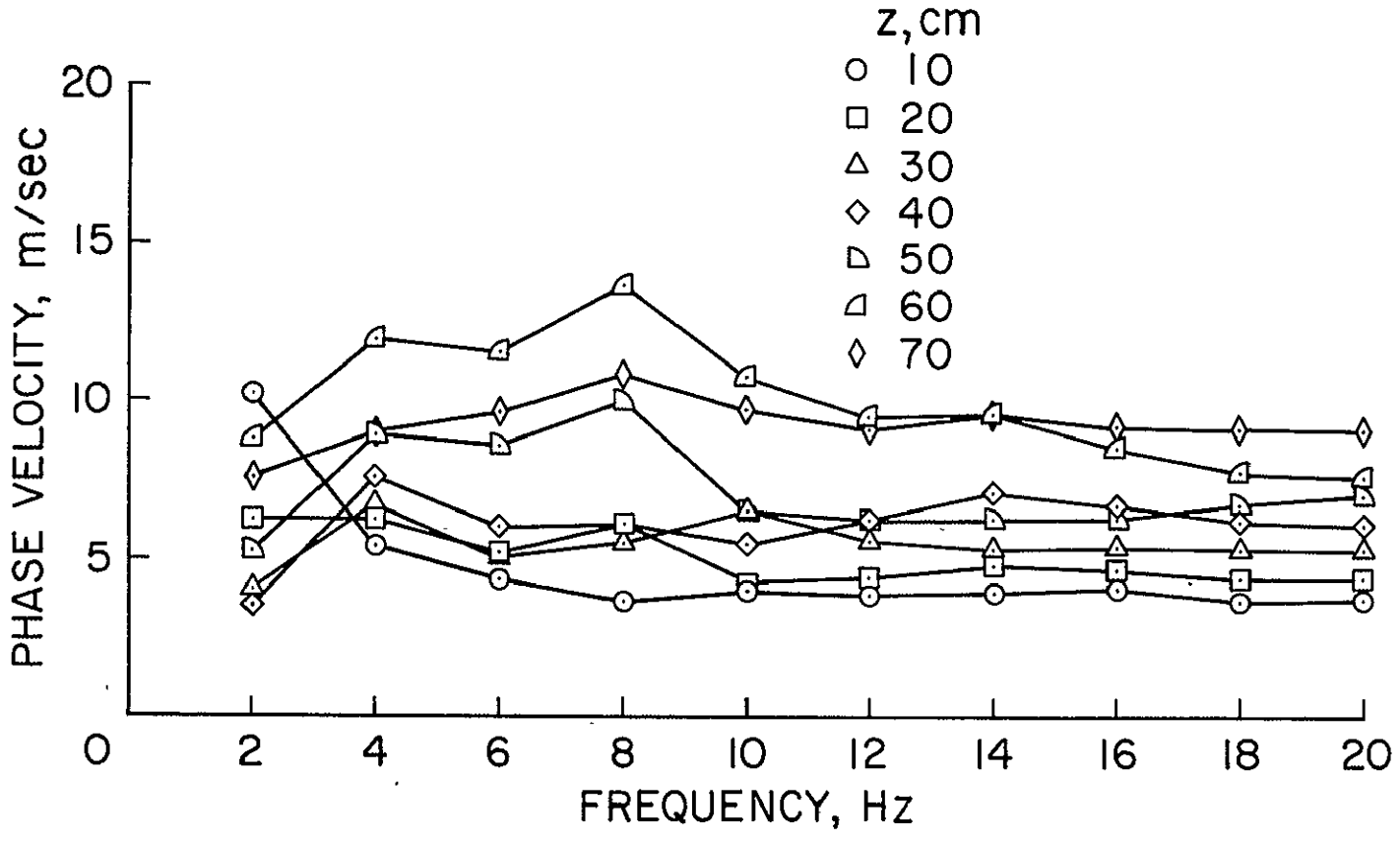

Figure 36. Frequency dependence of apparent phase velocity of flow pulse, calculated from the Standard Case.

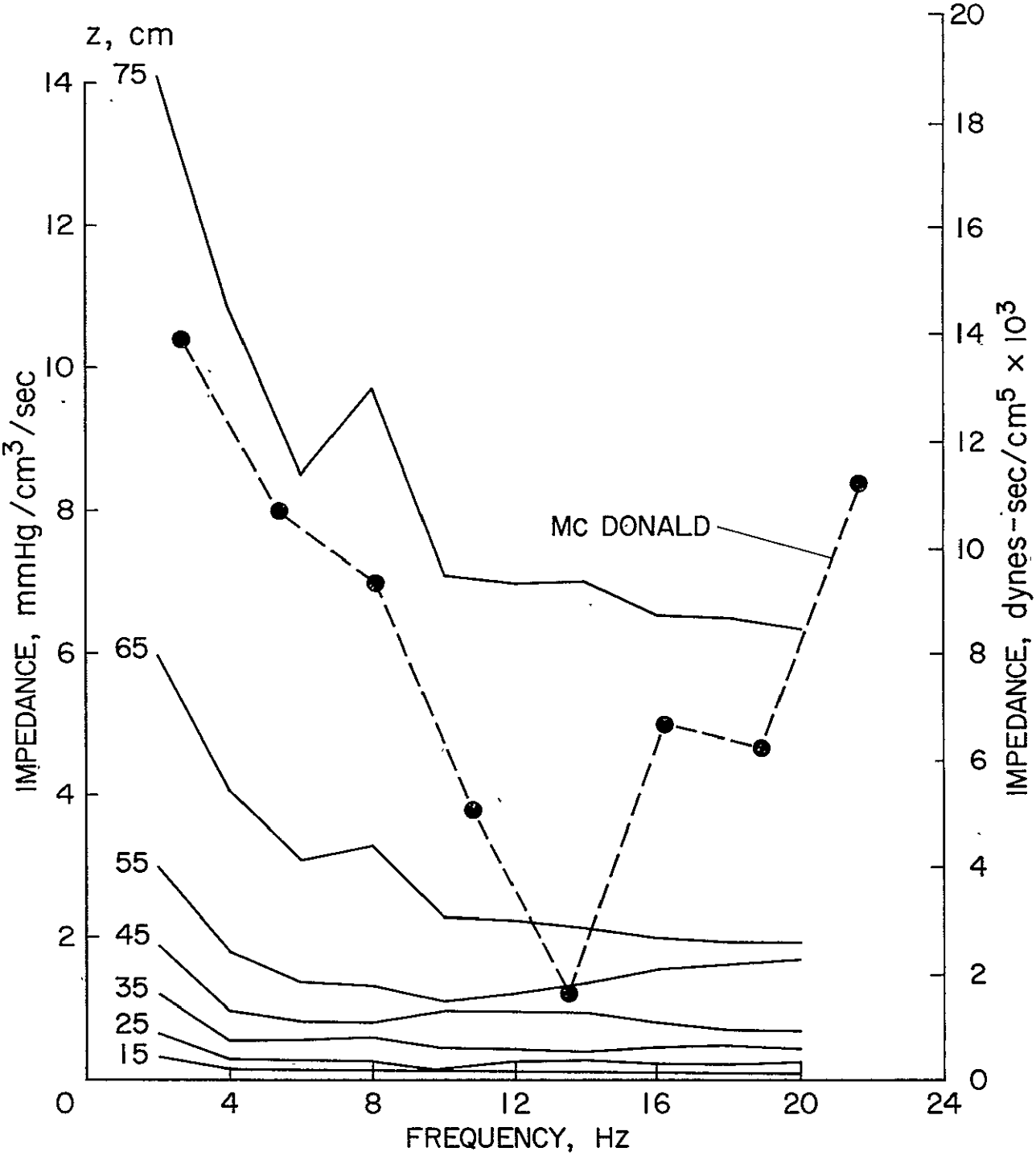

Figure 37. Frequency dependence of impedance modulus for different locations, determined by Fourier analysis of the pressure and flow pulses of the Standard Case. The dashed curve was obtained from measurements on the femoral artery of a dog.[35]

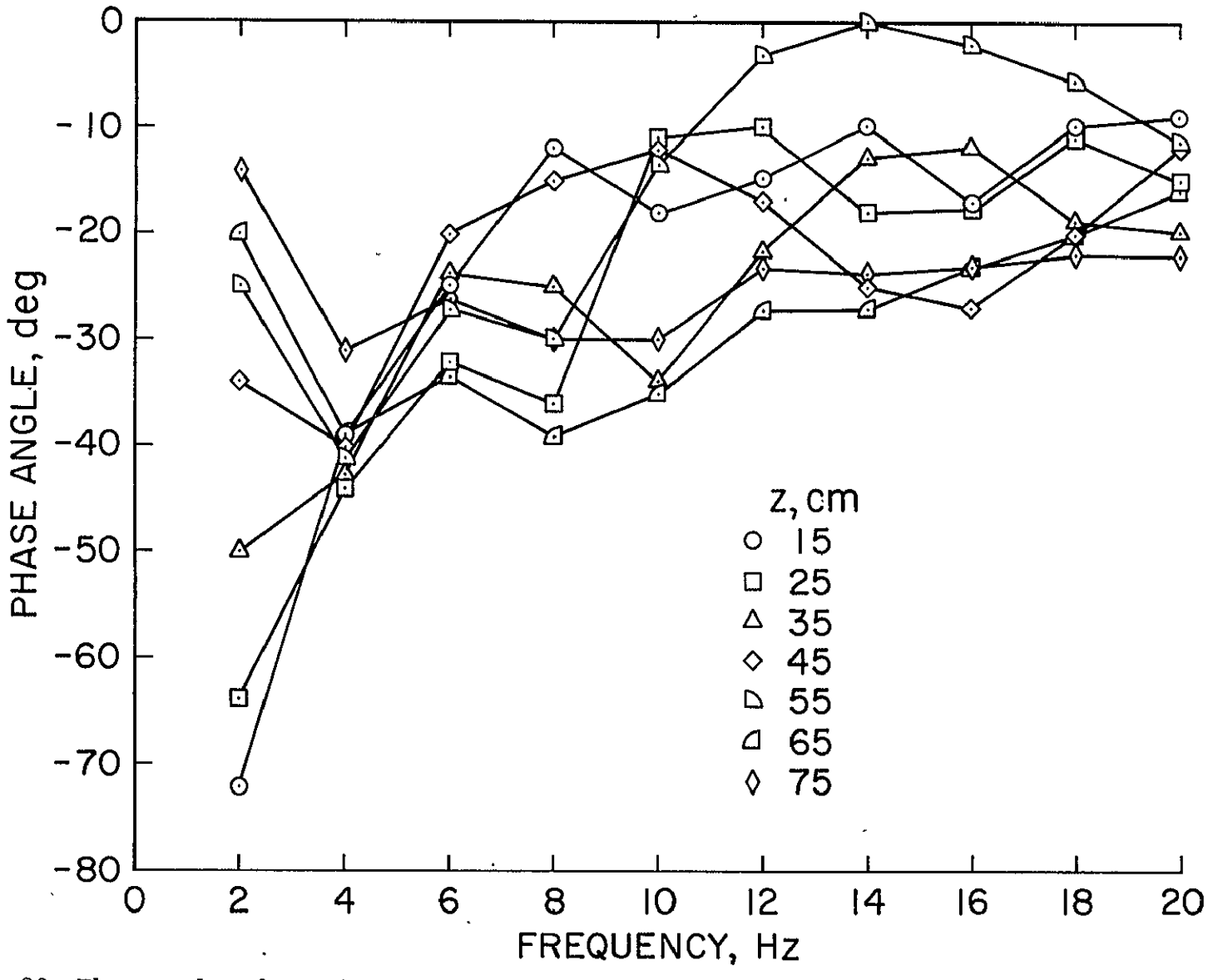

Figure 38. Phase angles of impedances corresponding to moduli given for the Standard Case in Figure 37 and different distances from the heart. A negative phase angle means that the flow leads the pressure.

G. TWO LIMITING CASES OF ARTERIAL WALL PROPERTIES

The effect of the elastic properties of the arterial wall is accounted for in the specification of the wave speed as a function of distance and pressure. Thus, in order to assess the consequences of alternative models we must change the form of the wave speed function. Specifically we intend to inquire into the characteristics associated with a rigid artery, and also one which is distensible but whose wave speed is independent of pressure.

A rigid wall has no distensibility, and so according to Equation (10) the wave speed should be infinite. However we have ignored so far the compressibility of blood in this analysis, and if the wall is rigid this property can no longer be neglected. Since the wave speed is the speed of propagation of small signals relative to the medium at rest, the wave speed for a compressible fluid is equal to the speed of sound in the fluid. Accordingly we choose $c = 1.5 \times 10^5$ cm/sec as the wave speed relation for a rigid arterial wall. Keeping all other parameters of the Standard Case unchanged we obtain the results displayed in Figures 39 and 40. Although the pressures are very much elevated due to the nondistending walls the velocity magnitudes remain at reasonable levels. Both profiles follow the shape of the ejection curve very closely.

For the case of a wave speed which is independent of pressure, one of the sources of nonlinearity is removed. However, the Moens-Korteweg equation (Appendix A) indicates that the elastic modulus of the arterial wall will still increase with pressure, since the thickness-to-radius ratio decreases as the wall becomes more distended. An artery with constant elastic modulus would display a wave speed relation which decreases with increasing pressure.

Using as the wave speed function that of the Standard Case with $P = 88$ mm Hg and leaving all other parameters defining the Standard Case

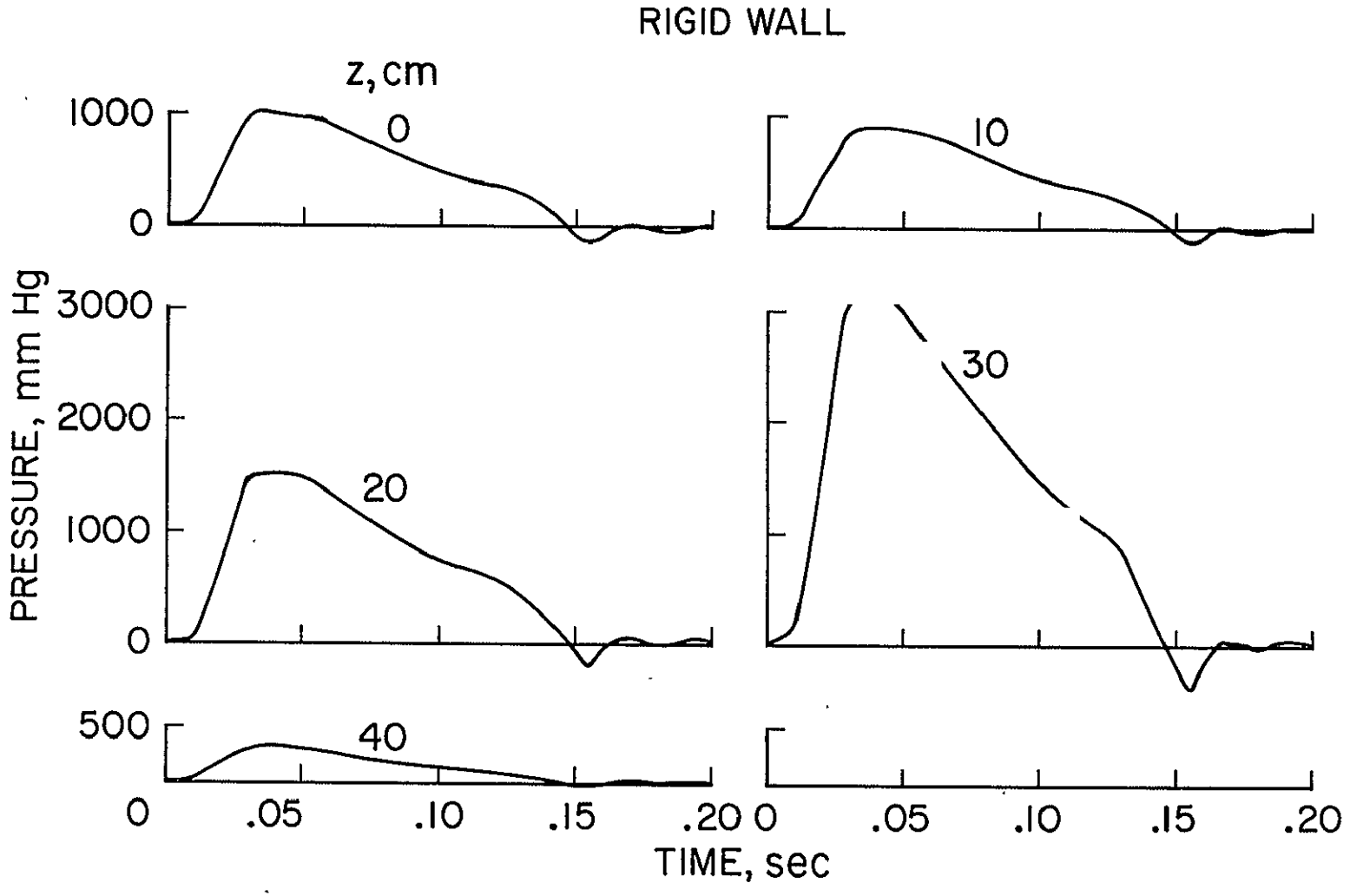

Figure 39. Pressure profiles for a rigid artery. As wave speed we have taken the speed of sound in blood, $c = 1.5 \times 10^5$ cm/sec. Otherwise the conditions are the same as in the Standard Case.

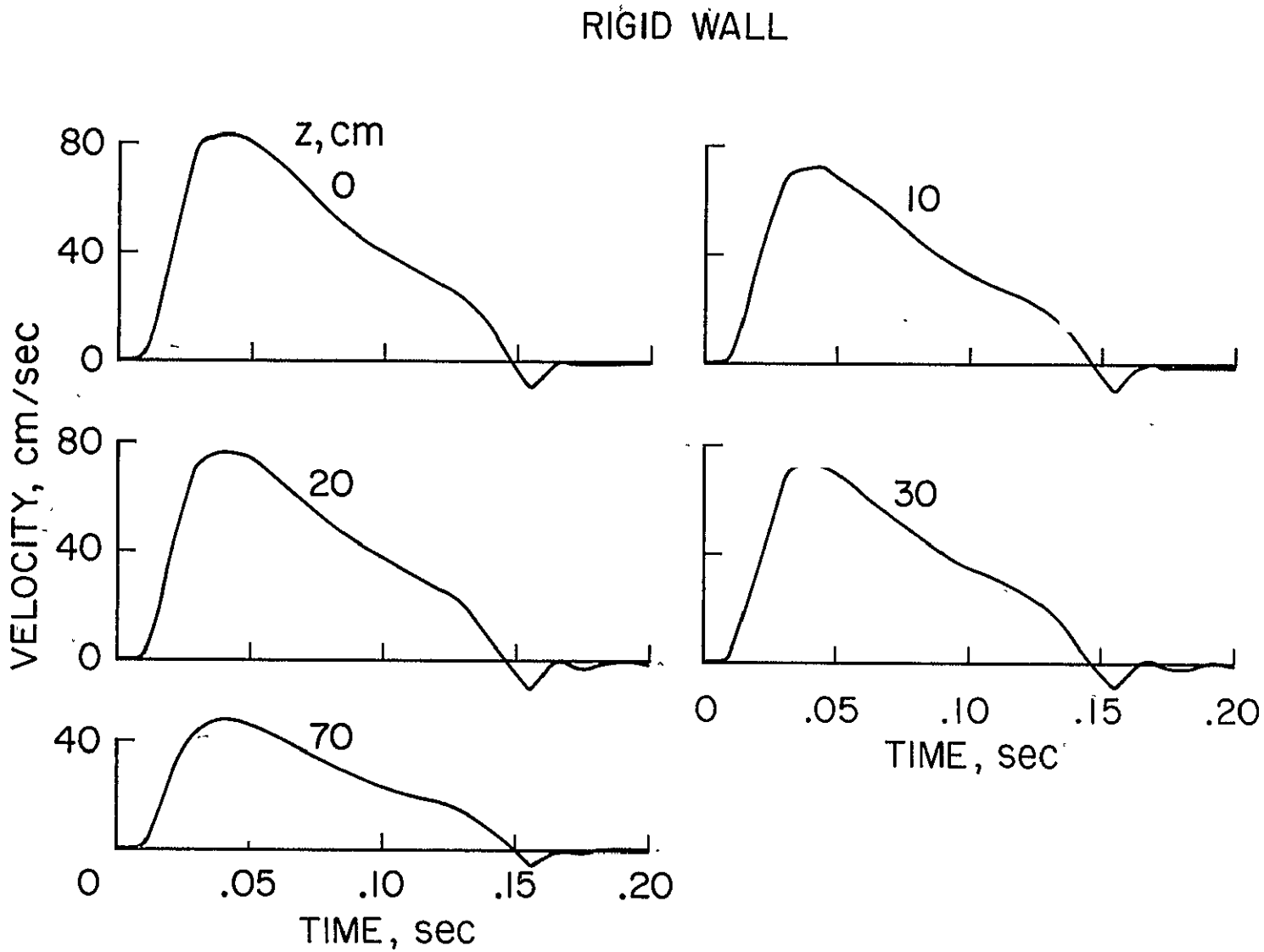

Figure 40. Velocity profiles for a rigid artery. As wave speed we h
$c = 1.5 \times 10^5$ cm/sec. Otherwise the conditions are the sa

unaltered we find the pressure and flow patterns given in Figures 41 and 42. The pressures are not significantly affected by this assumption, but they are somewhat lower. Also, the changes in the slopes of the pulses are analogous to those noted in the linearized treatment (see section IVB) and can be explained by the same reasoning. As in the linear solution the dicrotic wave is larger than in the Standard Case. This may again be caused by the fact that for large distances from the heart the pressure of 88 mm Hg assumed in the wave speed function exceeds the mean pressures of the Standard Case. Hence the distensibility of the distal portions of the artery is also reduced here and would tend to intensify any reflections.

H. EFFECT OF GENERALIZED VASOCONSTRICTION AND VASODILATATION

Generalized vasoconstriction and vasodilatation relative to the Standard Case can be simulated in the model by altering the resistance to outflow through the outflow constant α . This is only a partial simulation because the diameter of the artery of interest was kept constant. If we select a smaller value for α we produce a vasoconstriction which in turn should cause an increase in the mean pressure and in the pulse pressure because less blood is being removed from the artery while the stroke volume is the same as before. The pressure rise should lead to larger wave speeds and therefore pulses which travel somewhat faster. For vasodilatation the effects must be antithetic.

These expectations are corroborated by Figures 43 and 44 where the outflow constant α was changed by $\pm 15\%$. The Standard Case is also plotted for comparison purposes and naturally falls between the two sets of curves illustrating the effects of vasodilatation and constriction. From Figure 44 we conclude that the pressure rise induced by increasing the outflow resistance has apparently caused a sufficiently large distension of the proximal aorta to lower the peak and mean flow velocities.

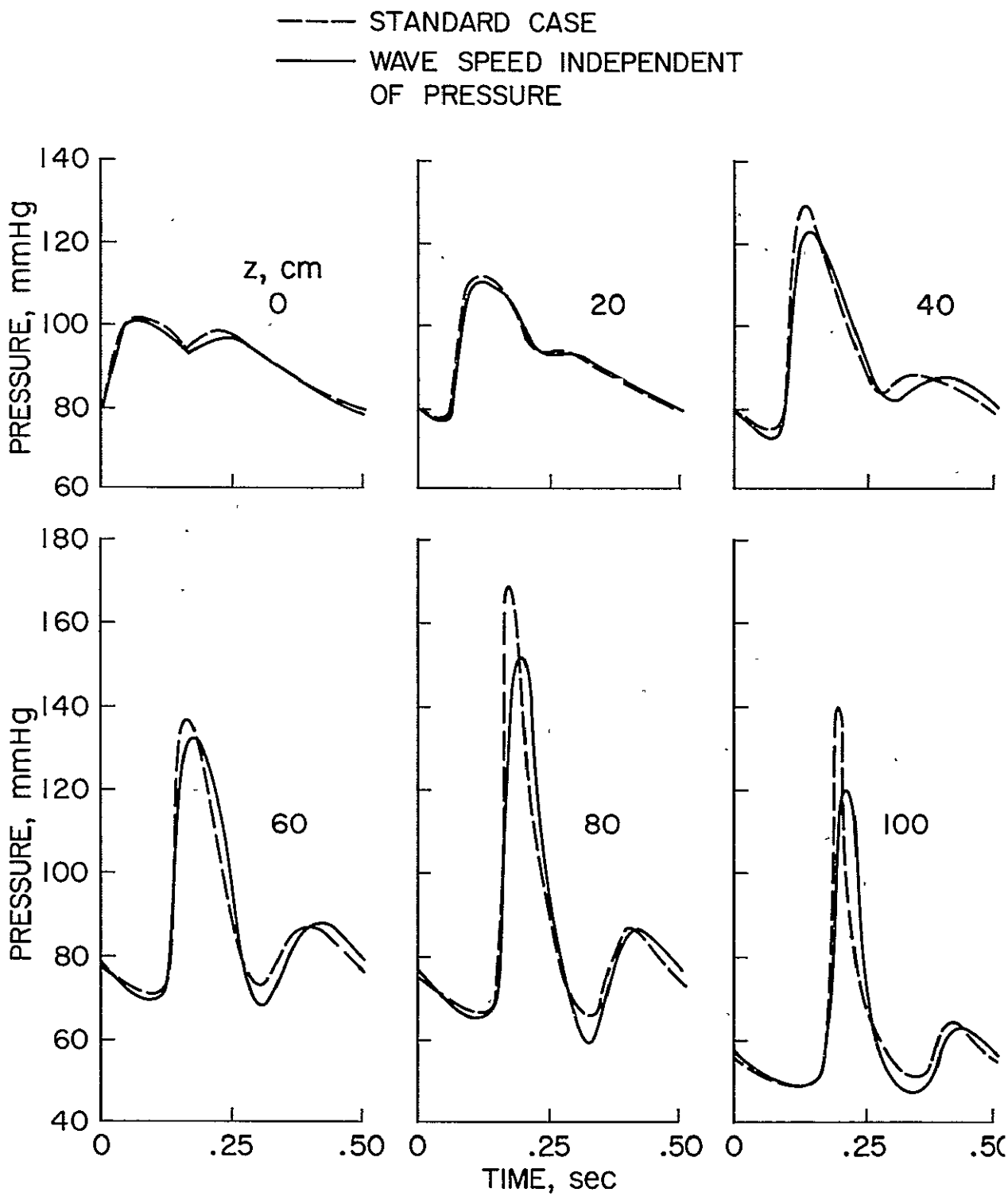

Figure 41. Changes in the pressure pulse produced by replacing the wave speed in the Standard Case by that corresponding to $p \equiv 88$ mm Hg. Otherwise the solution accounts for all nonlinear phenomena considered here.

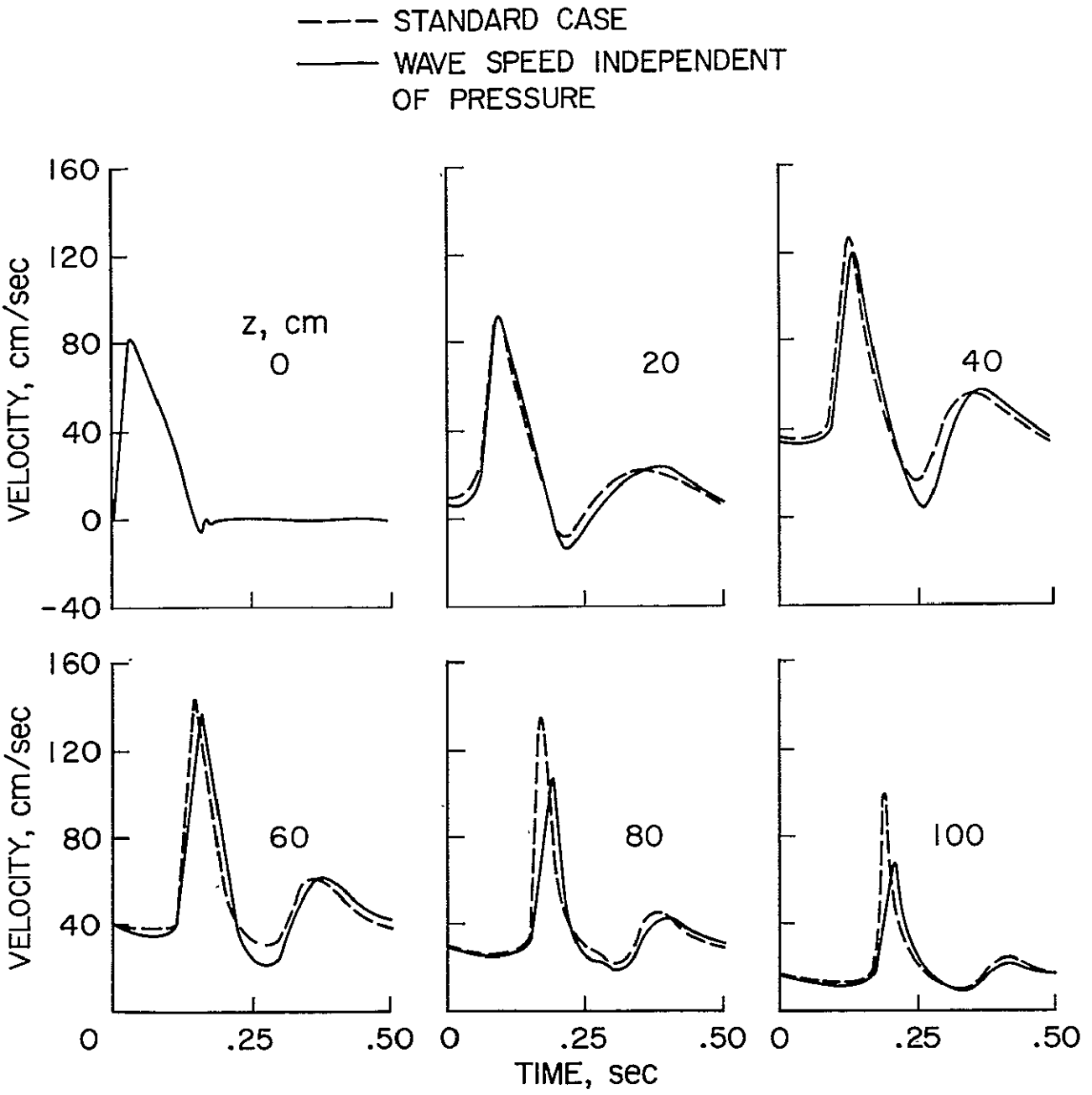

Figure 42. Flow velocity pulse produced by replacing the wave speed in the Standard Case by that corresponding to p ≡ 88 mm Hg.

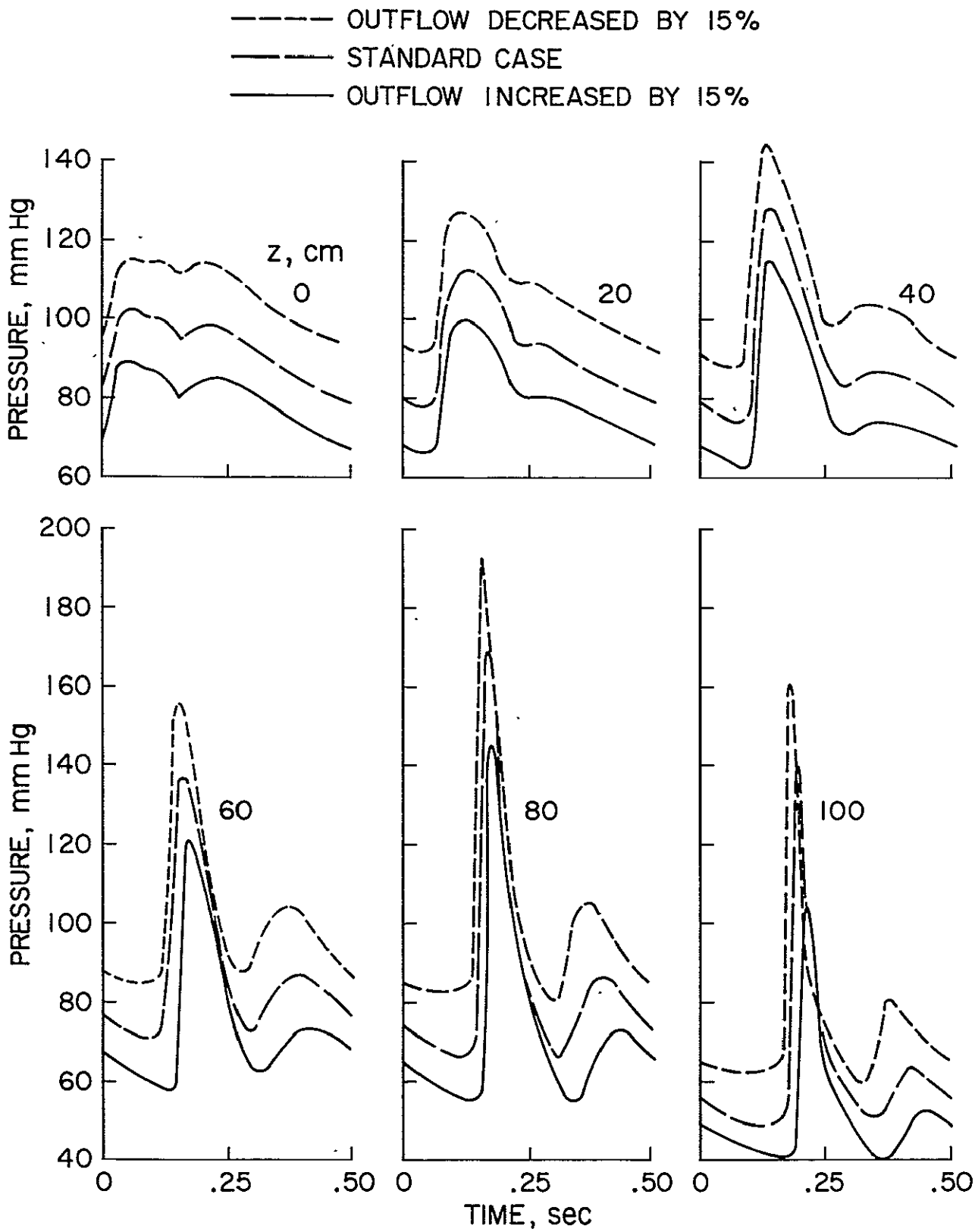

Figure 43. Effects of generalized vasoconstriction and vasodilatation on the pressure pulse produced by changing the outflow constant α by $\pm 15\%$ in the Standard Case.

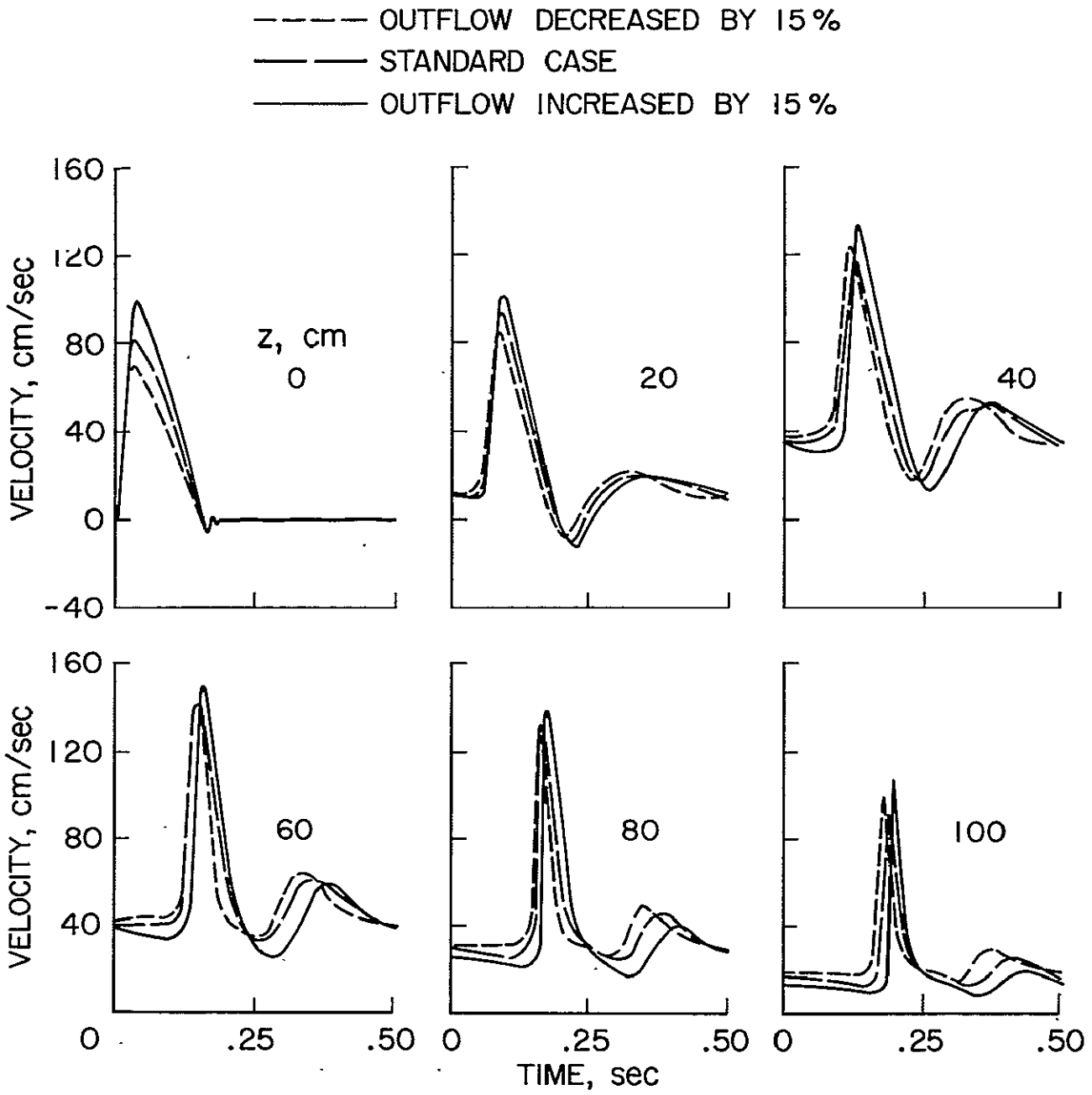

Figure 44. Velocity patterns for generalized vasoconstriction and vasodilatation produced by changing the outflow constant α by $\pm 15\%$ in the Standard Case.

I. EFFECT OF CARDIAC ARREST

Cardiac arrest was simulated by setting the cardiac ejection rate to zero after steady state was reached for the Standard Case. The results are given in Figure 45 and show the presence of small fluctuations in pressure and velocity after the ejection has ceased. It appears that these fluctuations including the dicrotic wave are manifestations of multiple reflections of the primary wave. But the dicrotic wave or any other wave can not be interpreted as a simple reflection at a discrete site because all pressure and flow peaks or valleys tend to appear later in time as the pulse travels down the artery. Retrograde waves should appear earlier in the distal and later in the proximal regions. No distinct retrograde waves can be discerned in Figure 45. The reflection mechanisms which seem to be responsible for the development of the dicrotic wave have yet to be identified in a quantitative manner.

J. A QUIESCENT STATE AS INITIAL CONDITIONS

If we are interested in steady state pressure and flow profiles the choice of initial conditions is not crucial. However, in order to minimize the computations we have regularly prescribed the initial conditions in terms of guesses for the ultimate end-diastolic pressures and flow. It was generally found that for all practical purposes the actual steady state condition was reached after two heart beats when the end-diastolic pressure at the heart was estimated to within a few mm Hg and when the end-diastolic velocity pattern of the Standard Case was used as the initial velocity distribution.

In a few situations however, initial conditions may be pertinent, for example, in determining the response of the cardiovascular system to renewed cardiac activity following a state of cardiac arrest. We now consider such a situation and assume that the period of cardiac arrest is sufficiently long to

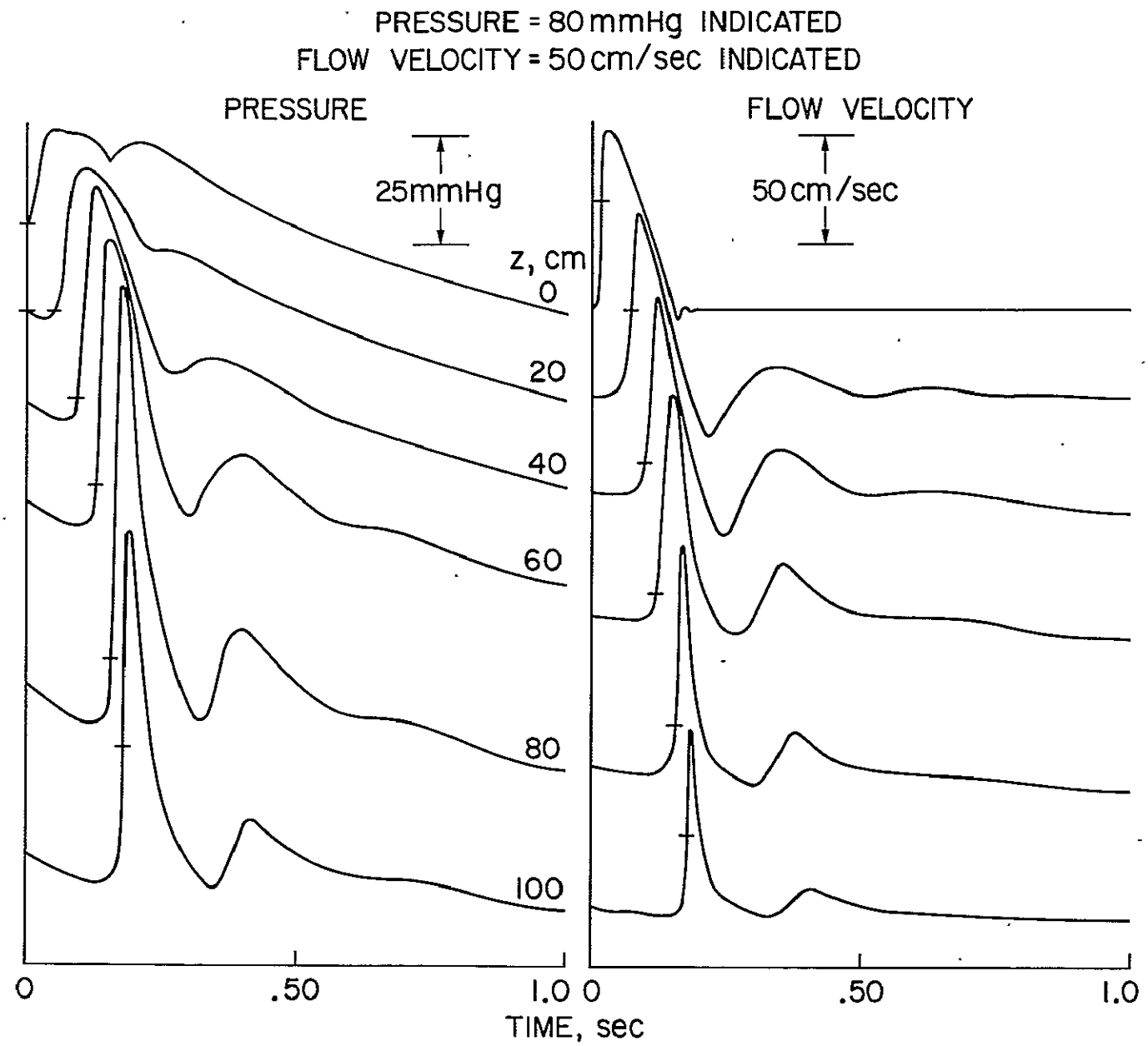

Figure 45. Effect of cardiac arrest on the pressure and flow patterns of the Standard Case.

produce in our model a quiescent state characterized by zero velocity and a pressure of 25 mm Hg (= p_c so that there is no outflow) everywhere in the artery. With such a quiescent state as initial conditions and for cardiovascular parameters corresponding to the Standard Case, we have computed the pressure and flow patterns over several heart beats.

Figures 46 and 47 show the gradual return of the pressure and flow to steady state profiles. The approach to steady state appears to be roughly exponential. After five heart beats the transient response still differs by perhap 5 mm Hg in pressure and by about 5 cm/sec in velocity from the steady state values. However, life-sustaining pressures are evidently attained already after two or three heart beats.

There are significant differences between the shapes of the profiles during the first cardiac ejection, and those occurring later. Most striking is the large velocity pulse in the vicinity of the heart which can only be explained in terms of the narrowing of the aortic cross section at lower pressures (see also Appendix B). We also notice intervals of relatively large negative flows during the first few beats. In addition, the dicrotic wave occurs later relative to the primary pulse during the first few beats in this numerical experiment. By interpreting the dicrotic wave as a manifestation of some reflection phenomena, this delay may be attributable to the lower wave speeds associated with the lower pressures in the beginning.

K. AORTIC INSUFFICIENCY AND SHOCK WAVES

It has already been noted that the system of one-dimensional differential equations for blood flow is hyperbolic, just as is the system of equations for the supersonic flow of a compressible fluid. Since the occurrence of shock waves is a familiar feature in high-speed compressible flow, it is

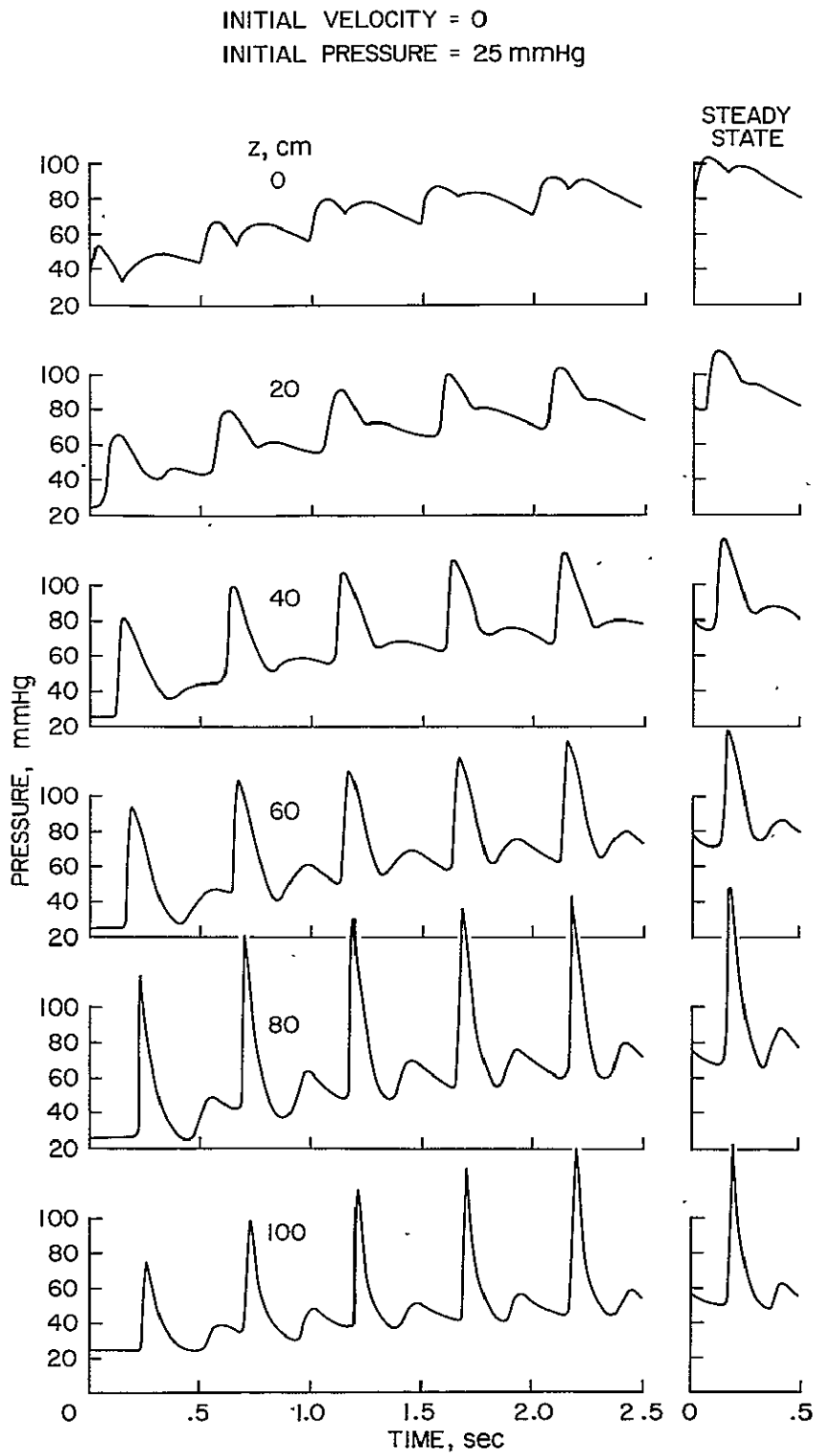

Figure 46. Pressure profiles for the Standard Case caused by a normal cardiac ejection pattern after a period of cardiac arrest sufficiently long to produce a quiescent state.

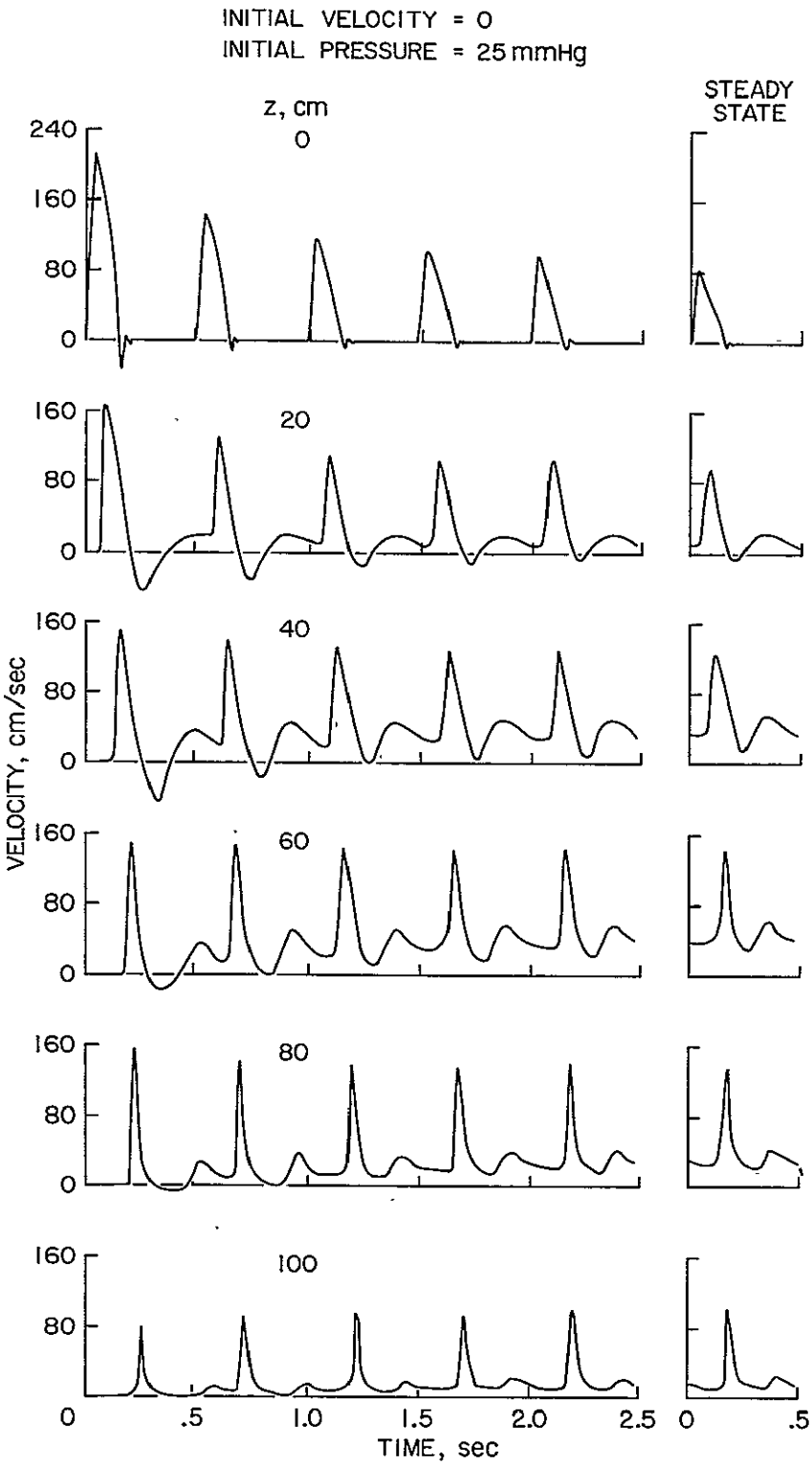

Figure 47. Velocity profiles for the Standard Case caused by a normal cardiac ejection pattern after a period of cardiac arrest sufficiently long to produce a quiescent state.

reasonable to ask under what conditions similar phenomena could occur in the cardiovascular system. Reality does not allow for true discontinuities. However we can envision shock waves in the form of abrupt rises in pressure and flow or spike-type perturbations which may evolve from relatively gradual changes in pressure.

While we have noted the steepening of the pressure wave for the Standard Case with increasing distance from the aortic valve, under normal conditions the pressure pulse generated by the heart is not sufficiently steep or strong to produce a shock wave within the dimensions of the body. However, in the case of an incompetent aortic valve (aortic insufficiency) the situation is quite different. The large amount of backflow associated with a leaking valve would reduce the normal net cardiac output per beat unless the size of the heart and the gross ejection volume are increased. A larger heart, and correspondingly larger positive and negative flow rates, are indeed clinically observed in patients with aortic insufficiency. Finally, any increase in the ejection volume for a given systolic time interval produces pressure pulses which are steeper and stronger than normal, and can therefore generate shock waves within a shorter distance from the heart.

Lacking actual recordings of cardiac ejection patterns in instances of aortic valve incompetence, we have assumed the ejection rate function shown in Figure 48. We arrived at this function by utilizing the information given in Reference 36 according to which regurgitation can exceed 80% of the net aortic flow. Also the diastolic pressure at the heart should be of the order of 40 mmHg or less to allow for the filling of the ventricle with oxygenated blood from the lung. In addition, we have kept the shape of the ejection curve approximately the same as in the Standard Case for the positive ejection phase of the cardiac cycle;

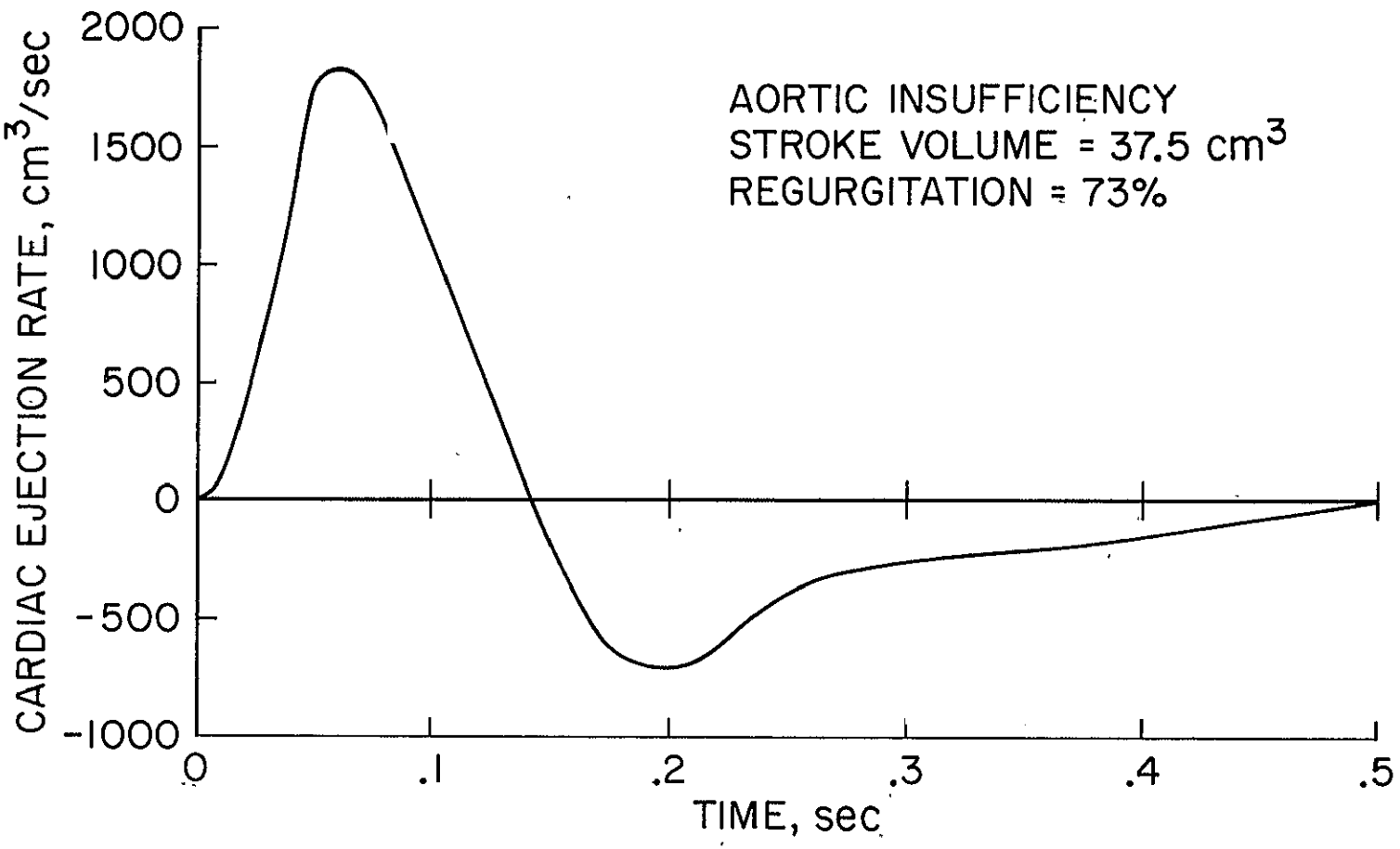

Figure 48. Hypothetical cardiac ejection rate pattern simulating aortic insufficiency. Amount of regurgitation is 73% of the gross stroke volume. Heart Rate 120 beats/minute.

but we increased the net stroke volume from 30 to 37.5 cm^3. All other cardiovascular parameters are identical with those of the Standard Case.

Since the peak ejection rate is much higher we expect a marked increase in pulse pressure as well as a much steeper wave front at the heart. Also, the inordinate regurgitation through the incompetent valve should cause significant backflow over a large segment of the aorta.

These predictions are verified by the computed results which are shown in Figures 49 and 50 together with the Standard Case. While normally the pressure remains elevated behind shock waves encountered in supersonic flow problems, it decays rapidly in our case due to the reversal in slope of the cardiac ejection curve and due to the outflow.

For many years, it has been observed clinically that the so-called pistol shot phenomenon is associated with aortic valve incompetence. This phenomenon manifests itself with a sharp pulse which can actually deflect the palpating fingers at the radial or femoral artery. We can readily demonstrate that the pistol shot sounds must be generated locally. They can not emanate from the heart, because they would be dissipated long before they could reach the extremities by the damping mechanism provided by the viscoelasticity of the arterial wall. The origin of the term "pistol shot" stems from the sharp cracking sound heard through a stethoscope placed at the site.

Just as an ordinary shock wave induces audible vibrations in air, the large and rapid rise in pulse pressure noted in Figure 49 can be expected to induce vibrations in the elastic arterial wall. When these vibrations are within the audible frequency range and have a sufficiently large amplitude then they would represent a sound. Since the pressure pulse has a very peaked and narrow shape and is traveling at a speed of 5 to 15 meters per second, such a sound

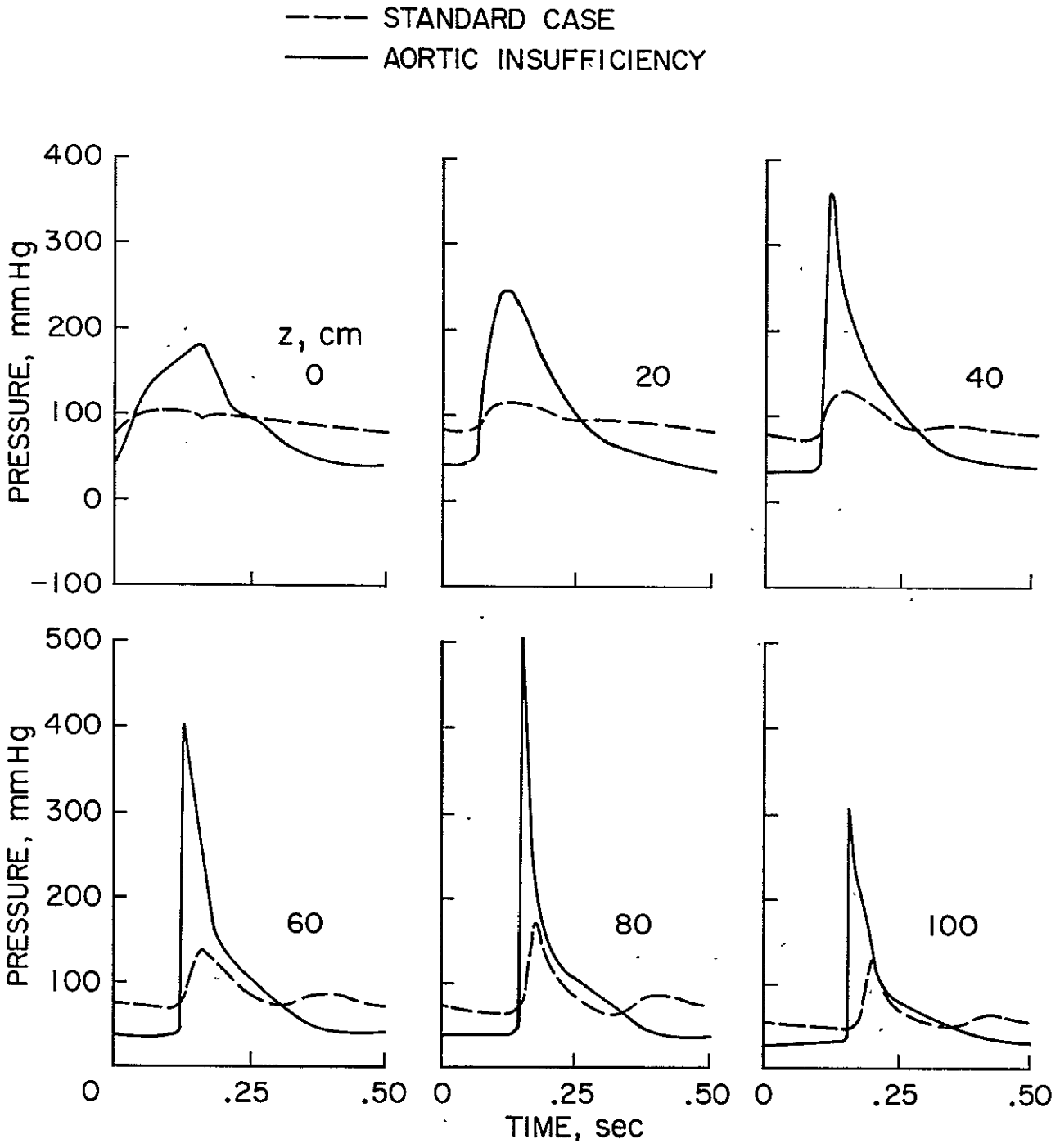

Figure 49. Pressure profiles for hypothetical aortic insufficiency corresponding to cardiac ejection rate given in Figure 48. Other parameter values are those for the Standard Case. First indication of a shock wave is suggested by the steepness of the pressure front at 40 cm from the heart.

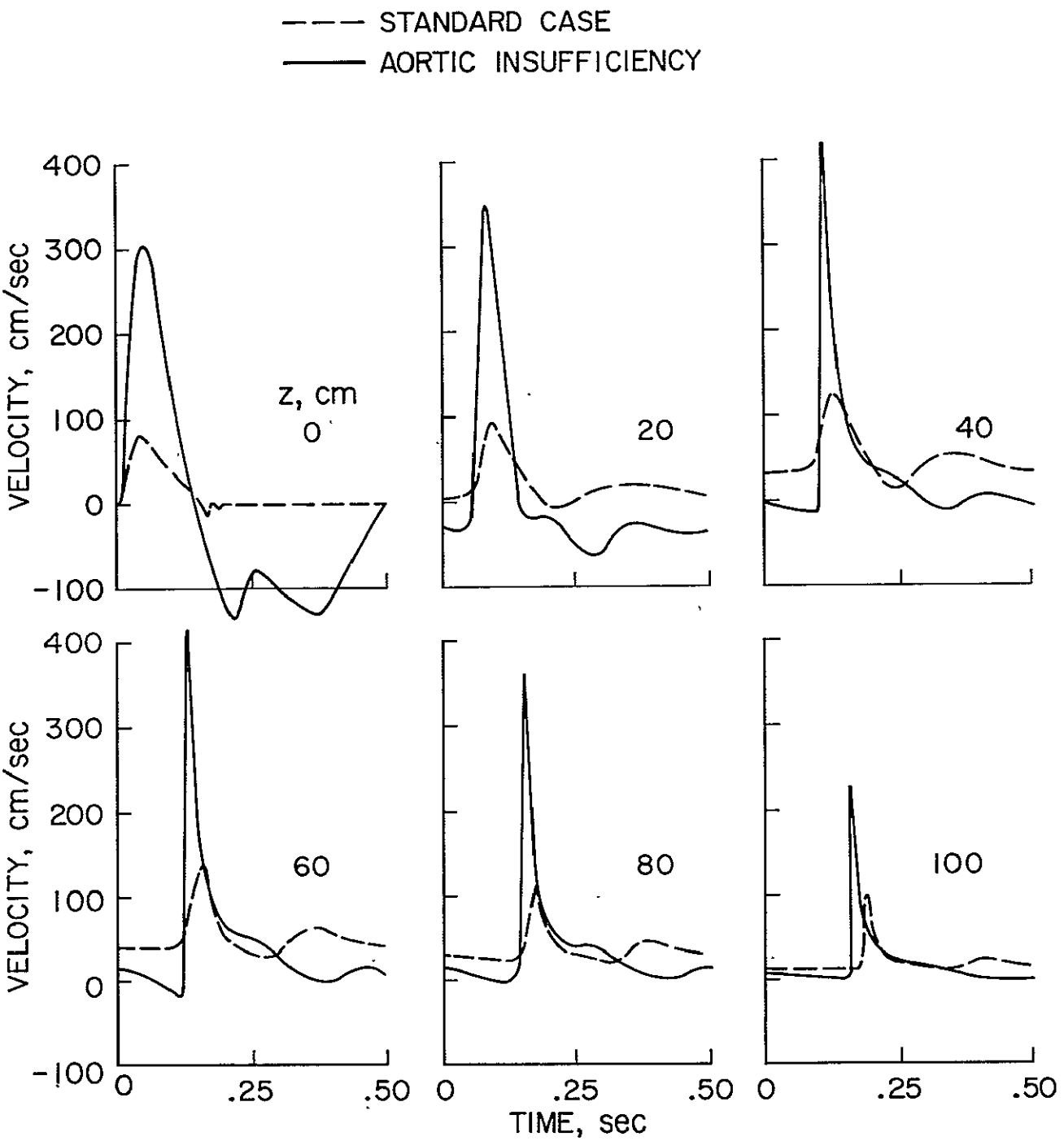

Figure 50. Velocity profiles for hypothetical aortic insufficiency corresponding to the pressure profiles of Figure 49. The flow pattern for $z=0$ does not faithfully reproduce the ejection pattern imposed on the system and given in Figure 48. The apparent discrepancy however vanishes when we multiply the instantaneous flow velocity by the corresponding cross-sectional area. Our model allows for the variation of the cross-sectional area at the root of the aorta with pressure.

should be of very short duration. The findings here are in apparent agreement with clinical observations on the characteristics of the pistol shot sounds.

Although we have been discussing the arterial pistol shot, a similar occurrence can arise on the venous side of the heart if the tricuspid valve is incompetent[22]. The venous pistol shot is normally detected over the jugular and femoral veins.

Figure 51 shows the development of the shock wave from a different viewpoint where we have plotted the local pressure gradient as a function of time on an expanded scale. (The local time rate of change of pressure $\frac{\partial p}{\partial t}$ would show similar features.) The differences from the Standard Case are very evident. For x = 100 and 120 cm the gradient $\frac{\partial p}{\partial x}$ does not return immediately to zero because the pressure here is decreasing with distance.

The difference in the travel times for the shock wave and the pressure pulse of the Standard Case is particularly noticeable in Figure 51. It is caused in part by the nonlinear effects of the variation of signal speed with pressure and velocity.

We can estimate the "thickness" of the shock wave by multiplying the speed at which the wave travels relative to the fluid by the time necessary for its passage. The former can be approximated by the wave speed at the average pressure of the pulse, and the latter by the time interval during which the local pressure gradient exceeds 10% of its maximum value. Table 3 shows the results for this calculation.

In compressible flow problems the shock wave thicknesses are extremely small compared to the physical dimensions of the bodies involved. The thicknesses given in Table 3 are much larger, of the order of ten times the arterial diameter. They also indicate that the shock wave does not form

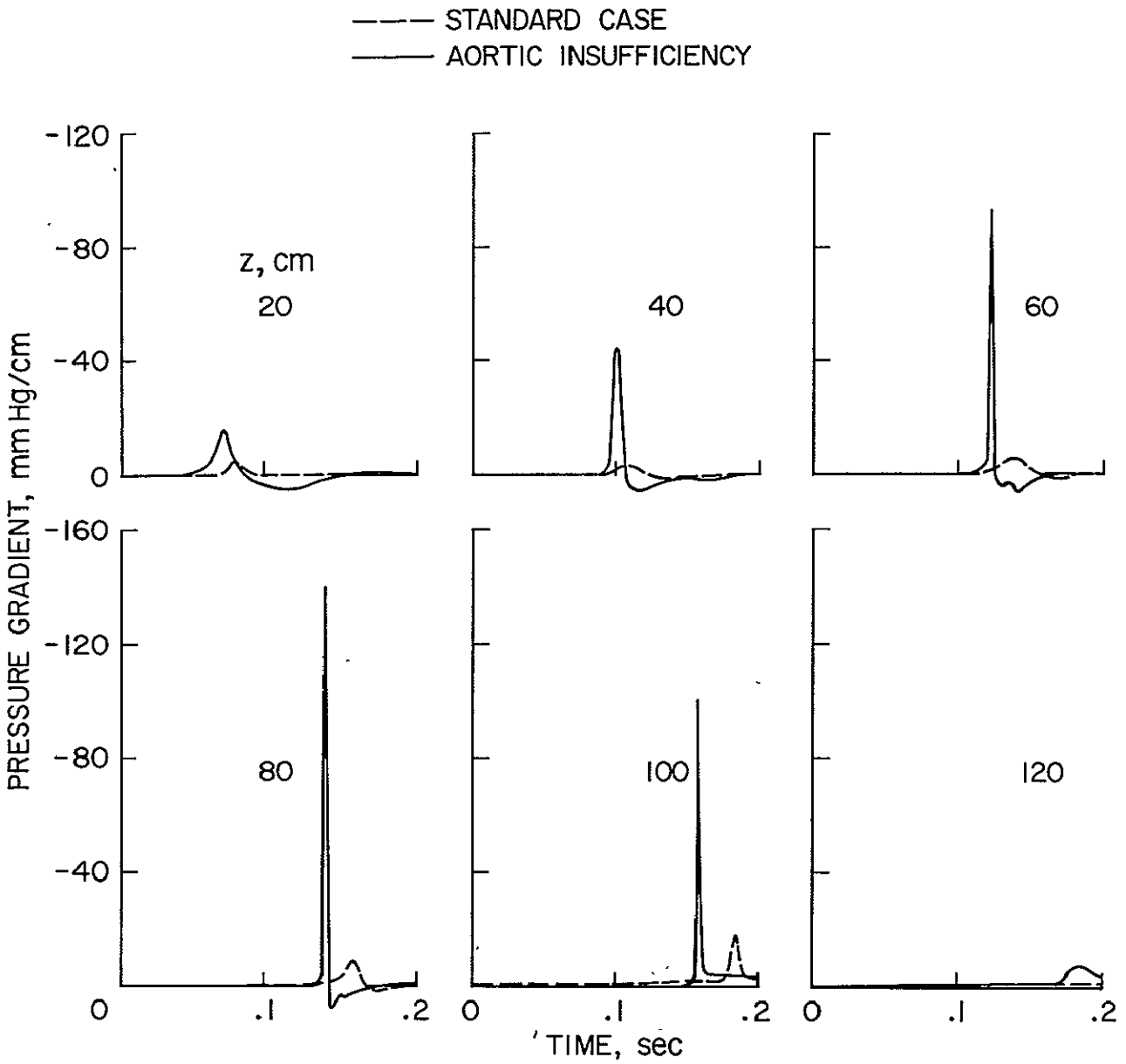

Figure 51. Local pressure gradients in the case of hypothetical aortic insufficiency.

abruptly, but in a gradual manner. In the case considered it approaches a minimal thickness of about 6 cm and then broadens again.

TABLE 3

Thickness of the Arterial Shock Wave

Distance cm	Wave Speed cm/sec	Time to Pass sec	Thickness cm
0	340	.120	41
20	560	.025	14
40	900	.010	9
60	1100	.006	7
80	1700	.004	7
100	1200	.005	6
120	670	.030	20

The peak pressures exceed 500 mm Hg at $z = 80$ cm and as such are probably somewhat high. Presumably this may partly be due to the fact that we have disregarded the viscoelastic damping which is particularly pronounced for spike-type perturbations. Yet it should be mentioned that systolic pressures beyond 300 mm Hg have been observed in man[37]. In general, the gross features associated with aortic insufficiency predicted here for the dog seem to be in qualitative agreement with observations on man. Even the fact that backflow is still present for $z = 60$ cm (near the external iliac artery) appears to be realistic[37].

V. DISCUSSION AND CONCLUSIONS

The results of this study have shown that the familiar features of the natural pressure and flow pulses in arteries can be reproduced mathematically with the help of the method of characteristics if we specify the physical and geometric cardiovascular parameters properly. In examining the effects of changes in these parameters it became apparent that the incisura develops even when there is no backflow as long as the time interval of diminishing ejection rate is sufficiently short. This means that towards the end of cardiac ejection the flow rate (Figure 8) must decay rapidly to zero to give rise to an incisura. Also, for the wave speeds considered we did not observe the phenomenon of backflow in the aorta beyond a distance of 30 cm from the heart except at low heart rates, low pressures and when we have incompetent aortic valves. Generally speaking, for stiffer arteries the backflow was less pronounced and vanished at shorter distances from the heart.

As the pulse wave propagates, we can always notice a marked steepening of the wave front and a peaking of the pressure pulse when we take the nonlinear effects into account. By contrast, the linearized analysis predicts less peaking of the pulse and essentially no steepening of the wave front. It also yields a significantly different diastolic pressure, a wider pulse and a more prominent dicrotic wave. These differences between the results of a linear and a nonlinear treatment of the propagation of large-amplitude pressure waves suggest that nonlinear effects must be accurately accounted for if we are interested in the interpretation of small changes in the flow and pressure pulses.

A decrease of 36% in cross-sectional area of the artery and an increase in arterial wall stiffness corresponding to a 40% rise in wave speed produced substantial changes in the pressure and flow pulses, suggesting that

they may possibly serve as diagnostic indicators. The potential use of the flow pulse for diagnostic purposes seems particularly promising in view of the recent development of ultrasound echo-ranging devices[5] and pulsed doppler flowmeters.[3] Both the reduction in diameter and the increase in wave speed effectively produced a diminished distensibility which accounts for the elevation of the pulse pressure in the major arteries predicted by the model. While the increase in wave speed primarily affected the shape of the flow pulse and not so much the peak flow velocities, the reduction in diameter mainly increased the peak flow velocities and left the shape of the flow pulse essentially unchanged. Figures 14 and 15 hint that a sufficiently large increase in wave speed might lead to the development of a second dicrotic wave. They also demonstrate that backflow can virtually be eliminated by raising the wave speed. Moreover, they clearly show that relatively small changes in the pressure gradient alter extensively the flow pattern. This again suggests that the results to be obtained by prescribing the pressure variation at the root of the aorta (instead of specifying the ejection pattern) as a boundary condition may exhibit large errors in the predicted flow pattern unless we know the pressure at the heart with extreme accuracy. In addition, it shows that the pressure gradient technique for determining the cardiac output[38] is prone to large errors.

Many of the features of the dicrotic wave indicate that it is caused by the reflection of the primary pressure pulse from the more distal regions of the arterial tree. However, the quantitative aspects of this reflection phenomenon are not yet established and additional investigations will be necessary. As we do not observe a dicrotic wave when the model artery is infinitely long and has neither taper nor outflow, we may infer that the dicrotic wave is a consequence of taper or outflow. Also, since the dicrotic wave appears progressively later in time

with increasing distance from the heart it can not be the result of a discrete reflection from a single site. This conclusion is also supported by the fact that the dicrotic wave occurs essentially at the same time for a given distance from the heart irrespective of whether we impose the terminal boundary condition at 71, 103, 120 or 150 cm from the heart.

Cardiac arrest and the subsequent resumption of the normal heart beat were simulated to seek evidence of transient phenomena. When the heart is stopped, extra waves which are normally obscured by following heart beats are observed but they have very small amplitudes. This suggests that they are caused by multiple reflections of the primary pressure pulse and that the dicrotic wave is the first of these reflections. When the normal cardiac ejection is resumed after a quiescent state of zero velocity and uniform pressure of 25 mm Hg has been reached, it takes only 2 or 3 heart beats to restore the pressure and flow pulses to life-sustaining levels.

The simulation of rest and of exercise by considering pulse rates of 60 and 180 beats per minute and modifying the resistance of the vascular bed to enforce normal pressure levels revealed distinct changes in the pressure and flow pulses. The lower heart rate produced significantly higher pulse pressures and larger dicrotic waves but much smaller average flow velocities as compared with the Standard Case. It also allowed for backflow at distances beyond 40 cm from the heart. In addition, as sometimes observed experimentally,[27] multiple diastolic (dicrotic) waves, which may even exhibit backflow, are predicted at the lower heart rate. The higher pulse rate simulating exercise produced generally opposite effects, i.e. lower pulse pressures, higher mean flow velocities, reduced backflow and a smaller dicrotic wave.

Overall modifications of the outflow resistance as might be caused

by vasoconstriction, vasodilatation, and by removing an abdominal organ seem to yield the expected changes in the pressure level but only mild alterations in the flow patterns.

It is questionable whether the effects of fluid viscosity have been accounted for in a satisfactory manner since the friction expression is based on the assumption of quasi-steady flow. For a nominal value of $\mu = .049$ poise or less, the results are essentially the same for laminar or turbulent flow. However when we increase the effective viscosity coefficient to 0.49 poise, then the pulse waves exhibit a much more rapid decay with distance for laminar flow but not in the turbulent case, yet the basic shape of the pressure and flow pulses is not markedly altered.

The concept of a peripheral resistance for the distal boundary condition was found to be remarkably satisfactory provided that this boundary condition was applied no closer to the heart than the femoral region in the cases examined. Attempts to utilize a peripheral resistance in the abdominal aorta yielded drastic alterations in the pressure and flow patterns.

The wave front velocity for the Standard Case compared rather favorably with experimentally obtained data. Likewise, harmonic analyses of the computed results for various stations along the artery show that the apparent phase velocities of the different harmonics as well as the impedances resemble those obtained from dog experiments.

Simulating aortic insufficiency, we find that the wave front is rapidly steepened with increasing distance from the heart in a fashion reminiscent of shock waves in high-speed compressible flow. Indeed a first indication of a shock wave in our particular case could be observed at 40 cm from the heart. Its effective thickness was estimated to be as small as 6 cm. The occurrence of shock

waves in our model of the cardiovascular system should not be too surprising since the governing differential equations form a hyperbolic system. Normally the dimensions of the body are too small to allow for the development of a shock wave. It is only in cases of circulatory disorders such as aortic insufficiency, where we have a very steep pressure front at the heart and an unusually large pulse pressure, that a shock wave can develop within a realistic distance from the heart.

APPENDIX A

We shall demonstrate that the wave speed expression (10) appearing in the derivation of the characteristic equations is indeed equivalent to the classical Moens-Korteweg relation. According to equation (10) of Chapter II:

$$c = \sqrt{\frac{S}{\rho\left(\frac{\partial S}{\partial p}\right)_z}} \tag{A1}$$

Restricting ourselves to a tube of circular cross section we consider a segment for which the cross-sectional area does not change appreciably with axial distance. Then S is essentially a function of pressure alone $S = S(p)$, and

$$\left(\frac{\partial S}{\partial p}\right)_z \approx \frac{dS}{dp}$$

Denoting by r the internal radius of the circular cross section, we have

$$S = \pi r^2$$

and

$$\frac{dS}{dp} = 2\pi r \frac{dr}{dp} = \frac{2}{r} S \frac{dr}{dp}$$

For a thin-walled tube with a wall thickness h we can take r to approximate also the radius of the middle surface $r + \frac{h}{2} \approx r$.

With the expressions for S and $\left(\frac{\partial S}{\partial p}\right)_z$ given above we can write for equation (A1)

$$= \sqrt{\frac{r}{2\rho}\frac{dp}{dr}} \tag{A2}$$

We now consider a change of state of the tube from a radius r to $r+dr$ from a pressure p to $p+dp$, and from a circumferential wall tension T to $T+dT$. The differential strain produced by dr is

$$d\epsilon = \frac{2\pi(r+dr) - 2\pi r}{2\pi r} = \frac{dr}{r}$$

while the differential wall stress can be given as

$$d\sigma = \frac{dT}{h}$$

Hence the tangential elastic modulus becomes

$$E = \frac{d\sigma}{d\epsilon} = \frac{r}{h}\frac{dT}{dr} \qquad \text{(A3)}$$

Static equilibrium requires that the tension in the wall be balanced by the pressure in the fluid, which means $T = pr$ and

$$dT = p\,dr + r\,dp$$

Neglecting the contribution of the small term $p\,dr$ we have

$$\frac{dT}{dr} = r\frac{dp}{dr}$$

and equation (A3) can also be written in the form

$$E = \frac{r^2}{h}\frac{dp}{dr}$$

Combining this relation with (A2) we finally obtain

$$c = \sqrt{\frac{Eh}{2\rho r}} \qquad \text{(A4)}$$

which is the classical Moens-Korteweg equation for the local speed of propagation of small pressure signals in elastic tubes.

We note that this equation has been derived from the more general equation (A1) with the assumptions of

(i) a circular cross section

(ii) a thin wall

(iii) a cross-sectional area that changes slowly with axial distance.

These are the standard assumptions for deriving the Moens-Korteweg equation from alternate considerations.

APPENDIX B

At a uniform pressure p_o equation (16) shows that the cross-sectional area of the artery varies exponentially with distance from the aortic valve. If we plot the function $\xi(z; p)$ defined by

$$\xi(z;p) = e^{\frac{p - p_o}{\rho c(p,z) c(p_o,z)}} \tag{B1}$$

for various values of p (see Figure B1), we can assess the changes in the local geometry of the artery produced by deviations of the local pressure from p_o. In computing the curves displayed in Figure B1 we have chosen the wave speed to be that for the Standard Case, and $p_o = 100$ mm Hg. The figure clearly indicates how the artery stiffens as z increases. It also shows that the local changes in cross-sectional area produced by the natural pressure pulse can easily exceed 10%, especially in the proximal aorta.

3

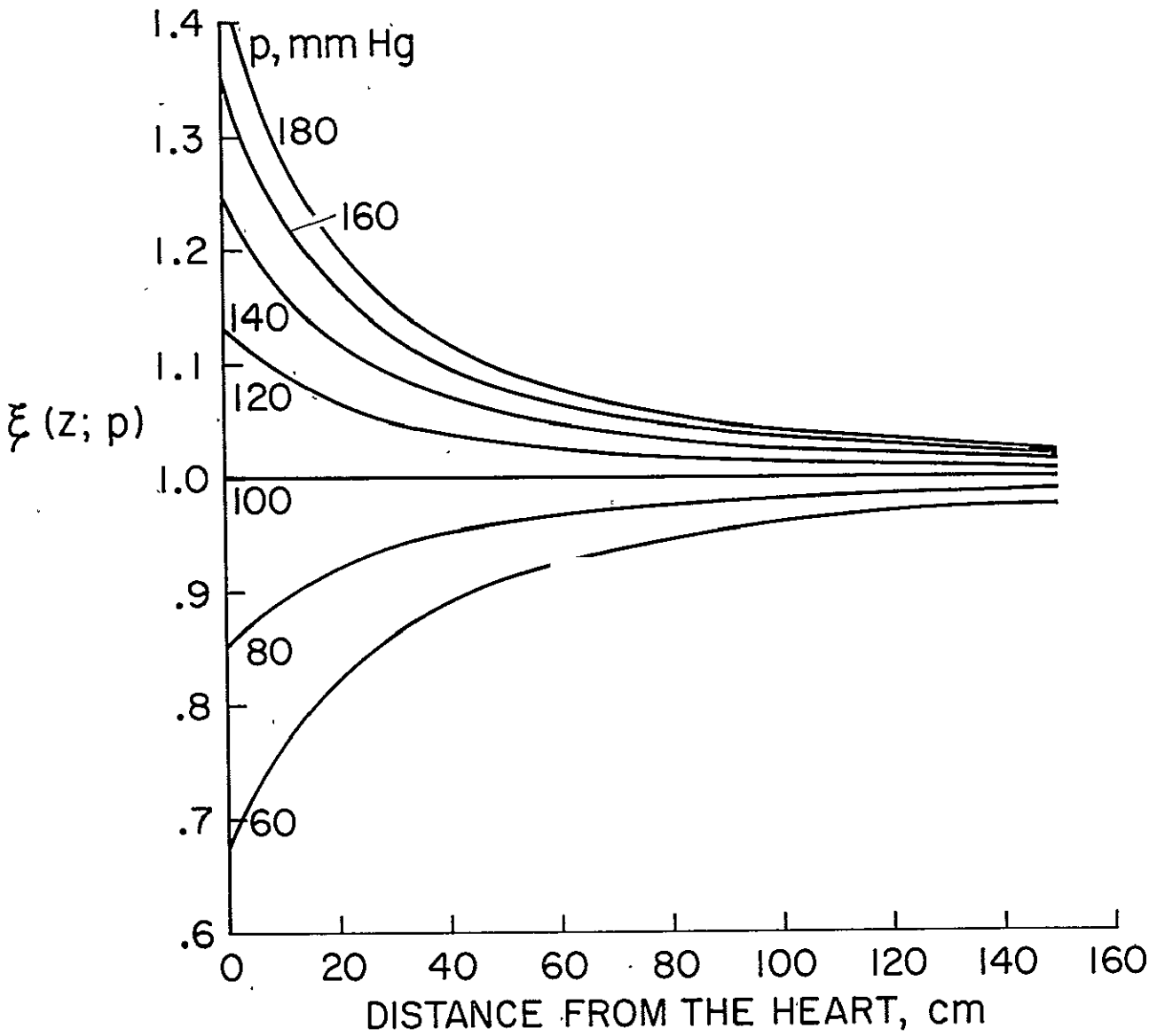

Figure B1. Effect of pressure on the arterial cross section in the Standard Case.

REFERENCES

1. Wetterer, E. and Kenner, Th.: Grundlagen der Dynamik des Arterienpulses. Berlin, Springer-Verlag, 1968.

2. McDonald, D.A.: Blood Flow in Arteries. London, Edward Arnold, Ltd., 1960.

3. Peronneau, P.A. and Leger, F.: Doppler Ultrasonic Pulsed Blood Flowmeter. Proceedings of the 8th International Conference on Medical and Biological Engineering, Chicago, Illinois, 1969.

4. Baker, D.W. and Strandness, D.E.: Instrumentation for the Early Detection of Arterial Occlusive Disease. Proceedings of the 8th International Conference on Medical and Biological Engineering, Chicago, Illinois, 1969.

5. Arndt, J.O.: Über die Mechanik der intakten A. carotis communis des Menschen unter verschiedenen Kreislaufbedingungen. Archiv für Kreislaufforschung, 59:153, 1969.

6. Anliker, M., Histand, M.B. and Ogden, E.: Dispersion and Attenuation of Small Artificial Pressure Waves in the Canine Aorta. Circulation Research 23:539-551, 1968.

7. McDonald, D.A.: Regional Pulse-Wave Velocity in the Arterial Tree. J. of Applied Physiology, 24:73, 1968.

8. Anliker, M., Moritz, W.E. and Ogden, E.: Transmission Characteristics of Axial Waves in Blood Vessels. J. of Biomechanics, 1:235-246, 1968.

9. Physiology in the Space Environment. I, Circulation. NAS-NRC Publ. 1485A Nat. Acad. Sci. - Nat. Res. Council, Washington, D.C., 1968.

10. Womersley, J.R.: An Elastic Tube Theory of Pulse Transmission and Oscillatory Flow in Mammalian Arteries. WADC Tech. Report TR 56-614, Defense Documentation Center, 1957.

11. Skalak, R.: Wave Propagation in Blood Flow. In Biomechanics Symposium, edited by Y.C. Fung, New York, ASME, 1966, pp. 20-46.

12. Rudinger, G.: Review of Current Mathematical Methods for the Analysis of Blood Flow. In Biomedical Fluid Mechanics Symposium, New York, ASME, 1966, pp. 1-33.

13. Lambert, J.W.: On the Nonlinearities of Fluid Flow in Nonrigid Tubes. J. Franklin Institute, 266:83, 1958.

14. Streeter, V.L., Keitzer, W.F. and Bohr, D.F.: Pulsatile Pressure and Flow Through Distensible Vessels. Circulation Research 13:3, 1963.

15. Rudinger, G.: Shock Waves in Mathematical Models of the Aorta. 12th International Congress of Applied Mechanics, Stanford University, California, 1968.

16. Barnard, A.C.L., Hunt, W.A., Timlake, W.P. and Varley, E.: A Theory of Fluid Flow in Compliant Tubes. Biophysical Journal 6:717-724, 1966.

17. Barnard, A.C.L., Hunt, W.A., Timlake, W.P. and Varley, E.: Peaking of the Pressure Pulse in Fluid-Filled Tubes of Spatially Varying Compliance. Biophysical Journal 6:735-746, 1966.

18. Jones, R.T.: Blood Flow. Annual Review of Fluid Mechanics 1:223-244, 1969

19. Anliker, M., Wells, M.K. and Ogden, E.: The Transmission Characteristics of Large and Small Pressure Waves in the Abdominal Vena Cava. IEEE Transactions on Bio-Medical Engineering, BME-16:262-273, 1969.

20. Lange, R.L. and Hecht, H.H.: Genesis of Pistol Shot and Korotkoff Sounds. Circulation 18:975-978, 1958.

21. Ruch, T.C. and Patton, H.D.: Physiology and Biophysics. Philadelphia, Saunders Co., 1965.

22. Hultgren, H.N.: Venous Pistol Shot Sounds. Am. J. of Cardiology 10:667, 1962.

23. Histand, M.B.: An Experimental Study of the Transmission Characteristics of Pressure Waves in the Aorta. Ph.D. Dissertation, SUDAAR Report No. 369, Department of Aeronautics and Astronautics, Stanford University, California, 1969.

24. Patel, D.J., deFreitas, F.M., Greenfield, J.C., Jr. and Fry, D.L.: Relationship of Radius to Pressure Along the Aorta in Living Dogs. J. of Applied Physiology 18:1111, 1963.

25. Attinger, E.O., Sugawa, H., Navarro, A., Riccetto, A. and Martin, R.: Pressure-Flow Relations in Dog Arteries. Circulation Research 19:230, 1966.

26. Sapirstein, L.A.: Regional Blood Flow by Fractional Distribution of Indicators. Am. J. of Physiology 193:161, 1958.

27. O'Rourke, M.F.: Pressure and Flow in Arteries. M.D. Thesis, University of Sydney, 1965.

28. Spencer, M.P. and Denison, A.B.: Pulsatile Blood Flow in the Vascular System. In Handbook of Physiology, sect. 2, Circulation, Vol. II, Washington D.C., 1963, pp. 839-864.

29. Lister, M.: The Numerical Solution of Hyperbolic Differential Equations by the Method of Characteristics. In Mathematics for Digital Computers, New York, John Wiley and Sons, 1960.

30. Wiggers, H.C.: Cardiac Output and Total Peripheral Resistance Measurements in Experimental Dogs. Am. J. of Physiology 140:519, 1944.

31. Schlimmler, W.: Untersuchen zu Elastizitätsproblemen der Aorta. (Statistical Correlation of Pulse Wave Velocity with Age, Sex and Blood Pressure.) Archiv für Kreislaufforschung 47:189, 1965.

32. Jones, E., Chang, I-Dee and Anliker, M.: Effects of Viscosity and External Constraints on Wave Transmission in Blood Vessels. SUDAAR Report No. 344, Department of Aeronautics and Astronautics, Stanford University, California, 1968.

33. Jones, R.T.: Simple Correction of the Windkessel Theory for the Dynamic Impedance of the Aorta. Proceedings of the 8th International Conference on Medical and Biological Engineering, Chicago, Illinois, 1969.

34. Nichols, W.W., Webster, J.E. and McDonald, D.A.: Pulse Wave Velocity in the Ascending Aorta of the Dog. Am. Physiological Society Proceedings, Davis, California, 1969.

35. McDonald, D.A.: Frequency Dependence of Vascular Impedance. In Pulsatile Blood Flow, edited by E.O. Attinger, New York, McGraw-Hill Book Co., 1964, pp. 115-133.

36. Regan, T.J., Defazio, V., Binak, K. and Hellems, H.K.: Norepinephrine Induced Pulmonary Congestion in Patients with Aortic Valve Regurgitation. J. of Clin. Invest. 38:1564-1571, 1959.

37. Friedberg, C.K.: Diseases of the Heart. Philadelphia, W.B. Saunders Co., 1955.

38. McDonald, D.A., Nichols, W.W. and Kouchoukos, N.T.: Methods for Monitoring Cardiac Output. Proceedings of the Annual Conference on Engineering in Medicine and Biology. Houston, Texas, 1968.